2009

Hybrid thermochemical/biological processing of biomass for the production of polyhydroxyalkanoates and hydrogen gas from *Rhodospirillum rubrum* cultured on synthesis gas

David Craig Chipman
Iowa State University

Hybrid thermochemical/biological processing of biomass for the production of polyhydroxyalkanoates and hydrogen gas from *Rhodospirillum rubrum* cultured on synthesis gas

by

David Craig Chipman

A thesis submitted to the graduate faculty

in partial fulfillment of the requirements for the degree of

MASTER OF SCIENCE

Co-majors: Mechanical Engineering; Biorenewable Resources and Technology

Program of Study Committee:
Robert C. Brown, Major Professor
Thomas A. Bobik
Theodore J. Heindel
Shihwu Sung

Iowa State University

Ames, Iowa

2009

TABLE OF CONTENTS

LIST OF FIGURES

LIST OF TABLES

ABSTRACT

The goal of this research is to optimize PHA production in the syngas fermenting organism *Rhodospirillum rubrum*. Syngas fermentation is the hybrid thermochemical/ biological approach to processing biomass into valuable fuels and chemicals. The process begins with the gasification of biomass to produce syngas, a flammable gas mixture consisting primarily of carbon monoxide (CO), hydrogen (H_2), and carbon dioxide (CO_2). Microorganisms are then used to ferment the syngas into biofuels and chemicals.

Rhodospirillum rubrum, a non-sulfur purple bacterium, utilizes the CO in syngas to produce H_2 and polyhydroxyalkanoates (PHAs), biobased-biodegradable polymers. Information is limited pertaining to the optimization of growth media as well as the optimal harvest point for *R. rubrum* in terms of H_2 and PHA production.

RRNCO growth media was optimized on the small scale (40 ml). The resulting media recipe was scaled up to 10L for the evaluation of the optimal harvest point. A syngas fermentation facility and control system was designed and developed for fermentation scale (10L) experiments. The results of the small scale experiments did not agree with literature in terms of the effect of the carbon to nitrogen balance on cellular PHA content. Yeast extract may have been acting as an additional source of available carbon and nitrogen in the media.

The results of the harvest point optimization indicated that cell density and media acetate levels may serve as good indicators of maximum PHA production. PHA production appeared to maximize when cell growth reached late exponential phase or early stationary phase. Maximum PHA production corresponded well with the point of media acetate exhaustion.

CHAPTER 1. INTRODUCTION

The goal of this research is to optimize PHA production in the syngas fermenting organism *Rhodospirillum rubrum*. The concept of a biorefinery has expanded beyond the separation and fractionation of biomass feedstocks into bio-based products. The new concept of a biorefinery also includes the separation and fractionation of biomass feedstocks, but on a molecular level by means of hybrid thermochemical and biological processing. Syngas fermentation is such a hybrid process.

In syngas fermentation, recalcitrant biomass enters the system and is thermally degraded through gasification to produce a gaseous product mixture called syngas or producer gas (the latter containing dilutant nitrogen from air used in the process). The resulting product gas is cleansed of solid particulates and tars and fed to fermentors containing syngas utilizing organisms. These organisms then use the available carbon monoxide (CO), hydrogen (H_2), methane (CH_4), and carbon dioxide (CO_2) as sources of energy and carbon to produce valuable products.

Rhodospirillum rubrum, a purple non-sulfur gram negative bacterium, is capable of utilizing the CO in syngas and producer gas as a carbon and energy source. *R. rubrum* is an attractive syngas utilizer for its ability to produce polyhydroxyalkanoates (PHA) as an energy storage molecule, as well as for its ability to biocatalyze the water-gas-shift reaction.

$$CO + H_2O \rightarrow CO_2 + 2H^+ + 2e^- \qquad \textbf{Equation 1}$$

This conversion is advantageous because the hydrogen content of the syngas is increased and PHA can be processed into biodegradable plastics. Recent techno-economic analysis has shown that with a hydrogen coproduction credit, PHA production via syngas fermentation could compete with traditional methods of production [1].

Studies have shown that varying media composition and carbon sources in the media affect PHA production by *R. rubrum* [2-4]. *Rhodospirillum rubrum* no-light CO (RRNCO) growth medium is used for anaerobic dark growth [5, 6]. Do and colleagues noticed that changing acetate concentration in the RRNCO media affected PHA production in *R. rubrum* grown on simulated syngas [5]. Information is limited pertaining to the optimization of growth media for *R. rubrum* for its effect on the co-production of H_2 and PHA. The point of harvest for PHA produced from *R. rubrum* also is not well understood. Understanding how to optimize PHA and hydrogen production from *R. rubrum* could increase its value as a biocatalyst and potentially reduce the cost of the growth media. This thesis investigates the optimization of RRNCO growth media on a 40 ml fermentation scale. The results of the small scale experiments are to be scaled up to the 10 L fermentation scale. It is hypothesized that the optimal growth medium will have a high carbon to nitrogen ratio.

A challenging aspect of this investigation was the design and development of a syngas fermentation facility. Generating a continuous flow of syngas from a gasifier was not possible for the duration required by the fermentation experiments. A syngas fermentation system was developed to provide a consistent and controllable supply of artificial syngas to the experimental fermentors. Control software was also written to control the system both locally and remotely.

CHAPTER 2. BACKGROUND

2.1 GASIFICATION

2.1.1 *Principles of Gasification*

Gasification is the thermochemical breakdown of carbonaceous substrates to condensable and non-condensable gaseous products as well as char (solid particulate consisting of carbon an ash). This complex set of reactions occurs in several steps [7]. First the carbonaceous substrate is heated and dried. Next, pyrolysis begins once the temperature of the substrate reaches 300-400^{o}C. Pyrolysis produces intermediate products of char, CO, CO_2, H_2, water vapor (H_2O), light hydrocarbons, and condensable vapors with distribution based on the substrate, temperature, and heating rate. Gas-solid reactions convert carbon into CO, H_2, and CH_4 as described by the carbon-oxygen reaction (Equation 2), Boudouard reaction (Equation 3), carbon-water reaction (Equation 4), and hydrogenation reaction (Equation 5).

$C + ½O_2 \leftrightarrow CO$ ΔH_R = -110.5 MJ/kmol **Equation 2**

$C + CO_2 \leftrightarrow 2CO$ ΔH_R = 172.4 MJ/kmol **Equation 3**

$C + H_2O \leftrightarrow H_2 + CO$ ΔH_R = 131.3 MJ/kmol **Equation 4**

$C + 2H_2 \leftrightarrow CH_4$ ΔH_R = -74.8 MJ/kmol **Equation 5**

The final step of gasification involves the gas phase reactions which include the water-gas shift reaction (Equation 6) and methanation (Equation 7).

$CO + H_2O \leftrightarrow H_2 + CO_2$ ΔH_R = -41.1 MJ/kmol **Equation 6**

$CO + 3H_2 \leftrightarrow CH_4 + H_2O$ $\Delta H_R = -206.1$ MJ/kmol **Equation 7**

2.1.2 *Gasification Product Distribution*

The products of gasification include non-condensable gases, condensable vapors, tars (short chain hydrocarbons, polyaromatic hydrocarbons, etc.), and char. The product distribution of gasification depends on several factors including reaction time, temperature, and inlet oxygen and steam levels. When the process uses air as a fluidizing and/or carrier gas, the resulting nitrogen-diluted gas stream is referred to as producer gas. When the gasification occurs with steam and oxygen (O_2) as the fluidizing and/or carrier gas, the resulting gas stream is referred to as synthesis gas or syngas.

2.1.3 *Types of Gasifiers*

The three major types of gasifiers are moving-bed, fluidized-bed, and entrained flow gasifiers [8]. In moving-bed gasifiers, the feedstock moves downward by gravity against a counter flowing heated gas. The counter-current arrangement allows for preheating of the entering feedstock by the exiting syngas. The exiting gas is relatively low in temperature (425-650^{o}C) and contains hydrocarbons in the gas stream [9].

Fluid-bed gasifiers provide excellent heat transfer and mixing conditions. The efficient heat transfer allows for rapid equilibrium and thus high throughput [10]. Feedstock is mixed with bed material and both are fluidized by the gas flowing through the bed. This type of gasifier can be heated both directly and indirectly. The particle size of both the feedstock and bed material is important to the operation of this type of gasifier. Small particles can be entrained in the fluidizing gas and leave the reactor

prematurely resulting in lower carbon conversion. Outlet gas temperatures for fluidized bed gasifiers are moderate (900-1050^{o}C) [9].

Entrained flow gasifiers are noted for high carbon conversion and output gas purity. In an entrained flow gasifier, the feedstock and carrier gas flow in the same direction. The most common entrained flow gasifier is the entrained flow slagging gasifier. Since the operating temperatures (1250-1600^{o}C) are higher than the ash melting point, the ash agglomerates and exits at the bottom of the reactor [8, 9].

2.1.4 *Gas Clean-up and Product Upgrading*

Syngas has several industrial uses. In addition to being combusted for use as process heat or for power generation, syngas is a valuable intermediate in the synthesis of many industrial chemicals. Carbon monoxide is used in the synthesis of several organic chemicals including acetic acid, phosgene, butanols, acrylic acid, and formic acid [8]. These chemicals serve as precursors to other valuable industrial products from polyurethanes to paints to preservatives [11]. In air blown gasification, ammonia can be produced from the hydrogen and nitrogen in the syngas. Syngas can also be used as a substrate for Fisher-Tropsch synthesis for the production of hydrocarbons and alcohols. The upgrading of synthesis gas to the products mentioned above usually requires the use of catalysts at elevated pressure and temperature.

Catalyst poisons as well as solid particulate must be removed before the syngas is upgraded. Depending on the size, solid particulate is removed with cyclones and/or barrier filters. High efficiency cyclones are capable of removing particles greater than 5 μm. Smaller diameter particles, down to 0.5 μm, are removed with barrier filters, such as

candle filters and bag filters [12-14]. This particulate removal occurs at elevated temperatures to prevent the condensation of tars and other vapors [13]. Tars are removed from the syngas stream once the solid particulate has been removed. Oil and water are commonly used to scrub tar from syngas, but the resulting waste is toxic and can be costly to treat for disposal [13, 15]. Tar can also be removed via chemical or thermal "cracking" into CO and H_2.

2.2 SYNGAS FERMENTATION

Syngas fermentation offers a unique approach to processing the recalcitrant components of biomass. Instead of using microorganisms to breakdown cellulose and lignin, the "thermodynamic hammer" is used to break these complex molecules into simpler compounds that can be utilized by microorganisms. Syngas utilizing organisms can produce a variety of chemicals including acetic acid, biopolymers, butyric acid, butanol, ethanol, hydrogen, and methane [16]. Syngas fermentation has several advantages over mineral-based catalytic upgrading. Such advantages include higher reaction specificity, higher yields, lower energy costs, greater resistance to poisoning, and complete conversion [17-19]. The biocatalysts used by syngas fermenting organisms also operate at lower temperatures and pressures compared to most mineral-based catalysts. Some catalytic syngas upgrading processes, such as Fisher-Tropsch synthesis, require very specific ratios of carbon monoxide to hydrogen in order for the process to work properly, however, biocatalysts are less sensitive to such ratios. Slower reactions and the need for sterility are disadvantages to syngas fermentation [20].

2.2.1 *Syngas Utilizers*

Many organisms are capable of utilizing the components of syngas as carbon and energy sources. Products from these organisms range from CO_2 to alcohols to acids.

Table 1 lists organisms capable of utilizing syngas and the products produced by those organisms.

2.2.2 *Rhodospirillum rubrum*

Rhodospirillum rubrum is a purple, non-sulfur, photosynthetic, gram-negative bacteria. This loose spiral-shaped organism can range in size from 0.8 to 1 μm [21]. In nature, *R. rubrum* is found in pond water, mud, and sewage [22]. *R. rubrum* has a diverse metabolism. Its ability for anaerobic CO growth, hydrogen production, and PHA production makes *R. rubrum* an excellent candidate syngas organism. Several investigations have been made into *R. rubrum* as a syngas organism [5, 19, 20, 23-27].

2.2.3 *Carbon Monoxide Metabolism*

Several types of Bacteria and Archaea have demonstrated the ability to oxidize carbon monoxide. Carboxydotrophs, phototrophs, methanogens, acetogens, and sulfate reducers all have been shown to oxidize CO [28-31]. The ability of these organisms to utilize CO as an energy and/or carbon source is due to the presence of the enzyme carbon monoxide dehydrogenase (CODH). CODH in *R. rubrum* provides a source of reductant, energy, carbon, and serves as a protective mechanism by expanding its metabolic capabilities to utilize CO [32]. Previous studies at Iowa State University estimate that 20% of the CO fermented by *R. rubrum* is converted into cellular biomass, of which 35% is PHA. The remaining 80% goes into producing extra cellular hydrogen [33].

Table 1. Syngas utilizing microorganisms and associated products (adapted from Henstra et al. [34]).

Species	T_{opt} [^oC]	pH_{opt}	t_d [h]	Energy Source	Source
Acetate Producers					
Acetobacterium woodii	30	6.8	13	$CO + H_2$	[35]
Clostridium thermoaceticum	55-60	nr	nr	$H_2 + CO_2$ or CO	[36]
Eubacterium limosum	38-39	7.0-7.2	7	$CO + H_2$	[37, 38]
Moorella thermoacetica	55	6.5–6.8	10	$CO + H_2$	[16]
Moorella thermoautotrophica	58	6.1	7	$CO + H_2$	[39]
Peptostreptococcus productus	37	7	1.5	$CO + H_2$	[40]
Acetate, Ethanol Producers					
Clostridium autoethanogenum	37	5.8-6.0	nr	$CO + H_2$	[41]
Clostridium ljungdahlii	37	6	3.8	$CO + H_2$	[42]
Acetate, Ethanol, Butyrate, Butanol Producers					
Butyribacterium methylotrophicum	37	6	12-20	$CO + H_2$	[43-45]
Clostridium carboxidivorans	38	6.2	6.25	$CO + H_2$	[46]
Acetate, n-butyrate Producers					
Oxobacter pfennigii	36-38	7.3	13.9	$CO + H_2$	[47]
Acetate, formate, CH_4 Producers					
Methanosarcina acetivorans strain C2A	37	7	24	$CO + H_2$	[48]
Acetate, H_2					
Clostridium thermoautotrophicum	55-60	5.7	nr	$H_2 + CO_2$ or CO	[49]
Acetate, formate, H_2S Producers					
Archaeoglobus fulgidus	83	6.4	nr	$CO + H_2$	[50]
Acetate, H_2S Producers					
Desulfotomaculum kuznetsovii	60	7	nr	$CO + H_2$	[51]
Desulfotomaculum geothermicum	54	7.3-7.5	nr	CO_{2+} H2	[52]
Desulfotomaculum thermobenzoicum subsp. *thermosyntrophicum*	55	7	nr	$CO + H_2$	[51]
CH_4 Producers					
Methanosarcina barkeri	37	7.4	65	$CO + H_2$	[53]
Methanothermobacter thermoautotrophicus	65	7.4	140	$CO + H_2$	[54]
H_2 Producers					
Carboxydibrachium pacificus	70	6.8–7.1	7.1	$CO + H_2$	[55]
Carboxydocella sporoproducens	60	6.8	1	$CO + H_2$	[56]
Carboxydocella thermoautotrophica	58	7	1.1	$CO + H_2$	[57]
Carboxydothermus hydrogenoformans	70–72	6.8–7.0	2	$CO + H_2$	[58]
Citrobacter sp Y19	30-40	5.5-7.5	8.3	$CO + H_2$	[59, 60]
Rhodopseudomonas palustris P4	30	nr	23	$CO + H_2$	[61]
Rhodospirillum rubrum	30	6.8	8.4	$CO + H_2$	[6]
Rubrivivax gelatinosus	34	6.7-6.9	6.7	$CO + H_2$	[62, 63]
Thermincola carboxydiphila	55	8	1.3	$CO + H_2$	[64]
Thermincola ferriacetica	57–60	7.0–7.2	nr	$CO + H_2$	[65]
Thermococcus strain AM4	82	6.8	nr	$CO + H_2$	[66]
Thermolithobacter carboxydivorans	70	7	8.3	$CO + H_2$	[67, 68]
Thermosinus carboxydivorans	60	6.8–7.0	1.2	$CO + H_2$	[69]
H_2, H_2S Producers					
Desulfotomaculum carboxydivorans	55	7	1.7	$CO + H_2$	[70]

***Optimum temperature not explicitly given; nr – not reported**

2.2.3.1 *Carbon Monoxide Dehydrogenase*

CODH can be classified by its content (molybdenum or nickel containing), or by its function (monofunctional CODH or bifunctional CODH/acetyl-coenzyme A synthase (CODH/ACS) [71-73]. CO acts as both a σ bond donor and π bond acceptor, which makes it a good ligand for transition metals [74]. At the heart of CODH lies a transition metal ligand binding site. The reaction biocatalyzed by CODH is similar to the water gas shift reaction except CODH produces two protons and two electrons as opposed to H_2 [74]. Two mechanisms for CO oxidation by CODH have been proposed. Oelgeschläger et al. [75] proposes:

$$CO + H_2O \rightarrow CO_2 + 2H^+ + 2e^- \qquad \textbf{Equation 8}$$

Ferry et al. [76] propose the role of an acceptor:

$$CO + H_2O + acceptor_{ox} \rightarrow CO_2 + 2H^+ + acceptor_{red} \qquad \textbf{Equation 9}$$

Aerobic CO utilizers have CODH with a molybdenum (Mo) based metal center and oxidize CO slower than its nickel-based counterpart. CO oxidation by this Mo-CODH generates electrons which are then transferred through an electron transport chain ending ultimately with O_2 [77]. Anaerobic CODHs contain a nickel (Ni) based metal center. CODH/ACS activity, found in methanogens, acetogens, and sulfate reducers, gives the ability to form/cleave acetyl-CoA from/into a methyl group, CoA, and CO [75].

Not all CO utilizers have CODH/ACS activity. *R. rubrum* lacks ACS activity [74]. CODH in *R. rubrum* is an oxygen labile nickel, iron-sulfur, and zinc-containing protein that is induced by the presence of carbon monoxide CO [78]. The enzyme is soluble, however, when in the presence of CO, CODH in *R. rubrum* becomes membrane bound [78, 79]. Bound *R. rubrum* CODH is a peripheral membrane protein and can be

made soluble when the membrane is reduced and subjected to detergents or by heating [80], [78]. More specifically, it is tightly bound to the chromatophore membrane [6, 80]. Binding to the chromatophore membrane suggests that CODH is associated with the photosystem's ability of donating electrons. In *R. rubrum*, oxidation of CO is coupled to the H^+ reduction by a hydrogenase resulting in hydrogen evolution [80]. CO is oxidized by the Ni-CODH (CooS) and is coupled to the reduction via the Fe/S protein CooF [32]. This coupling of the oxidation of CO with the production of hydrogen is exergonic [81].

R. rubrum, and other phototrophic carboxidotrophs, contain homodimeric CODH [75]. The CODH found in *R. rubrum* contains two metal centers, cluster C (Ni-X-$[Fe_4S_4]^{2+/1+}$) and cluster B ($[Fe_4S_4]^{2+/1+}$). The C-clusters are fully reduced at < -500 mV. [82]. The C and B-clusters form what is called the β subunit. Each CODH contains two β subunits linked by the $[Fe_4S_4]$ D-cluster. The C-cluster is where the CO ligand binds CODH (see Figure 1). Both the B and D clusters act as transporters of electrons between the C-cluster and whatever is external to the CODH [83] (see Figure 2).

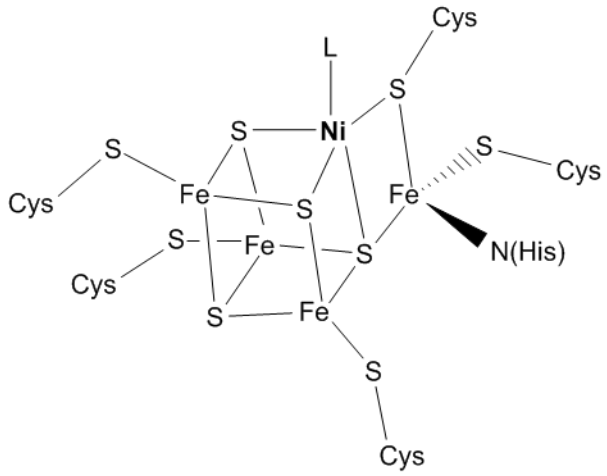

Figure 1. Model of $[Ni_1\text{-}Fe_4\text{-}S_5]$ cluster of CODH in *R. rubrum*. The L represents the ligand (CO) binding site [84, 85].

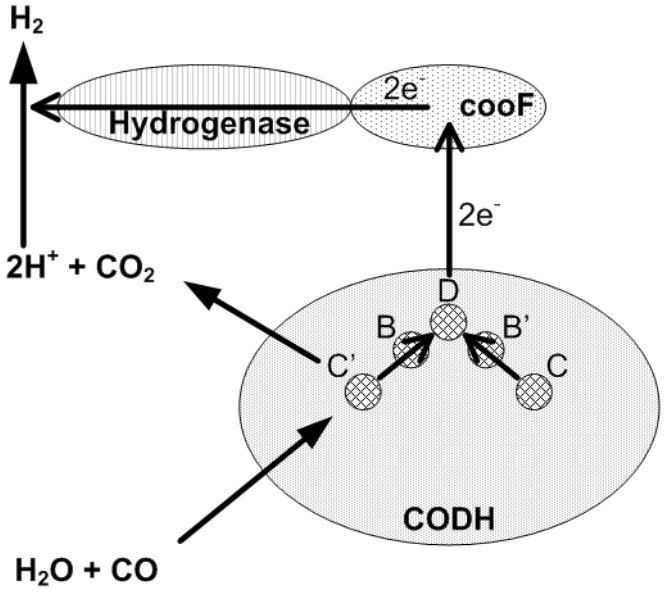

Figure 2. *R. rubrum* CODH with coupled hydrogenase activity via cooF (membrane associated protein) resulting in an exergonic reaction (20.1 kJ mol^{-1}) [84].

The CODH active site for CO oxidation is cluster C [74]. There are at least four redox states of cluster C: CO-reduced (C_{red2}), diamagnetic form (C_{ox}), one-electron reduced state (C_{red1}), and a state where the 3 g values are above 2 (C_{red3}) [74]. Feng and Lindahl classify the 4 redox states as C_{ox}, C_{red1}, C_{int}, and C_{red2} [83].

CODH in *R. rubrum* is inactive at redox potentials > -300 mV. In the presence of CO, autocatalysis can occur (CODH goes from an oxidized inactive form to reduced active form). Autocatalysis is initiated by small amounts of activated CODH which oxidize CO and gradually lower the redox potential [86]. Feng and Lindahl attemped to reproduce the results of Heo et al, but had difficulty. Their experiments suggest that CO binds to state C_{red1} [83]. They also found that thionin, an oxidant used in Heo et al. experiments, irreversibly inactivates CODH in *R. rubrum*. Cyanide as well as other anions can bind to cluster C and act as inhibitors, however, this action is reversible [74].

2.2.4 *Hydrogen Production*

Hydrogenases are enzymes that biocatalyze the oxidation of gaseous hydrogen (Equation 10):

$$H_2 \leftrightarrow 2H^+ + 2e^- \qquad \textbf{Equation 10}$$

This reversible reaction favors H_2 production in the presence of a reducing agent, and H_2 uptake in the presence of an oxidizing agent, however, the direction of the reaction is usually committed one way or the other in vivo depending on the organism [87, 88]. These enzymes can be found in several types of organisms and are not limited to bacteria [89-96].

Hydrogenases can be categorized into three classes based on the composition of their metal centers: [NiFe] hydrogenases, [FeFe] hydrogenases, and [Fe] hydrogenases [97-102]. The [NiFe] hydrogenases are further subdivided into groups: Group 1 – membrane-bound H_2 uptake hydrogenases; Group 2 – cyanobacterial uptake hydrogenases / H_2 sensing hydrogenases; Group 3 – reducing hydrogenases, hyperthermophillic hydrogenases, and NAD-linked hydrogenases; Group 4 – membrane-bound H_2 evolving hydrogenases [87].

R. rubrum likely contains at least three unique hydrogenases. In addition to uptake hydrogenases, *R. rubrum* contains a formate-linked hydrogenase that is regulated at the transcriptional level and a Group 4 CO-linked hydrogenase that is induced by CO at the transcriptional level (via the CooH gene) [88], [103]. The CO-linked hydrogenase activity is membrane bound and complexes with carbon monoxide dehydrogenase (CODH) [78, 80, 104]. This CO-linked hydrogenase is what enables *R. rubrum* to grow

in the dark with CO as its sole source of energy, possibly by serving as a means of pumping H^+ out of the cell [104, 105].

The CO-linked hydrogenase has a higher tolerance to CO than other hydrogenases [106]. In fact CO stimulates the CO-linked hydrogenase activity, but CO concentrations greater than 60% can be inhibitory. This activity increase has been linked to hydrogenase association with CODH as well as de novo synthesis of hydrogenase upon exposure to CO [104, 106].

Like CODH, the CO-linked hydrogenase is sensitive to O_2 [106]. The hydrogenases found in *R. rubrum* are also sensitive to acetylene, which could be problematic for syngas fermentation as C_2H_2 can be found in syngas. As long as acetylene levels do not exceed 10% (v/v), CO-linked hydrogenases should not show much inhibition, however concentrations exceeding this level can lead to significant inhibition (>70% decrease in activity) [103]. Since syngas usually contains only trace amounts of acetylene, so inhibition is unlikely. The *R. rubrum* hydrogenase is heat sensitive above 70^o C [106]. The optimum extracellular pH for the CO-linked hydrogenase is 7.2 [103].

2.3 POLYHYDROXYALKANOATE SYNTHESIS

Polyhydroxyalkanoate(s) (PHA) are water insoluble inclusion bodies produced by many prokaryotes as an energy and carbon storage molecule [107]. PHAs are thermoplastics with properties similar to polypropylene and as such, offer an alternative to petroleum derived plastics. Since PHAs are produced by bacteria, they are also readily biodegradable by other microorganisms [108, 109]. PHAs have several applications

including biomedical implants, packaging items, coatings, diaper linings, and moldable plastic products [110]. PHAs can also be chemically modified for use as flexible rubber-like materials and polymer composites [111, 112].

2.3.1 *PHA Structure*

PHAs are bacterial polyesters which can take on many forms depending on their monomer composition. The PHA monomers are derived from hydroxyalkanoic acids used in the synthesis of the polymer. Poly(3-hydroxybutyratic acid) (PHB) was the first discovered and most well known PHA, however, there are up to 150 hydroxyalkanoic acids known as constituents of PHA [112, 113]. In the cell, PHA inclusion bodies are coated with a phospholipid monolayer containing catabolic and non-catabolic proteins [114, 115].

The general structure of a PHA molecule is a (R)-β-hydroxy fatty acid (Figure 3), however, the fatty acid composition can vary widely. PHAs can be classified based on polymer composition and akyl side chain-length. Short chain-length PHAs (*scl*PHA) encompass homo and heteropolymers with chain-lengths typically less than 5 carbons, while medium chain-length PHAs (*mcl*PHAs) typically encompass chain-lengths between 5 and 16 carbons [2, 116-118]. Alternating monomers of different composition can form co-polymers such as poly 3HV-co-3HB.

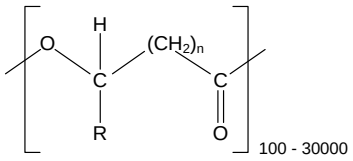

n	**R**	PHA
1	H_2	Poly(3-hydroxypropionate)
1	CH_3	Poly(3-hydroxybutyrate)
1	C_2H_5	Poly(3-hydroxyvalerate)
1	C_3H_7	Poly(3-hydroxyhexanoate)
1	C_5H_{11}	Poly(3-hydroxyoctanoate)
1	C_9H_{19}	Poly(3-hydroxydodecanoate)
2	H_2	Poly(4-hydroxybutyrate)
2	CH_3	Poly(4-hydroxyvalerate)

Figure 3. General structure of a PHA polymer. The alkyl group (R) is located on the the β carbon of the hydroxyl fatty acid (adapted from Lee [119].

2.3.2 *PHA Properties*

PHAs can range in molecular mass from 50,000 Da to 1,000,000 Da [110]. The properties of PHAs are dependent upon the monomer content. Short chain-length homopolymers, such as PHB, are typically stiff and brittle, while medium chain-length homopolymers can be more elastic, but typically have less mechanical strength [112]. Co-polymers of PHB and poly(3-hydroxyvalerate) (PHV) have both strength and elasticity. The PHB-co-PHV polymer exhibits properties similar to polypropylene including melting point, gas and water barrier properties, and processing capabilities [120-124]. Table 2 provides a look at the properties of PHA as compared to two popular petroleum based plastics.

Table 2. Comparison of PHAs with common petroleum derived plastics (adapted from Sudesh et al. [125]).

	Melting temperature (^oC)	Glass-transition temperature (^oC)	Young's modulus (Gpa)	Tensile strength (Mpa)	Elongation to break (%)
P(3HB)	180	4	3.5	40	5
P(3HB-co-20 mol% 3HV)	145	-1	0.8	20	50
P(3HB-co-6 mol% 3HA)*	133	-8	0.2	17	680
Polypropylene	176	-10	1.7	38	400
Low-density polyethylene	130	-30	0.2	10	620

2.3.3 *PHA Biosynthesis*

PHA accumulation occurs when bacteria are stressed from unbalanced growth conditions. This production can be initiated by limited availability of nitrogen, phosphorus, magnesium, sulfate, or oxygen (if aerobic) as well as conditions of excess carbon [107, 126-128]. Several pathways exist for PHA production, but the process can be generalized as shown in Figure 4. PHAs are produced when the carbon for growth, regardless if the carbon source is a product of metabolism or anabolism, is channeled to hydroxyacyl-CoA thioesters [110].

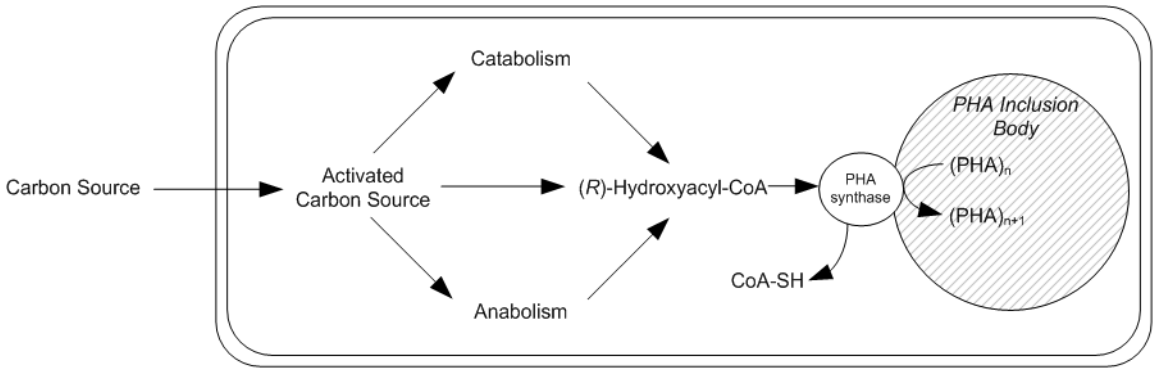

Figure 4. General process of PHA production from various carbon sources [125, 129].

The proteins associated with PHA biosynthesis are located on the surface of PHA inclusions [114, 130, 131]. In PHA production by *R. eutropha*, 2 acetyl-CoA molecules are condensed to acetoacetyl-CoA by the enzyme 3-ketothiolase (PhaA) [132]. Next, acetoacetyl-CoA is reduced by the NAHD-dependant enzyme, acetoactyl-CoA reductase (PhaB), to (*R*)-3-hydroxybutyryl-CoA. Finally, the previous product is polymerized by PHA synthase (PhaC) while CoA is released. PHA production in *R. rubrum* is similar to that in *R. eutropha*, however, the PhaB is an isoenzyme which yields (*S*)-3-hydroxybutyryl-CoA. Since PhaC usually only accepts the *R* stereoisomer of 3-

hydroxybutyryl-CoA, two enoyl-CoA hydratases must convert the *S* isomer to the *R* isomer [133]. A simplified pathway for PHA production *R. rubrum* is shown in Figure 5.

The PHA biosynthesis pathway described above is regulated by the inhibition of 3-ketothiolase by free coenzyme-A from the Krebs cycle. During nutrient limitation in the presence of excess carbon, the Krebs cycle is not using acetyl-CoA. This surplus acetyl-CoA is then utilized for PHA synthesis [134].

There are three different types of PhaC differentiated by substrate specificities as well as by structure [135]. The Type I PhaC, as found in *R. rubrum*, act on short chain-length hydroxyalkanoates [2]. The Type II PhaC act on medium chain-length hydroxyalkanoates. Type III PhaC enzymes are not as well studied. These enzymes generally act on short chain-length hydroxyalkanoates but have two subunits as opposed to the one subunit found in Types I and II [136].

Co-polymers of PHB-co-PHV can be produced in media containing propionic or valeric acid. This co-polymer can also be produced when propionyl-CoA is available as a substrate for a specialized 3-ketothiolase in the PHA pathway. Propionyl-CoA can be synthesized from an intermediate of the Krebs cycle, succinate. During anaerobic conditions, succinate is not readily oxidized to fumarate and accumulates. The accumulated succinate is forced to the formation of succinyl-CoA and is then converted to propionyl-CoA [137].

In *R. eutropha*, propionyl-CoA and acetyl-CoA combine to form acetoacetyl-CoA and 3-ketovaleryl-CoA [138]. Both acetoacetyl-CoA and 3-ketovaleryl-CoA continue through PHA synthesis and are modified into (*R*)-3-hydroxybutyryl-CoA and

(*R*)-3-hydroxyvaleryl-CoA respectively. The polymerization of PHB-co-PHV is then catalyzed by PHA synthase [138].

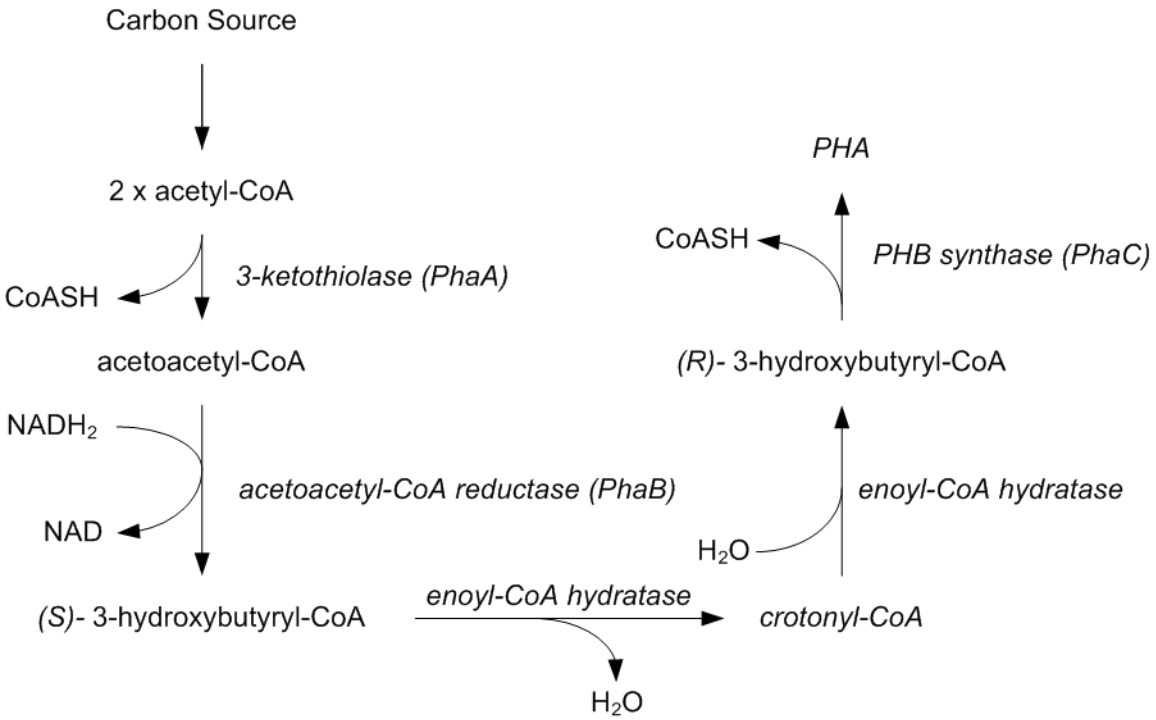

Figure 5. The simplified PHA production pathway for *R. rubrum* begins with two acetyl-CoA molecules derived from carbon metabolism [132, 133].

2.4 TECHNO-ECONOMICS

PHAs have the potential to replace petroleum based plastics. Although the advantages of replacement are numerous, current process economics make this transition challenging. Industrial scale PHA production has been explored with the use of microorganisms and plants. Currently, PHAs are produced commercially by only a few companies. Monsanto produced a compolymer of Poly(3HB-co-3HV) under the name Biopol™ [139]. In 2001, Massachusetts-based Metabolix bought the Biopol™ assets from Monsanto. Metabolix produces its own biopolymer, *Mirel*™, via sugar fermentation [140].

As of 2008, only one study had been published which evaluated the techno-economics for PHA production via a gasification-based biorefinery [1]. Choi, Chipman, et al. reported that PHA production by *R. rubrum* cultured on syngas was both economically viable and technically feasible. The co-production and sale of hydrogen gas subsidized the operating costs of the biorefinery. As a result, PHA production by syngas fermentation was $2 to $4 cheaper to produce per kilogram than PHA production by sugar fermentation [1, 141].

Increasing PHA production without decreasing hydrogen output could further drive down the price and make PHA more economically competitive with petroleum based plastics. The techno-economic analysis by Choi, Chipman, et al. included process optimization, but did not consider an optimized growth media or harvest point. This thesis investigates these additional optimization strategies.

CHAPTER 3. EXPERIMENTAL APPARATUS: SYNGAS FERMENTATION FACILITY

3.1 BACKGROUND

A syngas fermentation research facility was constructed to study the conversion of syngas to biofuels and biochemicals via syngas fermentation. This facility is located in the Black Engineering Gasification Lab which provides a source of syngas/producer gas. The lab houses a 5 kg/day fluidized bed gasifier with plumbing to five 14 liter New Brunswick Scientific BioFlo 110 fermentation units and a custom gas mixing system. The fermentors were plumbed so they could be operated in parallel or one fermentor could be operated in series with the remaining four in parallel (Figure 6). A gas mixing system was designed and built to supplement the fermentors with "artificial" syngas for controlled testing and culture feeding.

3.1.1 *System Requirements*

Computer control and monitoring of the fermentors and gas mixing system is necessary for data logging and system integration for manageable operation. Computer control and monitoring are also important for safety, data synchronization, and system upkeep.

Fermentation experiments in this lab can last several weeks. Having a fulltime operator to run the lab was not feasible, so it was important to be able to monitor and control the system remotely in order to be promptly alerted to problems should any arise.

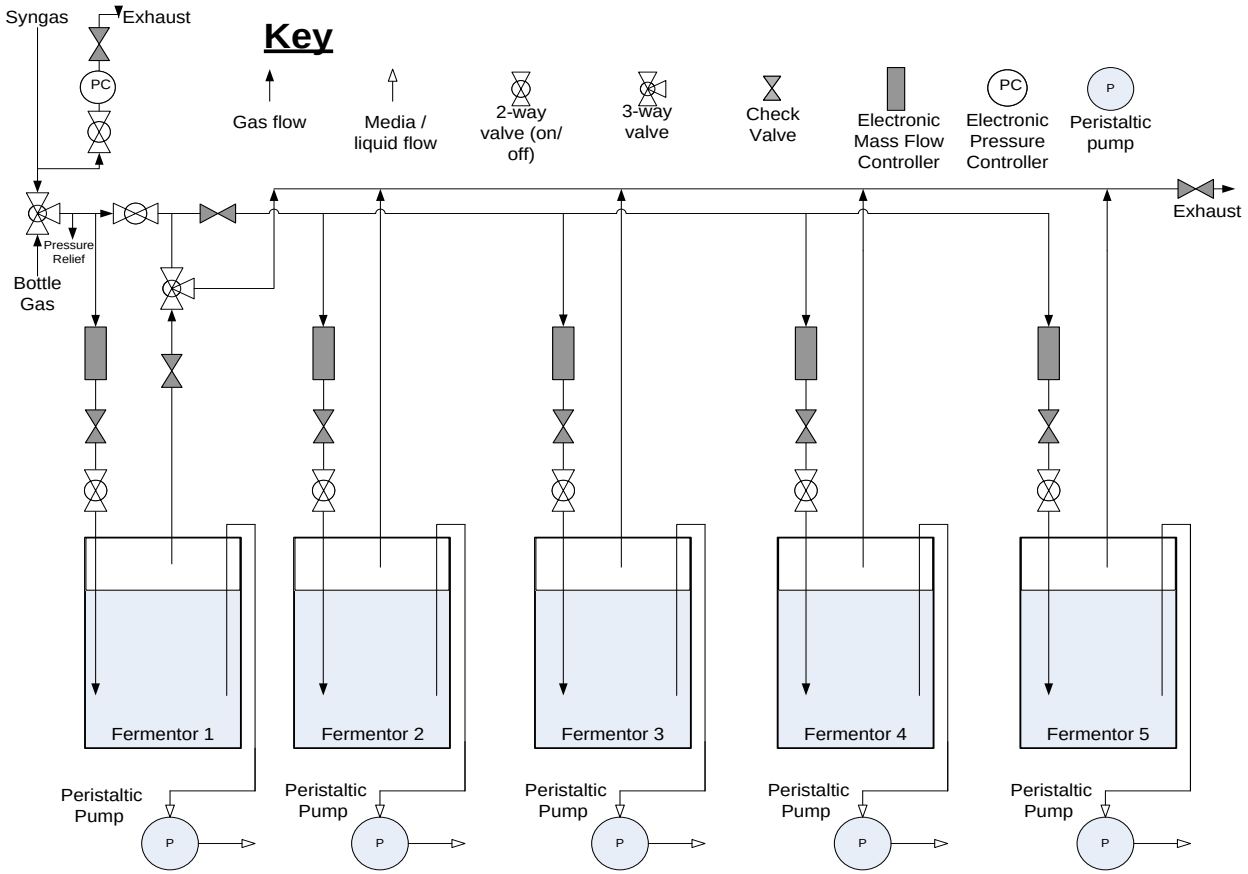

Figure 6. Syngas fermentation research facility reactor system schematic.

3.1.2 *Software*

The operating system used by the control computer was Microsoft XP Professional, Version 2002, Service Pack 2. A visual programming tool for measurement and automation systems, National Instruments LabView (Version 8.2), was used to code the fermentation control system program [142]. LabView drivers for the Alicat gas control hardware (LabView 8.0.1 Rev 5) available from the Alicat Scientific website were modified using LabView [143].

To integrate the fermentors with LabView an O*bject Linking and Embedding for* P*rocess* C*ontrol* (OPC) server from New Brunswick Scientific, BioCommand OPC Server Wizard was used [144]. An OPC server can be thought of as driver that acts as a translator between hardware and client (the program needing the translation, LabView in this case). Essentially, the server queried values from the fermentation hardware (agitation speed for example) using Modbus protocol, organized it, translated it, and made it available on a server so third party control software could access the data. An advantage to using an OPC server was the client software (LabView) could operate independently from the hardware. For example, if the New Brunswick BioFlo 110 fermentors were ever to be replaced by fermentors from a different manufacturer, the LabView program would require minimal changing. The variables that LabView uses would just be assigned by the new fermentors' OPC server or Modbus communicator. Modbus is an industry standard network protocol and can be interfaced with any program setup for Modus [145].

Other software used in the fermentation control system included Microsoft Office Outlook 2003 (11.8217.8202) SP3 and modified versions of publicly available code written by Kevin Valentine, and Michael Bauer [146, 147].

3.1.3 *Hardware*

A Dell Optiplex GX745 with a 2.13 GHz Intel Core 2 CPU and 1.99 GB of RAM was used as the system control computer. The computer was configured with an additional 2 communication (COM) ports using a PCI card.

The controllable components of the gas mixing system included of four gas mixing mass flow controllers (Alicat Scientific Inc. MC-5SLPM-D), five fermentor supply mass flow controllers (Alicat Scientific Inc. MC-5SLPM-D), and one pressure controller (Alicat Scientific PC-30PSIG-D) (Figure 7).

Each New Brunswick BioFlo 110 fermentation unit was comprised of the following modules: Primary Control Unit (PCU), dissolved oxygen(dO_2)/pH controller, and a power controller (Figure 8). Probes for dO_2 and pH attached to the dO_2/pH controller. The agitation motor, temperature probe, and optional heating jacket attached to the power controller, which supplied power to all of the modules. The sub components were controlled by the PCU. The PCU was the hardware communication link between the control program and each fermentor.

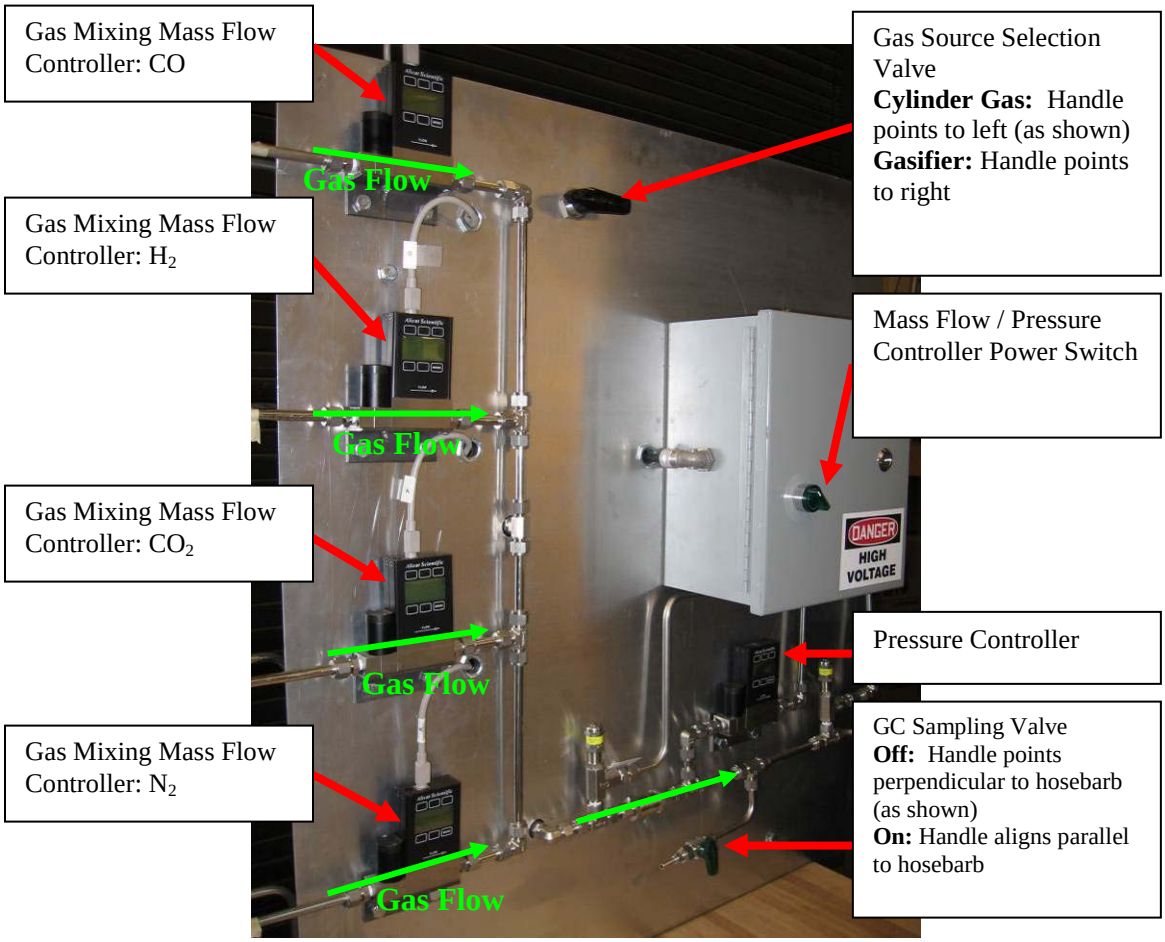

Figure 7. Gas mixing system hardware panel with Alicat mass flow and pressure controllers.

The BioFlo 110 could be controlled manually using the operator interface found on the front of the PCU. Alternatively, it could be controlled using serial communication with a computer. The BioFlo 110 communicated via RS-485, a robust serial communication standard [148], with either the Modbus communication protocol or the Andrew File System (AFS) protocol. The AFS protocol was used for connection with New Brunswick's BioCommand supervisory software. The fermentation control program utilized the Modbus feature of the BioFlo 110.

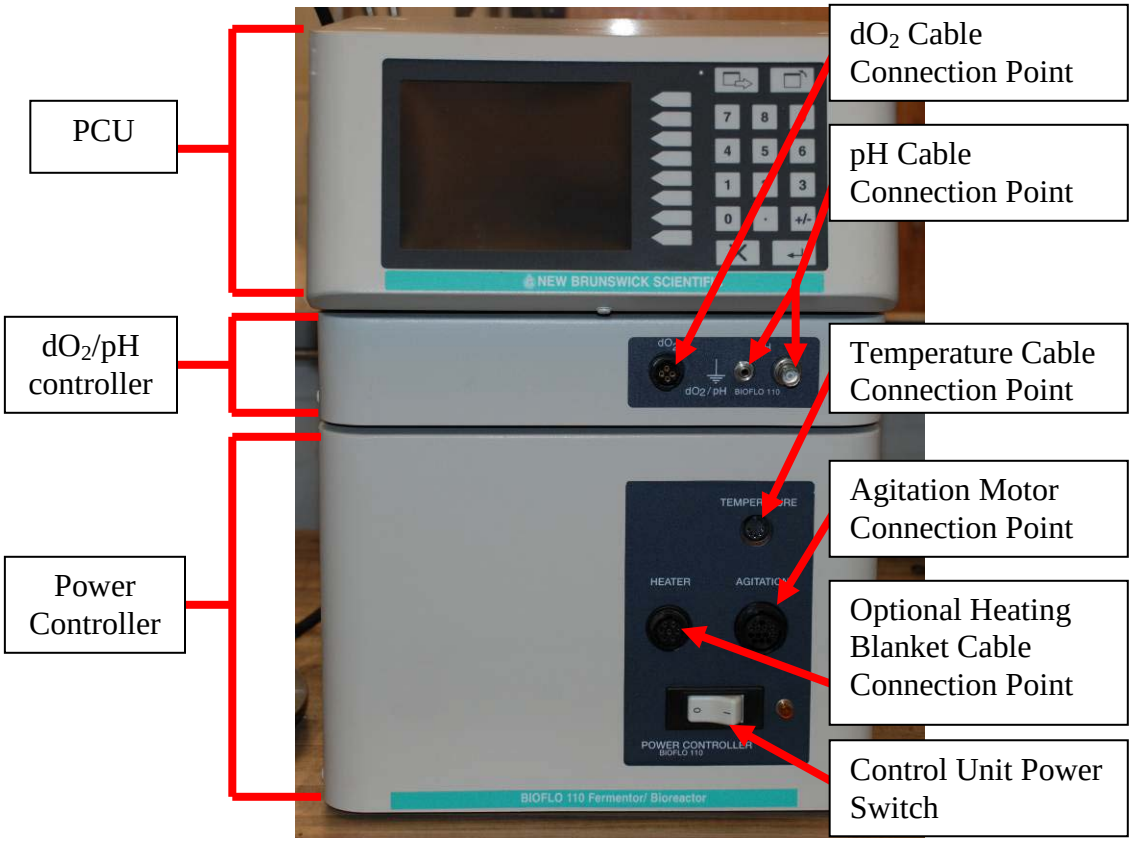

Figure 8. New Brunswick Scientific BioFlo 110 fermentation unit with PCU, dO_2/pH controller, and power controller.

3.1.4 *Mobile alerts and remote system monitoring*

The fermentation system control program took advantage of the fact that most major cell phone carriers allow Simple Message Service (SMS) text messages to be sent and received via email. For example, to send a text message to a Verizon cell phone an email is sent to the address with the pattern: *phonenumber*@vtext.com, where *phonenumber* is a valid 10 digit mobile phone number on the Verizon network. Conversely, a text message from a cell phone can be addressed to an email address instead of a phone number. Sending and receiving text messages in this manner does not require fees beyond the carrier's normal text messaging charges. These abilities were capitalized in the fermentation control program remote message and alert functions.

3.2 DESIGN METHODOLOGY

3.2.1 *Hardware Integration*

After construction of the system, the next major hurdle was getting all of the equipment to communicate with the control computer. Without system integration, 16 different pieces of hardware would have to be controlled individually and data logging would not be possible.

3.2.1.1 *Alicat Scientific Mass Flow and Pressure Control Devices*

The Alicat mass flow and pressure controllers used standard DC-62 type connecting cables for external communication. The Alicat Mass flow and pressure controllers were connected to a RS-232 multi-drop module (Alicat Scientific BB9 Multi-Drop Box). The multi-drop module connected the wires in the RS-232 configuration in parallel with each other. The BB9 had nine DC-62 input sockets as well as input screw terminals for serial transmit, receive, power, and ground wires (Figure 9) The BB9 nine pin output COM port was then connected to the COM 1 port on the computer.

Figure 9. Alicat Scientific BB9 Multi-Drop Box [149].

Before connecting the Alicat control devices to the computer, each was configured for serial input, a common baud rate (19200 bps), and a unique communication ID. This was accomplished by following the instructions in the user manuals [150, 151]. Computer communication was initially established by creating a HyperTerminal connection file. The HyperTerminal configuration was carried out as stated in the Alicat User Manual [150]. Integration of the Alicat control devices with LabView was made easy with drivers provided by Alicat Scientific [143].

Once Hyperterminal was configured, the read-only memory (ROM) image was saved for each controller. The ROM image contained firmware registry values for important settings such as factory calibrations, Proportional, Integral, Derivative (PID) values, etc. Saving the ROM image allowed for easy recovery from mass flow controller firmware related issues.

3.2.1.2 *New Brunswick Scientific BioFlo 110 Fermentation Units*

Each BioFlo 110 control module was interconnected for power and communication sharing between its sub modules as described in the Guide to Operations [152]. For communication with the computer, the control modules were daisy chained together using the New Brunswick Scientific RS-232/422 Adapter Kit (NBS part number M1291-800). For this application, Modbus communication protocol was used. The fermentor control units were configured for Modbus and given a unique address. BioCommand OPC server from New Brunswick Scientific was installed on the control computer. Variables were created on the OPC server for each fermentor.

3.2.2 *LabView Programming*

The control program for the system was developed in LabView version 8.2. LabView programs are organized hierarchically. The top level program is referred to as a Virtual Instrument (VI). Subroutines are referred to as Sub Virtual Instruments (Sub VI). Sub VIs for the control program were created and organized based on major subsystems of the control program.

3.2.2.1 *Device Interface*

The Alicat device drivers and New Brunswick OPC Server allowed the fermentation system hardware to communicate with LabView. The fermentation control program took advantage of the Alicat device's and BioFlo PCU's internal control loops. Set points were sent by the fermentation control program to each device and the response was monitored. The device hardware firmware/software managed the feedback and control loops, which allowed the fermentation control program to be simplified.

3.2.2.2 *Alicat Device Interface*

Each Alicat controller required its own driver in LabView (Figure 10). The Sub VI, "Alicat Cluster Out," was developed to utilize the drivers to collect the input set points of each Alicat controller and parse the output from each controller into clusters. The driver was "wired" with values for the VISA resource name (the name of the COM port that the devices were connected to: COM 1), UnitID (the unit address), and SetPoint (an integer value ranging from 0 – 64,000 where 64,000 = the full scale flow/pressure of the unit).

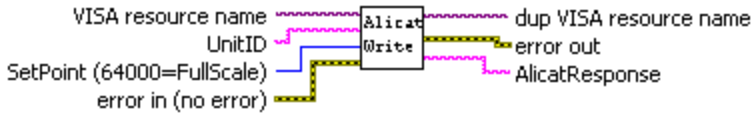

Figure 10. Alicat Scientific device driver (LabView 8.0.1 Rev 5) for LabView.

The Alicat devices were 16 bit and thus offered 65,535 selectable set points for mass flow or pressure over the controllers full scale range (including a 2% over range). A small Sub VI was developed to simplify the conversion from standard liters per minute (SLMP) to a value understood by the controller. The Sub Vi used Equation 11 to calculate the appropriate unsigned word (16 bit positive integer) when given a set point in SLPM.

$$Value = \left(\frac{Desired\ SetPoint \times 64000}{Full\ Scale\ Flow\ Range}\right) \qquad \textbf{Equation 11}$$

The response signal from the Alicat devices was a string with the pattern shown in Figure 11.

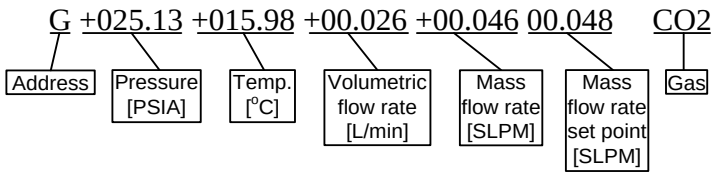

Figure 11. Alicat Scientific mass flow controller device output response.

The output was parsed into its main components of pressure, temperature, volumetric flow rate, mass flow rate, mass flow rate set point, and gas type. The output clusters in "Alicat Cluster Out" contained all outputs values of the Alicat controllers in both string form and double precision number form. This allowed the data to be accessible to other Sub VIs in the control program.

The pressure controller interfaced similarly but had an output response as shown in Figure 12. The parsing for the output variables was adjusted accordingly.

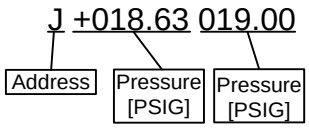

Figure 12. Alicat Scientific pressure controller device output response.

3.2.2.3 *New Brunswick Fermentor Interface*

Using the "Shared Variables Proprieties" tool in LabView, the variables on the OPC server were bound to variables that could be used and recognized by the block diagram in LabView. Once bound, the shared variables were added to the front panel of the "Ferm NBS OPC" Sub VI. The inputs to this Sub VI included the agitation and temperature set points for each fermentation station. A cluster data type served as the output of this Sub VI which contained the status (On/Off) of agitation and temperature control as well as values for agitation, dO_2, pH, and temperature for each of the five fermentation stations (Figure 13).

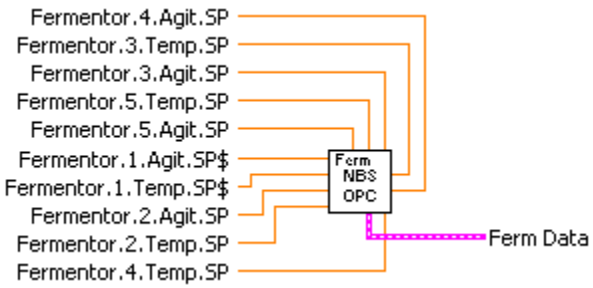

Figure 13. "Ferm NBS OPC" Sub VI used to control set point values and monitor the bound shared variables of the fermentors.

3.2.2.4 *Data Logging*

In the fermentation system control program, each fermentation station was configured with the option to log data. The Sub VI "Data Logging SubVI 1" was

developed for this purpose (Figure 15). All values (except the device address and gas name) from the mass flow controller associated with the fermentation station as well as all of the mass flow and pressure controllers in the gas mixing station were set to record to that station's data log file. Recorded values for the fermentor included agitation rate, temperature, dO_2 level, and pH. All data was configured to log synchronously with reference to the time stamp.

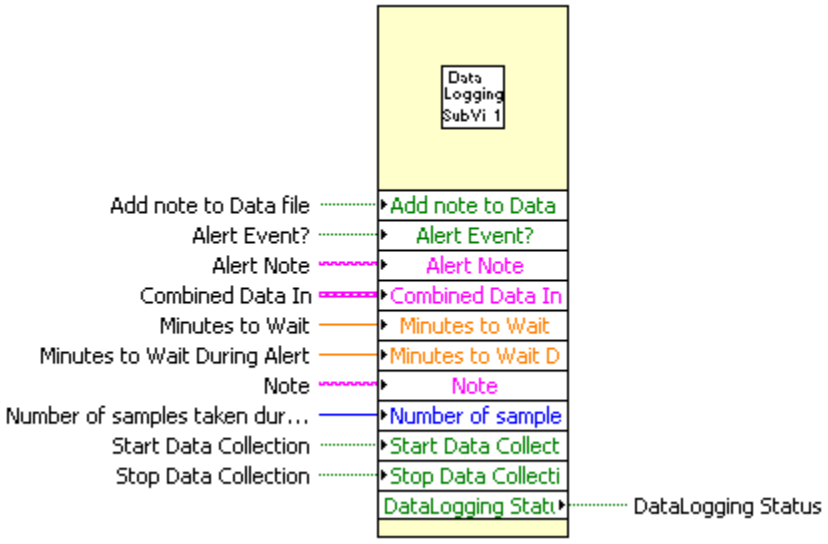

Figure 14. "Data Logging SubVI 1" Sub VI used to log data in the fermentation system.

The Sub VI was programmed to initiate a chain of events when the "*Start Data Collection*" Boolean was true. First a series of dialogs would prompt the user to create or append a comma separated value (csv) file and to fill out information to be placed in the file header (such as the operator name, test name, beginning gas mixture settings, etc.). Next, the Sub VI would create the data file and begin data logging. The rate of data collection was made configured as a user controlled input. Additional capabilities, such as adding a note to the data file and automatic logging of alert events, were programmed into the Sub VI as well.

3.2.2.5 *Overpressure Protection*

The 14 L glass fermentation vessels included with the New Brunswick Scientific BioFlo 110 fermentors were rated to a maximum pressure of 10 PSIG [152]. Code was written to prevent exceeding the maximum pressure. A Sub VI was built on the capability of the mass flow controllers to measure downstream pressure. Since the mass flow controller at each fermentation station was located so close to the inlet of the fermentor, the pressure measured in the controller was assumed to equal the head pressure of the fermentor. The code was designed to shut off gas flow to the fermentor if the set maximum pressure was exceeded and to restore flow should the pressure go below the set maximum pressure. An override was also included.

The pressure controller and mass flow controllers reported different units for pressure, PSIG and PSIA respectively. The downstream pressure in the gas mixing mass flow controllers was assumed to equal the system pressure controlled by the pressure controller given the proximity of the controllers (Figure 7). Using this assumption, Equation 12 was developed to bring all pressure measurements on the same basis:

$$P_{MFC-G} = P_{MFC-A} - \left(\bar{P}_{MFC_{GM}-A} - P_{PC-G}\right) \qquad \textbf{Equation 12}$$

where

$P_{MFC\text{-}G}$ = mass flow controller gage pressure

$P_{MFC\text{-}A}$ = mass flow controller absolute pressure

$P_{PC\text{-}G}$ = pressure controller gage pressure

$\bar{P}_{MFC_{GM}-A}$ = mean of the four gas mixing mass flow controllers' absolute pressure.

3.2.2.6 *Gas Mixture Control*

To simplify gas mixture controlling, a Sub VI, "Set Gas Mixture" was developed (Figure 15). A user dialog was made that would give the option of using a previously saved composition when the "Set Gas Mixture" Boolean is true. If the user chose not to load a previous gas composition, a new dialog would allow the user to enter the desired gas composition in volume percent as long as the total percentage equaled 100%. The Sub VI was written to allow the user to save the newly created composition. Saved gas compositions were stored in composition files. To ensure that the gas mixing mass flow controllers supplied enough gas to meet the system gas flow demand, a final dialog was made prompting the user to estimate the total gas flow demand on the system.

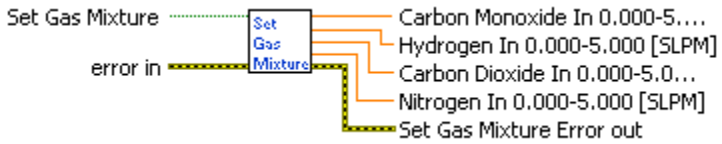

Figure 15. "Set Gas Mixture" Sub VI used control the gas mixture composition in the fermentation system.

3.2.2.7 *Alert System*

An alert system was developed to allow the user to monitor key values and to be alerted should those values deviate by a specified amount. Each "Email Alert System" Sub VI was programmed to monitor the mass flow rate and mass flow rate set point of one fermentation station as well as the gas mixing mass flow controllers (Figure 16).

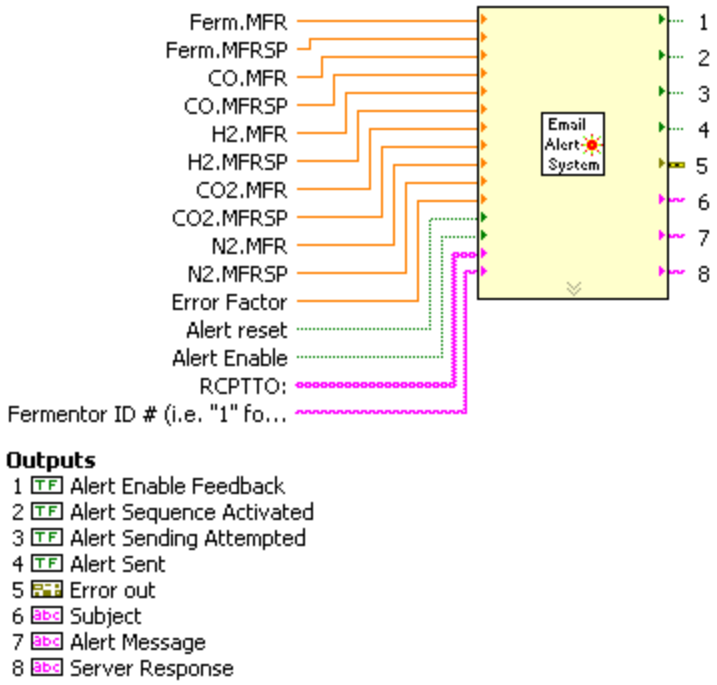

Figure 16. "Email Alert System" Sub VI used to monitor and send alerts for mass flow rates and mass flow rate set points in the fermentation system.

When enabled, the alert system would compare the mass flow rates to the mass flow rate set points. The alert system logic was based on Equation 13.

$$\frac{|mass\ flowrate - mass\ flowrate\ setpoint|}{mass\ flowrate\ setpoint} > Error\ Factor \qquad \textbf{Equation 13}$$

If the value on the left was greater than the user defined "Error Factor", the alert sequence would be activated. Once activated, the alert sequence would send an email to the "RCPTTO:" input with the offending value in the email subject and the current values and set points in the message body.

The email functionality of the "Email Alert System" Sub VI was made possible by a modified open source Sub VI [146]. Two email addresses were created for the syngas fermentation system, isu.syngas.fermentation.lab@gmail.com and syngas.fermentation.lab@iastate.edu. The former email address served as a default to

receive alerts. The latter email, which utilized the Iowa State University Simple Mail Transfer Protocol (SMTP) outgoing server, was used for all outgoing mail. Cell phone SMS text message alerts were made possible using the ability of most cell phone providers' capabilities to receive text messages from email.

3.2.2.8 *Remote Monitoring and Control*

LogMeIn Free remote login software from LogMeIn, Inc. was used for general remote monitoring and control of the fermentation system [153]. LogMeIn Free allowed for control of the remote computer via any internet connection. To allow for system monitoring and control of the fermentation system via email or cell phone text messages, the Sub VI "Email Cmnd." was developed (Figure 17).

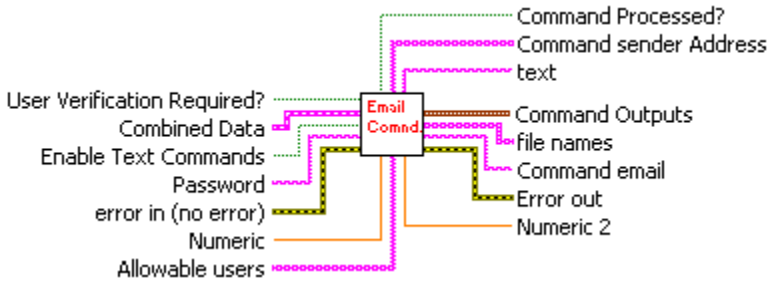

Figure 17. "Email Cmnd." Sub VI used to control the text message based control and monitoring function of the syngas fermentation control program.

The Sub VI scanned for email/text messages sent to the address isu.syngas.fermentation.lab@gmail.com. Since there was no real good way to access a Post Office Protocol version 3 (POP3) server with Secure Socket Layer (SSL) capabilities in LabView (required for receiving emails, and thus remote commands, from the Gmail POP server), another solution had to be found.

A solution for the POP3/SSL issue was developed that took advantage of LabView's ability to scan for files in file folders. If an incoming email could be saved as

a text file in a known folder location, LabView could then find that text file in the specified folder, read it, parse out the sender address, command password, and command codes, and move it to another folder to avoid repetitive reading of the same file. To convert incoming emails as text files, a publicly available macro written by Michael Bauer was modified and nested in Microsoft Outlook [147]. Microsoft Outlook was configured to check the server for messages every minute. The command email/text required the following format (text in italics is actual entered text):

To:
isu.syngas.fermetnation.lab@gmail.com
Subject: (password entered in subject; may not be available for cell phone text messages)
password (case sensitive)
Message Body: (a carriage return must follow the password and between subsequent commands; when texting from a cell phone, the carriage return can usually be found as the special symbol "LF")
password (case sensitive)
CommandName (case sensitive; refer to Table 3 for valid command names)
⋮
CommandName (multiple commands are allowed)

Once the password (and sender address if this security was enabled by the user) was verified, the text message was parsed for the command. Valid commands are shown in Table 3. If a valid command was received, the sender would receive a reply with all of the current system gas controller set points. The reply Sub VI, "SMS Cmnd. Confirm," utilized the same modified open source Sub VI as used in the alert system [146].

Table 3. Fermentation system control program email/text remote command list. (MFCSP = mass flow controller set point)

Command Name (case sensitive)	Command result
Status	Returns the values for all mass flow controllers and pressure controller set points to the sender of the *Status* command
CO #.###	Sets the CO MFCSP to #.### SLPM (example: CO 0.100)
H2 #.###	Sets the H_2 MFCSP to #.### SLPM (example: H2 0.100)
CO2 #.###	Sets the CO_2 MFCSP to #.### SLPM (example: CO2 0.100)
N2 #.###	Sets the N_2 MFCSP to #.### SLPM (example: N2 0.100)
F1 #.###	Sets the Fermentor 1 MFCSP to #.### SLPM (example: F1 0.100)
F2 #.###	Sets the Fermentor 2 MFCSP to #.### SLPM (example: F2 0.100)
F3 #.###	Sets the Fermentor 3 MFCSP to #.### SLPM (example: F3 0.100)
F4 #.###	Sets the Fermentor 4 MFCSP to #.### SLPM (example: F4 0.100)
F5 #.###	Sets the Fermentor 5 MFCSP to #.### SLPM (example: F5 0.100)
Pressure ##.##	Sets the Pressure Controller to ##.## PSIG (example: Pressure 20.00)

3.2.2.9 *Front Panel Design*

The front panel was divided into 5 major sections: a tabbed section, gas mixing section, system gas flow summary section, system pressure summary section, and the alert summary section (Figure 18). The gas mixing section displayed the controls and indicators for the gas mixing mass flow and pressure controllers. Located below the gas mixing section was the summary chart of all system mass flows as well as the summary chart for all system pressures. The Alert Summary section, which displayed the status of each fermentation station alerts, was located in the bottom right hand corner of the front panel. The first five tabs in the tabbed section displayed the controls for each fermentation station. Values for inlet gas mass flow, agitation speed, fermentor temperature, dissolved oxygen, and pH were displayed and controlled from each station's tab (Figure 19). The controls for that station's alert, data logging, and overpressure functions were also displayed in each of the fermentation station tabs.

The remaining tabs displayed the Alert Settings, Advanced Settings, and Error Reports tabs. The Alert Settings Tab allowed setup of the alert system via user dialogs for each fermentor station (Figure 20). The Advanced Settings included options for both gas mixture control and system control through SMS/email commands (Figure 21).

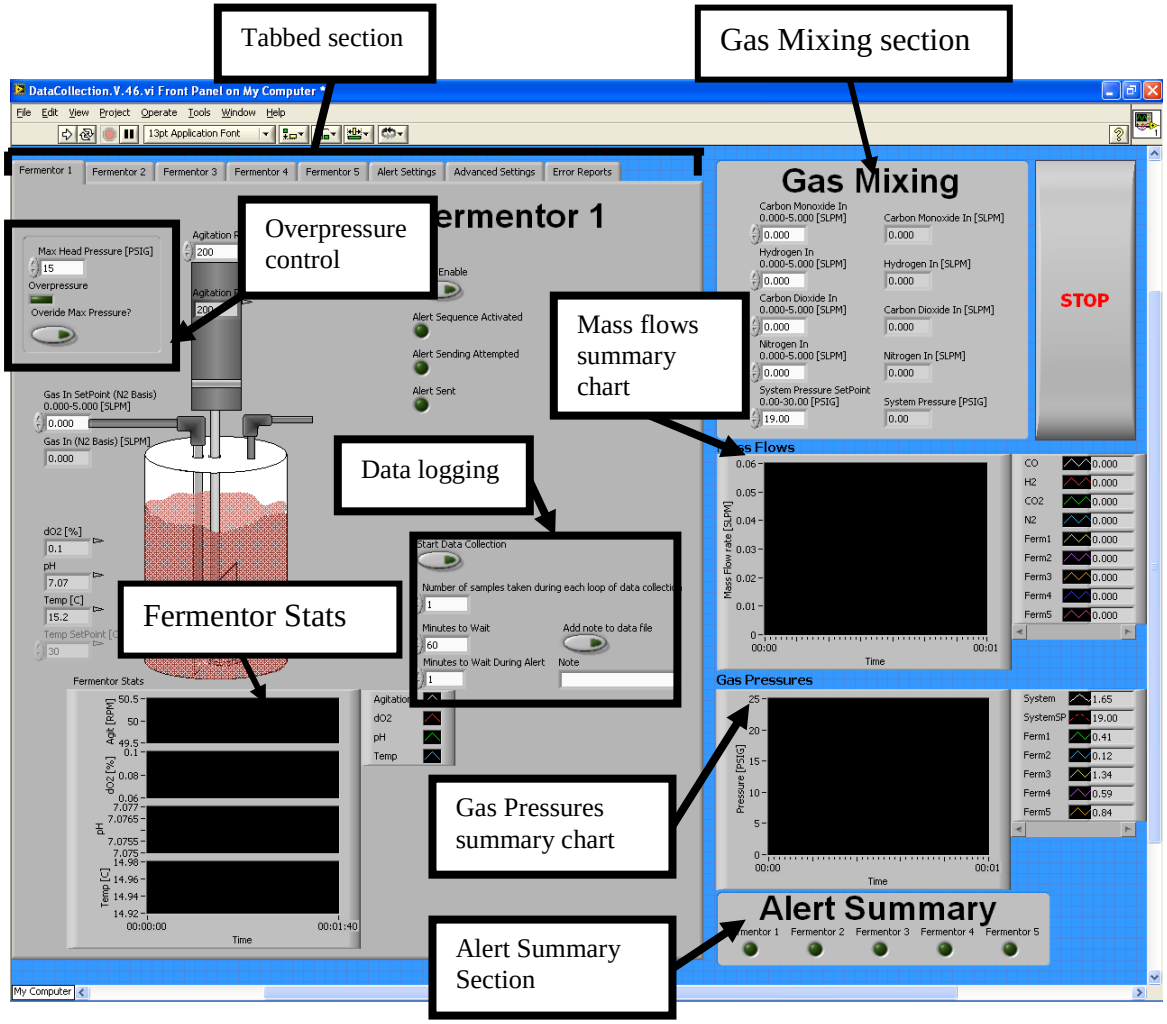

Figure 18. Syngas fermentation system control program front panel layout.

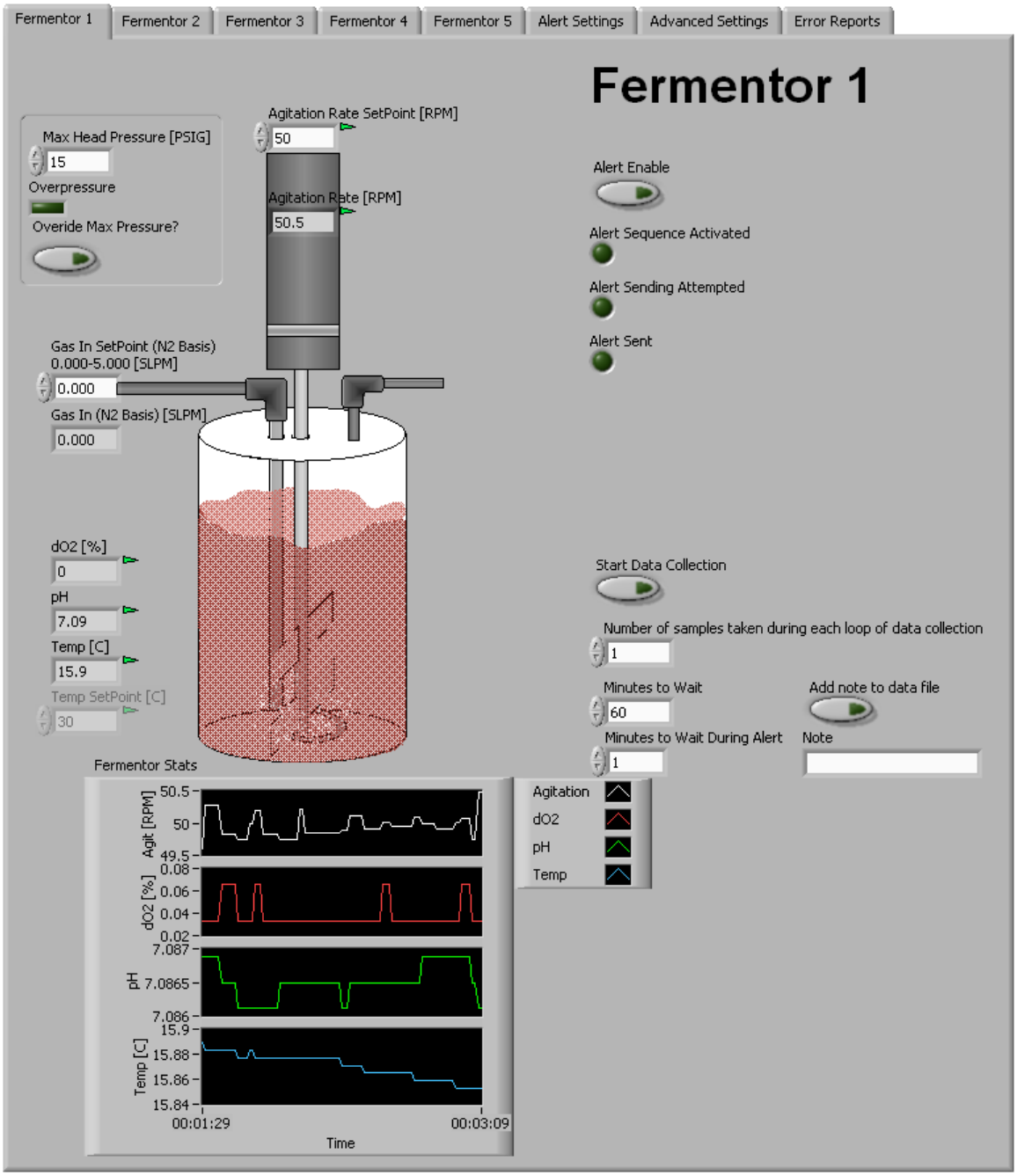

Figure 19. Fermentation system control program front panel "Fermentation Station" control tab.

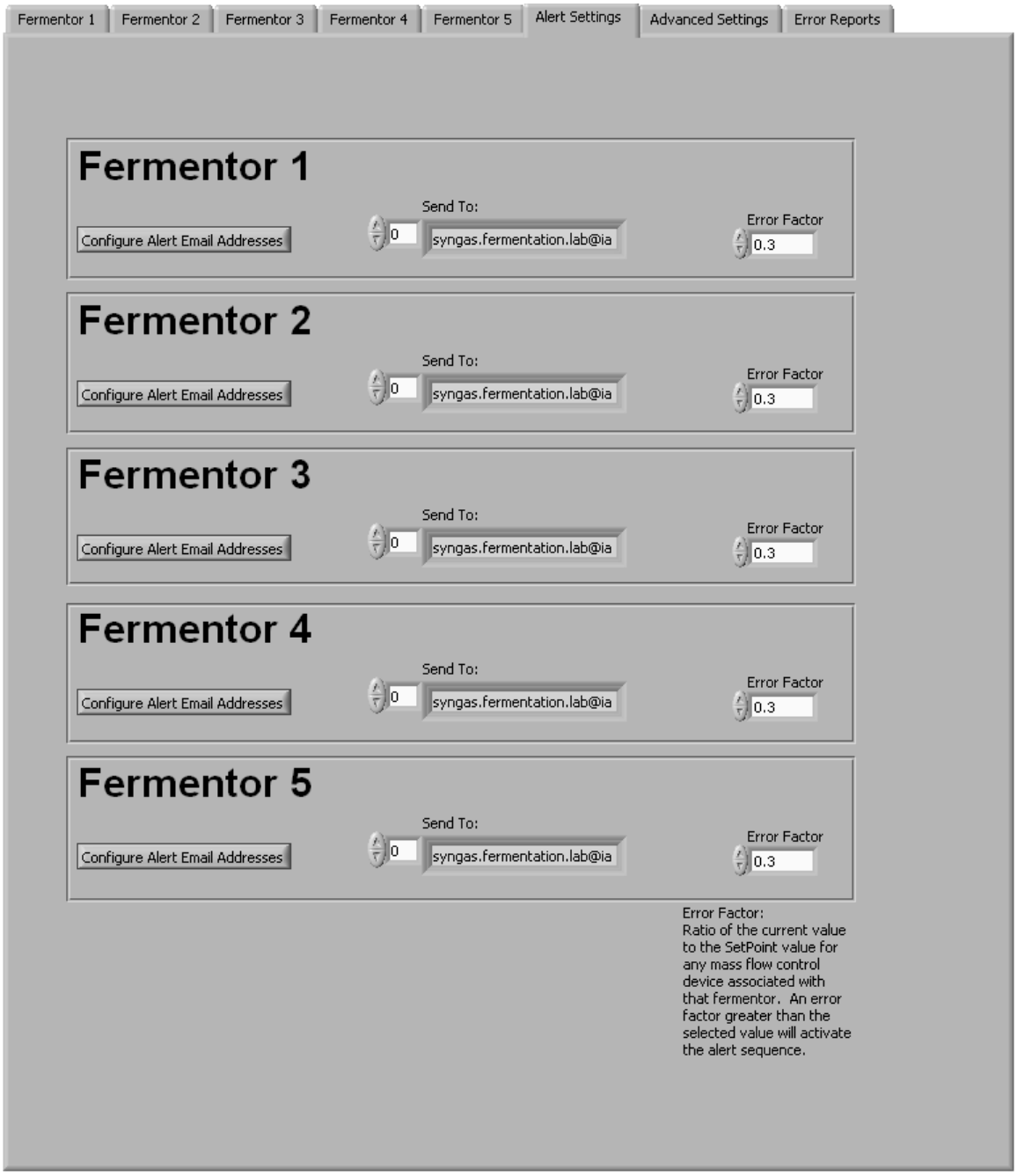

Figure 20. Fermentation system control program front panel "Alert Settings" control tab.

Figure 21. Fermentation system control program front panel "Advanced Settings" control tab.

CHAPTER 4. EXPERIMENTAL METHODS

4.1 EXPERIMENTAL DESIGN

4.1.1 *Media Optimization*

Two experimental approaches were used to determine an optimal media concentration on the 40 ml fermentation scale. Batch testing as well as a central composite design experiment was used to evaluate the optimum media component concentrations for PHA production. The media to be optimized, referred to as *Rhodospirillum rubrum* no-light carbon monoxide (RRNCO), was based off of the media described in Kerby et al. [6].

4.1.1.1 *Hypovial study*

Ammonium chloride (NH_4Cl), yeast extract (YE), and sodium acetate (NaAct) concentrations were varied to examine their effect on growth and PHA production. In each treatment, all media component concentrations were held constant except for the ingredient being evaluated. The experimental media concentrations are shown in Table 4.

Table 4. Experimental media component concentrations. All vials had the same concentration of media components except for the component being evaluated. An asterisk denotes the nominal media component concentration. The nominal NH_4Cl concentration was 18.7 mM.

Hypovial level number	Ammonium Chloride [mM]	Yeast Extract [g/L]	Sodium Acetate [mM]
1	0	0	0
2	2.5	0.25	2.5
3	5	0.50	5
4	10	1*	10*
5	25	2	25

All media was prepared anaerobically using the procedures described in the anaerobic preparation section. Stock solutions of 1 M NH_4Cl, 10 g/L YE, and 1 M NaAct were prepared anearobically. Concentrated RRNCO media lacking additives and the three experimental media components was also prepared anaerobically. The concentrated media was adjusted to pH 7.1 using NaOH. The concentrated media and component stock solutions were combined and reconstituted in the anaerobic chamber with anaerobically prepared deionized (dI) water. After autoclaving the vials, 1.9 M phosphate buffer, 0.5 M sodium bicarbonate, and 200 mM Na_2S were added.

Starter cultures were combined and mixed prior to inoculation to ensure uniformity between all of the cultures. Cultures were inoculated with 7% innoculum and grown in hypovials with 40 ml of fermentation volume and 60 ml of headspace. The headspace gas was purged daily with carbon monoxide. Each day, samples were taken from the cultures and analyzed for optical density (absorbance at 680 nm).

After reaching late exponential or early stationary phase, the cultures were harvested. The cultures were harvested at this time to ensure an adequate cell density for sample processing as well as to prevent any produced PHA from potentially degrading. Optical density and pH were measured for the last sample. The samples were then processed for dry cell mass, media acetate concentration, and PHA content.

4.1.1.2 *Central composite design*

A central composite design of experiments was used to determine an optimal hypovial media component concentration as well as to determine the presence of interaction effects between the media components. The central composite design is an

efficient means of evaluating the effects of several variables on a response. It is a powerful tool that can output a model to describe a system using a minimal number of experimental runs and has been recently used widely in microbial fields [154-157].

The central composite design for this study was based on a modified rotatable central composite design [158]. The levels evaluated in the central composite design were divided into three categories. The center point, coded *Level 0,* corresponded to the nominal RRNCO media concentrations of the three experimental variables. The star points, coded *Levels* $\pm\sqrt{3}$, were based on the distance of the center point to the corner of a theoretical design space cube with dimensions 2x2x2 ($\alpha = \sqrt{3}$). The remaining points, coded *Level ±1*, were based on the distance between the center point and the faces of the theoretical cube.

Three factors, yeast extract, ammonium chloride, and sodium acetate, were examined at five levels using the central composite design. The range for the variables was based on the lower limit of 0 for the concentration in the media. The upper limit was based on the maximums used in the hypovial studies. Table 5 displays the coded and actual values for the five-level-three factor design.

Table 5. Coded and actual values for component concentrations in the central composite design. Level 0 represents the nominal RRNCO media concentration of that component.

Variable Name	Level				
	$-\sqrt{3}$	-1	0	1	$\sqrt{3}$
Ammonium Chloride [mM]	0.0	7.9	18.7	29.5	37.4
Yeast Extract [g/L]	0.0	0.4	1.0	1.6	2.0
Sodium Acetate [mM]	0.0	4.2	10.0	15.8	20

The central composite design is shown in Table 6. The entire design was replicated once. The results of the central composite design were used to create a second

order polynomial to describe the affects of the response variables on dry cell mass and PHA production.

Table 6. Central composite design for PHA optimization showing both coded and actual values.

Standard Order	Coded			Actual		
	NH_4Cl	YE	NaAct	NH_4Cl	YE	NaAct
1	-1	-1	-1	7.9	0.4	4.2
2	1	-1	-1	29.5	0.4	4.2
3	-1	1	-1	7.9	1.6	4.2
4	1	1	-1	29.5	1.6	4.2
5	-1	-1	1	7.9	0.4	15.8
6	1	-1	1	29.5	0.4	15.8
7	-1	1	1	7.9	1.6	15.8
8	1	1	1	29.5	1.6	15.8
9	$-\sqrt{3}$	0	0	0.0	1.0	10.0
10	$\sqrt{3}$	0	0	37.4	1.0	10.0
11	0	$-\sqrt{3}$	0	18.7	0.0	10.0
12	0	$\sqrt{3}$	0	18.7	2.0	10.0
13	0	0	$-\sqrt{3}$	18.7	1.0	10.0
14	0	0	$\sqrt{3}$	18.7	1.0	20.0
15	0	0	0	18.7	1.0	10.0
16	0	0	0	18.7	1.0	10.0
17	0	0	0	18.7	1.0	10.0
18	0	0	0	18.7	1.0	10.0

As with the hypovial study, all media was prepared anaerobically using the procedures described in the anaerobic preparation section. Stock solutions of 1 M NH_4Cl, 10 g/L YE, and 1 M NaAct were prepared anearobically. Concentrated RRNCO media lacking additives and the three experimental media components were also prepared anaerobically. The concentrated media was adjusted to pH 7.1 using concentrated sodium hydroxide (NaOH). The concentrated media and component stock solutions were combined and reconstituted in the anaerobic chamber with anaerobically prepared dI water according to Table 6. After autoclaving the vials, 1.9 M phosphate buffer, 0.5 M

sodium bicarbonate, and 200 mM Na_2S were added. As with the hypovial study, cultures were inoculated with 7% innoculum and grown in hypovials with 40 ml of fermentation volume and 60 ml of headspace. The headspace gas was purged daily with carbon monoxide. Each day, samples were taken from the cultures and analyzed for optical density.

After 300 hours, the cultures were harvested. Optical density and pH were measured for the last sample. The samples were then processed for dry cell mass and PHA content.

4.1.2 *Harvest Point Optimization*

The optimal harvest point was determined by scaling up the results of the hypovial experiments to 10 L using the syngas fermentation system. A media recipe was developed based on the results of the hypovial study. The yield of PHA was multiplied by optical density to give the PHA Production Factor (Equation 14).

$$PHA\ Production\ Factor = O.D.\times \frac{PHA\ mass}{Dry\ Cell\ Mass} \qquad \textbf{Equation 14}$$

The measurement was compared across all of the treatments and the largest value was determined the optimal value for PHA production. The experiments on the fermentation scale were performed in triplicate.

The media was prepared aerobically. Heat stable ingredients were combined and the pH was adjusted to 7.1. The concentrated media was brought to a volume of 9.67 L (to compensate for the 0.33 liters of additives to be added later) in 14L New Brunswick Scientific fermentors and then autoclaved. Immediately after autoclaving, the media was cooled while purged with argon gas in order to make the media anaerobic. The additives

Na_2S, bicarbonate buffer, and phosphate buffer were prepared anaerobically by reconstituting the dry form of the additive with anaerobic dI water in the anaerobic chamber (Coy Laboratory Products, Inc.). Once the media was cooled to room temperature, the buffers and Na_2S were added to the media through a sterile rubber septum using a syringe and 0.2 µm syringe filter (Whatman).

The 14 L fermentors were equipped with dual six blade Rushton-type impellers. Impeller configuration and gas sparger location were patterned off of reactor geometry described by Ungerman and Heindel [159]. The fermentors were connected to the syngas fermentation system and purged with gas mixture containing 50% CO, 28.5% H_2, and 21.5% CO_2. The gas mixture composition was based on steam-oxygen gasification syngas compositions from literature [160-162]. Once the exhaust gas composition reached equilibrium, the fermentors were inoculated with 1-2% (by volume) light grown SMN *R. rubrum*. The cultures were agitated at 500 RPM and kept at 30^o C for the duration of the fermentation.

Initial samples were taken for optical density and pH. Exhaust gas was monitored semi-continuously with a gas chromatograph (Varian CP-4900). Fermentation media samples were taken every 12 – 24 hours and analyzed for optical density, pH, media acetate concentration, dry cell mass, and PHA content. An aliquot of each sample was saved for transmission electron microscopy analysis. Sample size decreased as optical density increased in order to maximize the number of samples. Samples were taken until the cells reached stationary phase or until the fermentation volume reached 7 liters.

4.2 ANAEROBIC MEDIA PREPARATION

All media for the hypovial studies was prepared anaerobically. Heat stable ingredients were combined and the pH was adjusted to 7.1. The concentrated media was then boiled and cooled under argon purge to drive off dissolved oxygen. The deoxygenated media was distributed to vials anaerobically in a Coy anaerobic chamber with an 3% H_2 97% Ar atmosphere (Coy Laboratory Products, Inc.). Vials were capped, removed from the chamber, and autoclaved.

Heat sensitive ingredients were brought into the chamber and reconstituted with anaerobic de-ionized water in the anaerobic chamber. These ingredients were filter sterilized and injected into the media.

4.3 STARTER CULTURE MAINTENANCE

Starter cultures were maintained with photosynthetic growth on supplemented malate-ammonium (SMN) medium developed by Kerby et al. [32]. The 40 ml cultures were contained in 100 ml Belco Glass serum vials and capped with butyl rubber septa. The growth media was prepared anaerobically. Starter cultures were inoculated with 5 ml of well grown (O.D. A680 > 2.0) photosynthetic SMN – grown *R. rubrum* in late exponential phase, early stationary phase. In some cases, light grown SMN *R. rubrum* in late stationary phase was used for inoculation.

Starter cultures were incubated in a lighted Innova 42R shaking incubator at 30^{o} C and 200 RPM (New Brunswick Scientific). A New Brunswick C76 water bath shaker with an external growth lamp was also used at the same temperature and agitation rate. The headspace was purged daily with CO.

Starter cultures not immediately used as inocula were stored in the dark at 3^{o} C until needed. Once needed, the cultures were reactivated with incubation and CO headspace purging prior to use as inoculums.

4.4 ANALYTICAL TECHNIQUES

4.4.1 *Cell Density*

A 200 µl aliquot from the well mixed sample was diluted with 800 µl of dI water in a 1.5 ml disposable polystyrene cuvette (Fisher Scientific). Cell density was measured using a Cary 50 Conc UV-Visible spectrophotometer (Varian). The Varian software, Simple Reads, was used to measure absorbance at 680 nm. A blank of deionized (dI) water was used as a zero reference. Each output value of the program corresponded to the average reading over a 2 second period at a sampling rate of 80 Hz. The blank cuvette was re-read at the end of each session in order to check for baseline drift during analysis.

4.4.2 *Media Acetate Concentration Determination*

Media acetate concentration was determined using high pressure liquid chromatography (HPLC). After harvesting the cultures, 30 ml of each sample was centrifuged at 9000 rpm for 10 minutes at 4^{o} C using a Beckman Avanti J-25 centrifuge. The supernatant was decanted and frozen. Prior to HPLC analysis, the supernatant was thawed and centrifuged at 14,000 rpm for 15 minutes in an Eppendorf 5415C desktop centrifuge to minimize any remaining particulate. A minimum of 500 µl of supernatant was then filtered with 0.2 µm filters (Whatman) into 1.8 ml autosampler vials (Thermo).

The supernatant was analyzed using a Varian ProStar HPLC system. The system included a ProStar 355 Refractive Index Detector, ProStar 230i Solvent Delivery Module, ProStar 325 UV-VIS Detector, and a ProStar 430 Autosampler. The system was controlled by Star Chromatography Workstation System Control Version 6.41. The sample was separated using an HPLC Organic Acid Analysis Column (Aminex HPX-87H Ion Exclusion Column, 300 mm x 7.8 mm) with 5 mM sulfuric acid as the mobile phase.

Standard solutions of 0 mM, 0.1 mM, 0.5 mM, 1 mM, 5 mM, 10 mM, and 25 mM sodium acetate were used to determine the retention time of acetate as well as to develop a standard curve. Sample peak areas were determined using forced peak and valley-peak integration methods. Acetate concentration was calculated using the calculated area and the standard curve.

4.4.3 *Dry Cell Mass Determination*

Dry cell mass was determined gravimetrically. Upon harvesting the cultures, an aliquot of each sample was centrifuged at 9000 rpm for 10 minutes at 4^{o} C using a Beckman Avanti J-25 centrifuge with a JA-25.50 rotor. The pellets were washed with 25 ml of DI water. The re-suspended pellets and rinses were transferred to pre-weighed centrifuge tubes and centrifuged at 9000 rpm for 10 minutes (Mettler Toledo AB54-S/FACT Classic Plus). The pellets were saved and frozen. Prior to lyophilization, the centrifuge tubes were covered with Kim wipes and placed in a -80^{o} C freezer for 30 minutes. The pellets were lyophilized for a minimum of three days (Labconco Centrivap Cold Trap). The vials were reweighed. The weights for the pre and post measurements

were made in triplicate and the difference of the averages was reported as the dry cell mass. Specific dry cell mass was determined by dividing the dry cell mass by the sample volume used to determine the dry cell mass.

4.4.4 *PHA Extraction*

PHA was extracted using chloroform and quantified gravimetrically. The procedure was developed at Iowa State University and based on a method by Brandl et al. [2]. In this procedure, 0.1 L/ g dry cell mass of 1.5% sodium hypochlorite solution was added to lyophilized cells. The mixture was vortexted until the cells were well mixed and then placed in a 37^{o} C bath. Once at temperature, the vials were incubated for one hour. The mixtures were transferred with dI water rinses to Kimbal HS No. 45600-15 15 ml glass centrifuge tubes. The tubes were centrifuged at 9500 rpm for 10 minutes in a Beckman Avanti centrifuge at 4^{o} C using a JA25.50 rotor.

Next, the pellets were washed once with dI water (0.1 L / g dry cell mass dI water), and twice with 190 proof ethanol (0.05 L 190 proof ethanol/ g dry cell mass). Each wash was followed by centrifugation at 9500 rpm for 10 minutes in a Beckman Avanti centrifuge at 4^{o} C using a JA25.50 rotor. The supernatant was discarded after each centrifugation.

After the second ethanol wash, pellets were sometimes flaky and not well formed. In these cases, the supernatant was filtered using a Whatman borosilicate glass filter (0.2 to 0.4 micron). This filter (with retentate) was then placed back into the centrifuge tube for subsequent PHA extraction.

Three ml of chloroform was added to each centrifuge tube. After vortexing for 30 seconds, the chloroform mixture was heated to a boil for 2 minutes. The mixture was hot-filtered through a Whatman borosilicate glass filter (0.2 to 0.4 micron) into a pre-weighed Fisher 5 ml culture tube (Mettler Toledo AB54-S/FACT Classic Plus). The centrifuge tube was rinsed with hot chloroform which was filtered as well. The centrifuge tube was checked for any remaining pellet. If detected, the pellet was loosened with a Pasteur pipette, washed with hot chloroform, and filtered. The filtrate was set aside to allow the chloroform to evaporate. The filter (with retentate) was placed back into the centrifuge tube. To ensure complete PHA extraction, the entire hot chloroform wash was repeated two more times. Once all of the chloroform evaporated, the culture tubes were weighed again. The sum of the difference between the average pre and post weight of the three repetitions was reported as the PHA mass. Specific PHA mass was calculated by dividing the PHA mass by the sample volume used to determine the PHA mass. PHA content was calculated by dividing the specific dry cell mass by the specific PHA mass for each sample.

4.4.5 *Exhaust Gas Analysis (Fermentation Scale)*

Exhaust gases from the fermentor were analyzed using gas phase chromatography. Prior to GC analysis, water was removed from the gas stream with an inline condenser and an inline Drierite moisture trap.

Gas compositions were analyzed using an on-line Varian CP-4900 Micro Gas Chromatograph. The gases were separated with CP740148 M5A and CP740143 PPQ columns (Varian). Argon was used as the carrier gas. Star Chromatography Workstation

System Control software was used to control the hardware and process the data (Version 6.30, Varian).

Before each use, the GC calibration was verified using custom calibration gases containing varying concentrations of the gases of interest. Peak areas were integrated by software methods based on expected gas retention times and calibration data. The CO peak retention time had a tendency to shift over long sampling periods. To correct for the shift, sample data was recalculated based on corrected CO retention times.

4.4.6 *Transmission Electron Microscopy (Fermentation Scale)*

An aliquot from each fermentor sample taken on the fermentation scale was saved for transmission electron microscope (TEM) imaging. Approximately 15 ml of sample was centrifuged at 2500 rpm for 10 minutes at 4^{o} C in a Beckman Avanti J-25 centrifuge. The supernatant was discarded. The pellet was re-suspended in 1ml of a fixative buffer containing 2% paraformaldehyde, 2% glutaraldehyde, and 0.1 M sodium cacodylate and stored at 4 C.

The fixed cells were placed on a copper grid with carbon film and observed using a 200kV JEOL 2100 scanning transmission electron microscope (STEM). Images were captured with a GATAN E1000 digital camera using Digital Micrograph software.

4.5 DATA ANALYSIS

4.5.1 *Statistical Analysis*

The statistical software package, JMP 7.0.2 (SAS Institute Inc.), was used for data analysis. For the hypovial study, Tukey-Kramer honestly significant difference (HSD)

tests were used to determine which means within the three treatments were significantly different.

The software package Design Expert 7.1.6, Stat-Ease, Inc., Minneapolis USA was used to analyze and fit a second order polynomial to the central composite design data as well as to determine interaction effects of the three variables. Dry Cell mass and PHA production were the responses optimized in the central composite design and were used to determine interaction affects. Response surface regression was used to develop a second-order polynomial model of the form:

$$Y_i = \beta_0 + \sum_i \beta_i x_i + \sum_{ii} \beta_{ii} x_i^2 + \sum_{ij} \beta_{ij} x_i x_j \qquad \textbf{Equation 15}$$

where Y_i was the predicted response, β_0 was the constant, x was the independent variables, and β_i, β_{ii}, and β_{ij} were the linear, quadratic, and interaction coefficients respectively. The equation with the three independent coded variables of the central composite design took on the form:

$$\begin{aligned} Response = {} & \beta_0 + \beta_1[NH_4Cl] + \beta_2[YE] + \beta_3[NaAct] \\ & + \beta_{11}[NH_4Cl]^2 + \beta_{22}[YE]^2 + \beta_{33}[NaAct]^2 \\ & + \beta_{12}[NH_4Cl] \cdot [YE] + \beta_{13}[NH_4Cl] \cdot [NaAct] \\ & + \beta_{23}[YE] \cdot [NaAct] \end{aligned} \qquad \textbf{Equation 16}$$

where *Response* was the dry cell mass or PHA production factor and [NH_4Cl], [YE], and [NaAct] were the concentrations of NH_4Cl, YE, and NaAct, respectively.

4.5.2 *Uncertainty Analysis*

Uncertainty analysis was performed on fermentation scale for dry cell and PHA mass measurements using the methodology of Figliola and Beasley [163]. The same

balance was used for both dry cell mass and PHA mass measurements. Manufacturer specifications reported repeatability and linearity errors of 0.0001 g and 0.0002 g respectively. Precision error of the mass measurements was also observed and used to calculate uncertainty.

The uncertainty for dry cell mass ranged from ±2% to 11% (4.3% average) (see APPENDIX III and APPENDIX IV). PHA mass uncertainty ranged from ±4% to 73% (34% average). The uncertainty associated with PHA yield (DCM mass/PHA mass) ranged from ±6% to 123% (34% average). The large uncertainty associated with PHA mass and PHA yield was due in large part to precision error being propagated through calculated response variables.

CHAPTER 5. RESULTS AND DISCUSSION

5.1 MEDIA OPTIMIZATION: HYPOVIAL STUDY

Growth in the hypovial scale was difficult to achieve. Often times the cell growth would stagnate with long lag phases or simply not grow at all. Several actions were taken which effectively improved growth including remaking of stock solutions, improved and more frequent seed culture maintenance, improvement of anaerobic techniques, and increased inoculation volume. The hypovial experiments were carried out once the growth issue was resolved. Detailed results of the hypovial studied can be found in APPENDIX I.

5.1.1 *Results*

5.1.1.1 *Growth*

Differences in growth between levels of concentration were observed for all treatments (Figure 22 - Figure 24). The final cell density for cultures containing 25 mM NH_4Cl was significantly greater than the other NH_4Cl concentration levels (Figure 22). Cell density increased with increasing concentration of YE. With an average final cell density of 1.7 absorbance units, cultures with 2.0 g/L yeast extract had the highest final cell density of all treatments (Figure 23). In the NaAct treatment cultures, cell growth was similar for all levels until early stationary phase. NaAct concentrations between 2.5 and 5 mM resulted in the highest final cell density for that treatment (Figure 24).

The mean final pH for all levels in each treatment was 7.31, 7.33, and 7.32 for the NH_4Cl, YE, and NaAct treatments respectively.

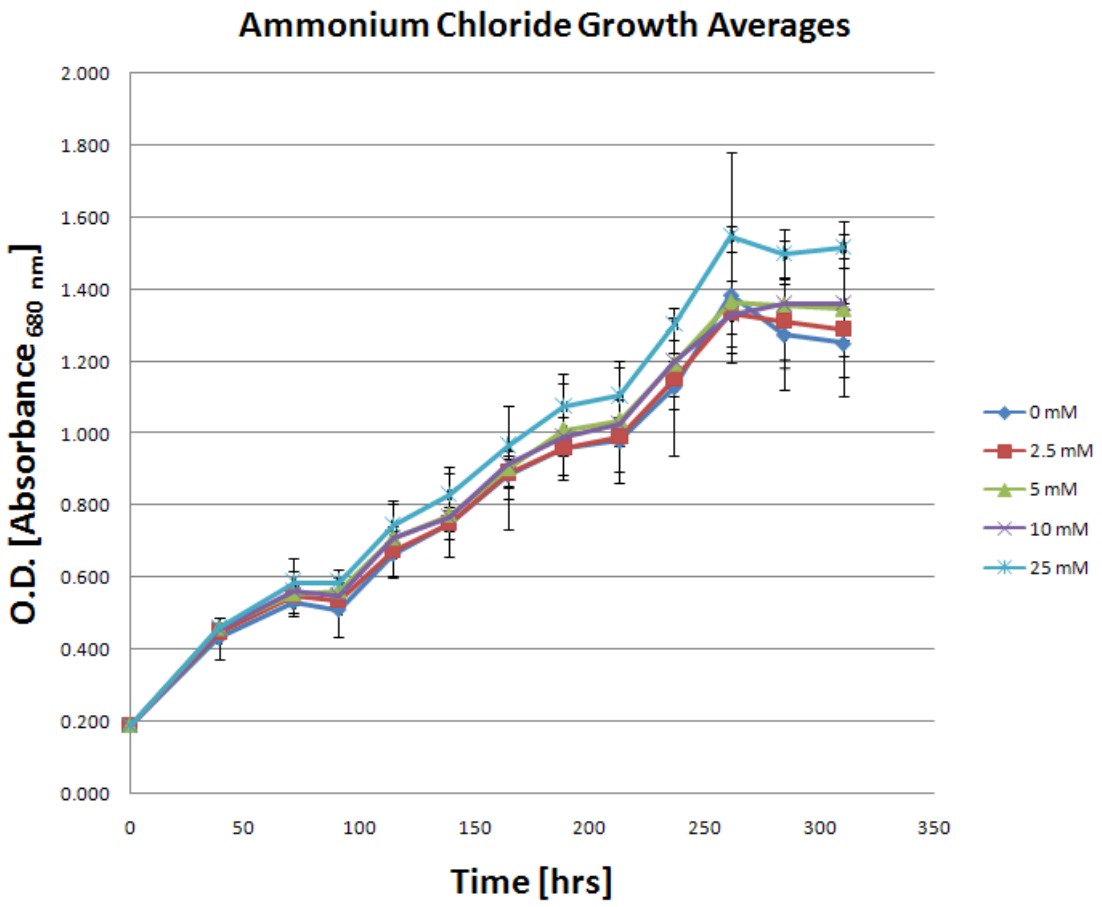

Figure 22. The dark, CO-dependent growth of *R. rubrum* in modified RRNCO media is displayed as a function of time for the NH_4Cl treatment. The concentration of NH_4Cl was varied while the remaining media component concentrations were kept at their nominal values. The cultures were incubated at 30^{o}C, shaken at 200 RPM, and purged daily with 100% CO. The data represents the average optical density (Absorbance 680nm) from three cultures per level per treatment. Error bars represent confidence intervals (CI) at ±95% (N=3).

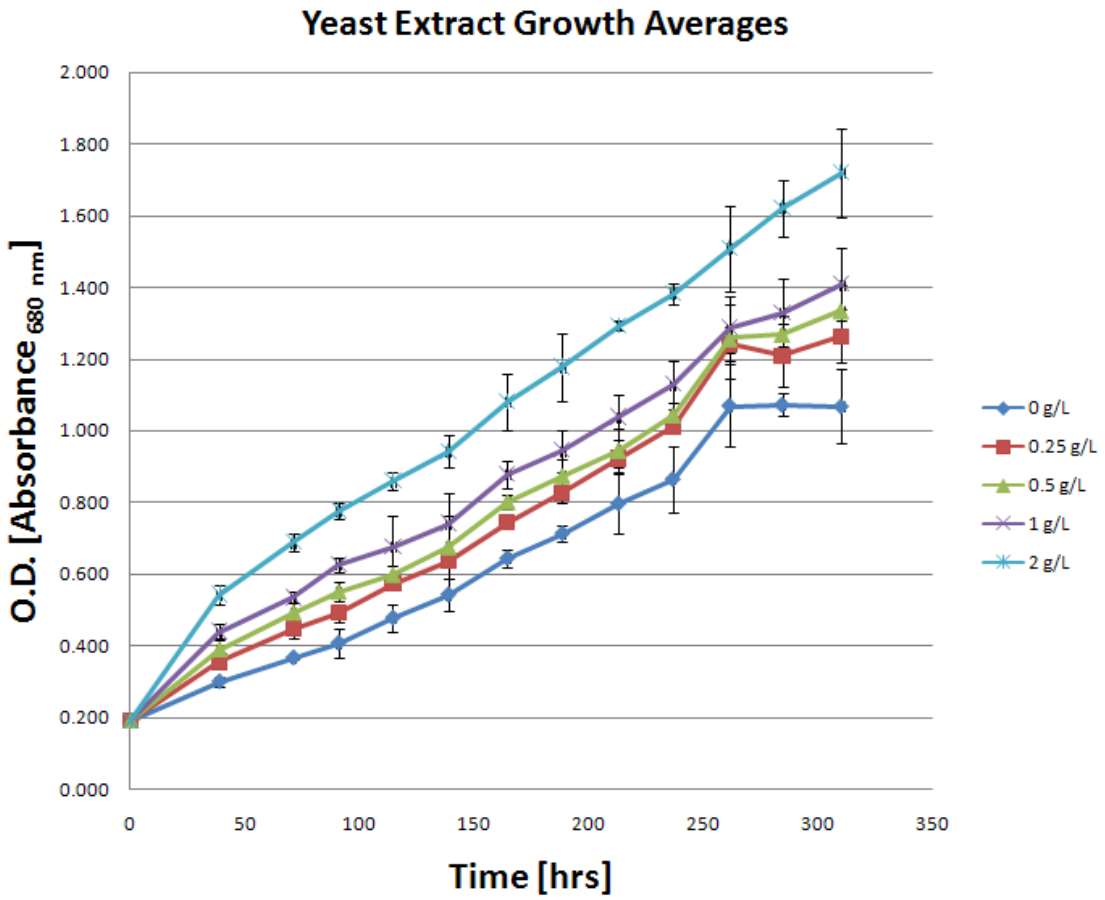

Figure 23. The dark, CO-dependent growth of *R. rubrum* in modified RRNCO media is displayed as a function of time for the YE treatment. The concentration of YE was varied while the remaining media component concentrations were kept at their nominal values. The cultures were incubated at 30°C, shaken at 200 RPM, and purged daily with 100% CO. The data represents the average optical density (Absorbance 680nm) from three cultures per level per treatment. Error bars represent confidence intervals (CI) at ±95% (N=3).

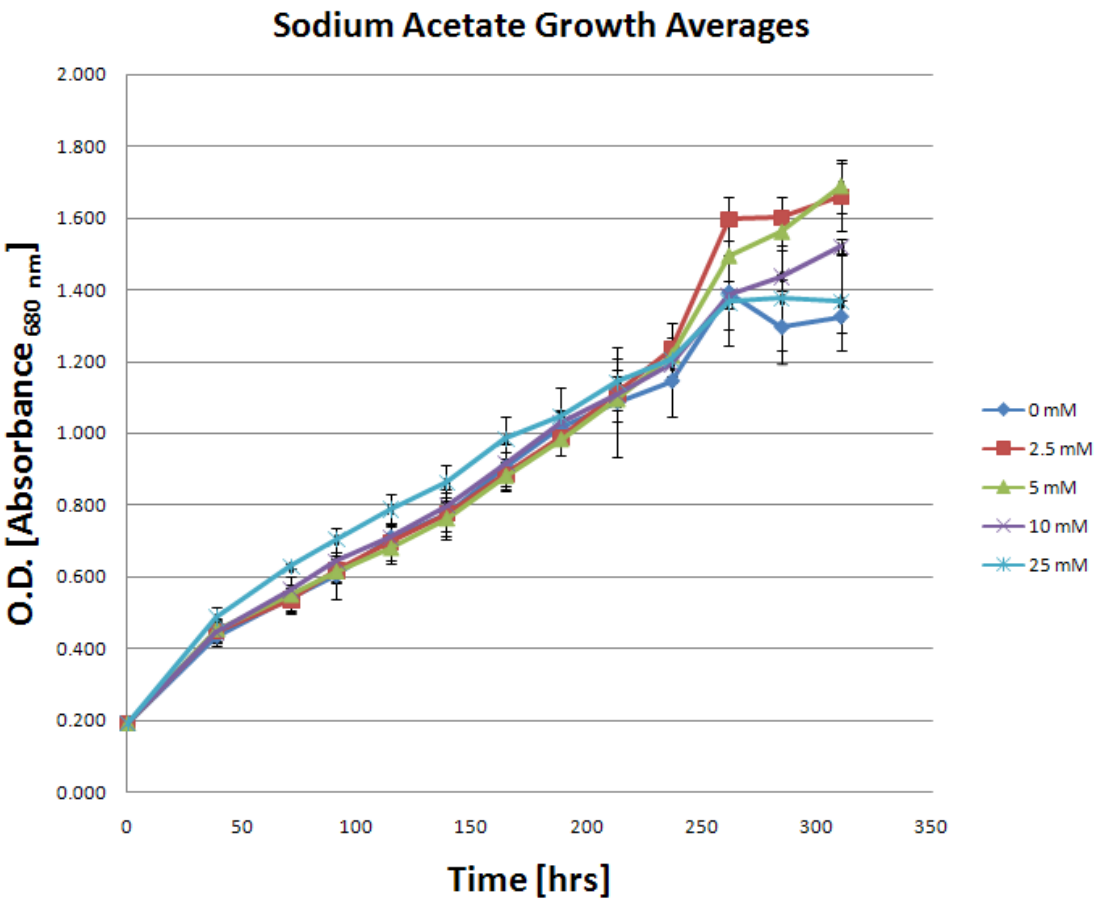

Figure 24. The dark, CO-dependent growth of *R. rubrum* in modified RRNCO media is displayed as a function of time for the NaAct treatment. The concentration of NaAct was varied while the remaining media component concentrations were kept at their nominal values. The cultures were incubated at 30°C, shaken at 200 RPM, and purged daily with 100% CO. The data represents the average optical density (Absorbance 680nm) from three cultures per level per treatment. Error bars represent confidence intervals (CI) at ±95% (N=3).

5.1.1.2 *Media Acetate Consumption*

Final media acetate concentration was measured using HPLC. Over varying concentrations of NH_4Cl, the amount of acetate consumed remained relatively constant at 4 mM (Figure 25). Acetate consumption decreased with increasing concentration of YE (Figure 26). For the NaAct treatment, acetate consumption increased with increasing concentration of NaAct (Figure 27).

5.1.1.3 *PHA Production Factor*

The yield of PHA (dry cell mass basis) was multiplied by optical density to give the PHA Production Factor (Equation 14). Figure 28 through Figure 30 display the PHA production factor for the three treatments. For levels 2.5 mM NH_4Cl, 5 mM NH_4Cl and 10 mM NaAct, calculations and statistics were based on two measurements for PHA mass instead of three.

The 25 mM NH_4Cl concentration had the largest PHA production factor for the NH_4Cl treatment group (Figure 28). The 25 mM concentration level was significantly different than the 0 mM and 2.5 mM levels.

The 2 g/L YE concentration had the largest PHA production factor for the YE treatment group (Figure 29). The 2 g/L concentration level was significantly different from the 1 g/L level, but not from the remaining levels.

The 2.5 mM NaAct concentration had the largest PHA production factor for the NaAct treatment group (Figure 30). The 2.5 mM concentration level was significantly different than all levels except the 5 mM concentration level.

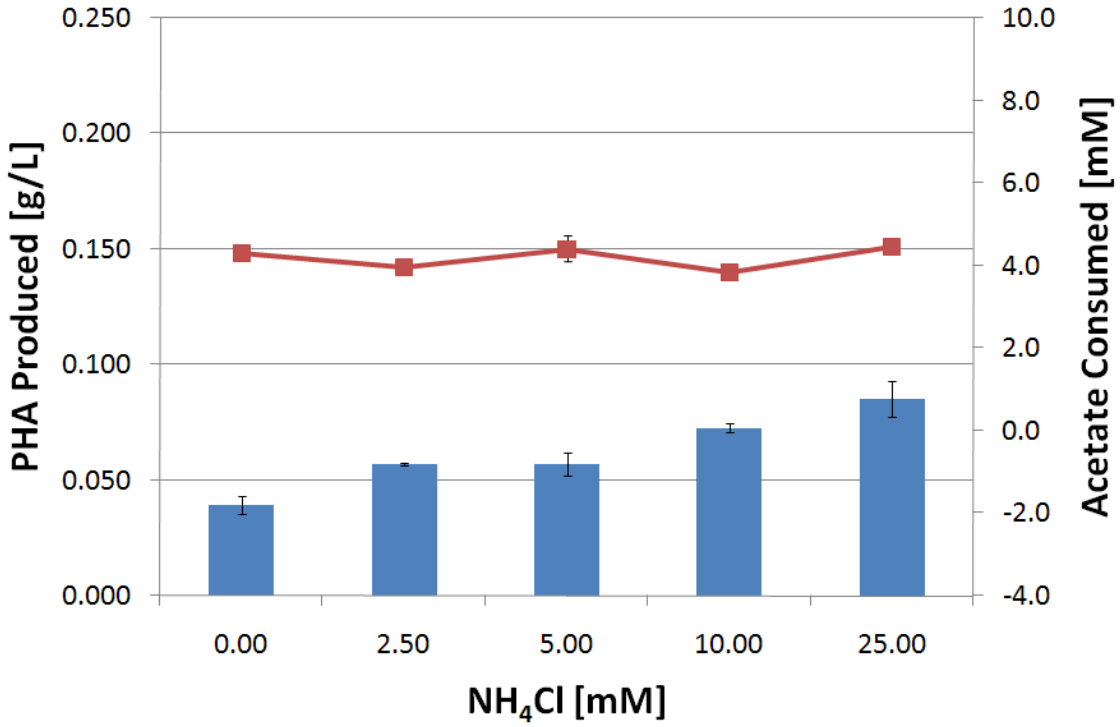

Figure 25. PHA production (blue bars) and acetate consumption (■) are plotted as a function of media component concentration for NH_4Cl. The nominal NH_4Cl concentration in the fermentation media is 18.7 mM. The error bars represent the standard error.

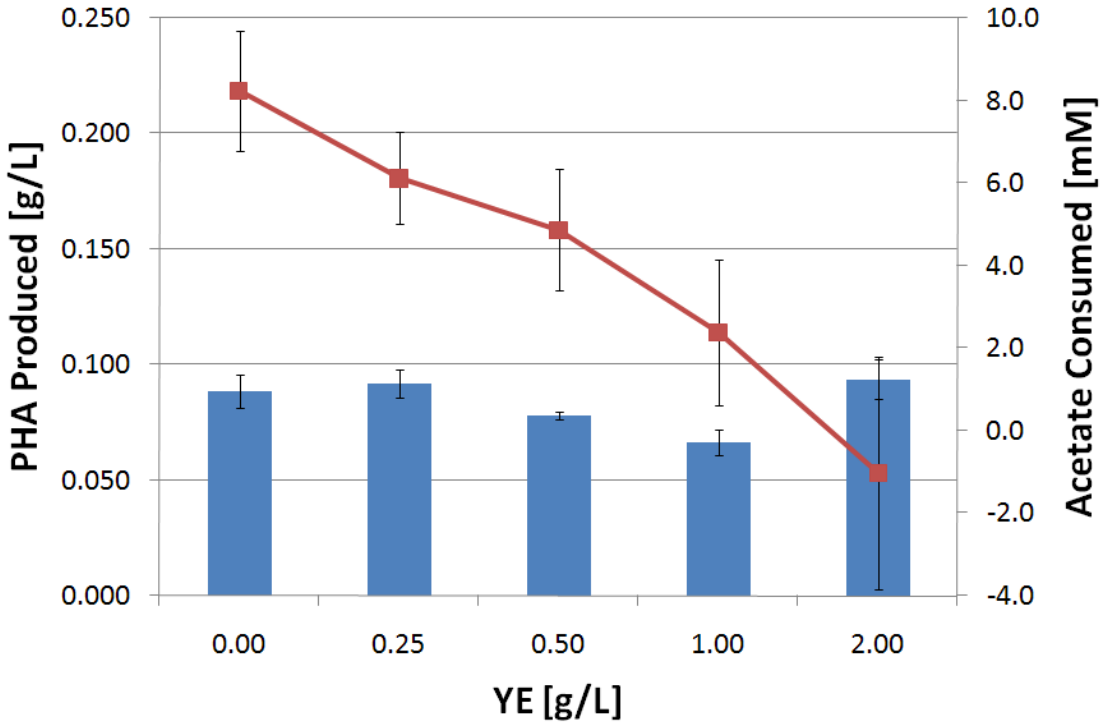

Figure 26. PHA production (blue bars) and acetate consumption (■) are plotted as a function of media component concentration for YE. The nominal YE concentration in the fermentation media is 1 g/L. The error bars represent the standard error.

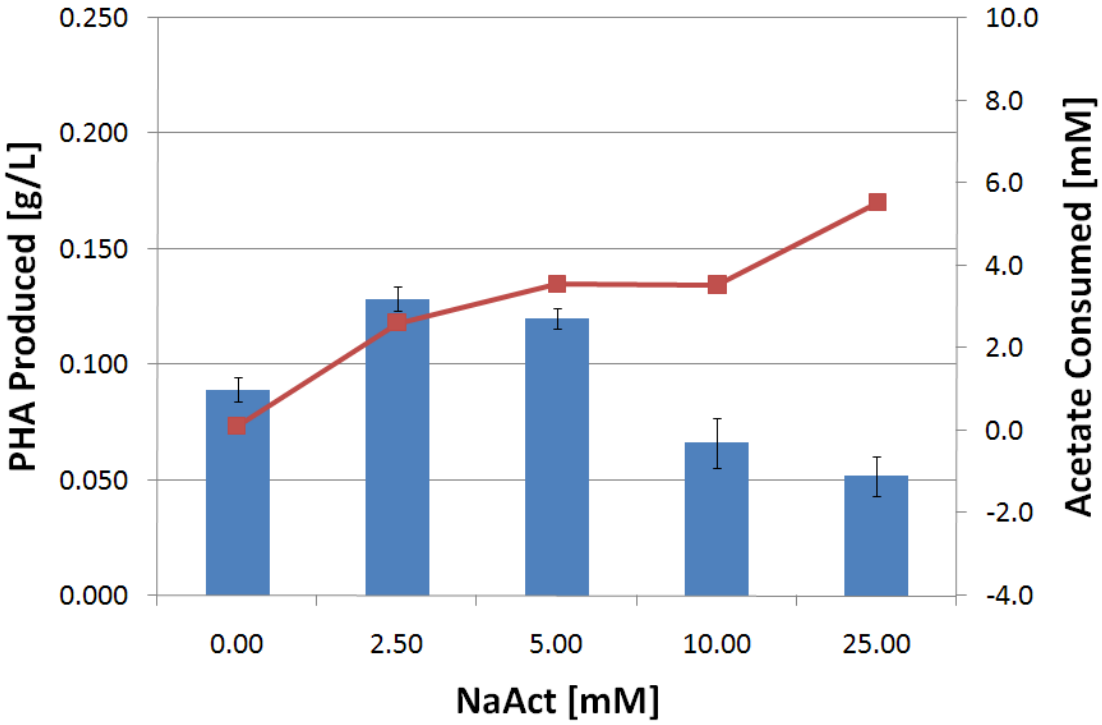

Figure 27. PHA production (blue bars) and acetate consumption (■) are plotted as a function of media component concentration for NaAct. The nominal NaAct concentration in the fermentation media is 1 g/L. The error bars represent the standard error.

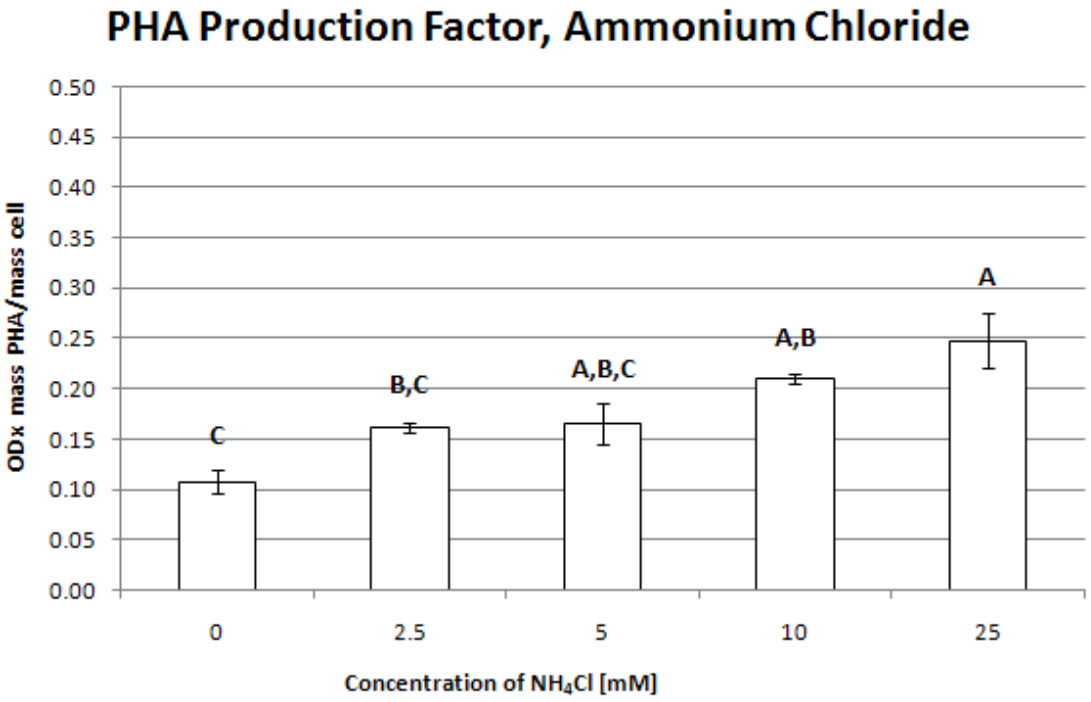

Figure 28. PHA Production Factor for various concentrations of ammonium chloride. The nominal RRNCO ammonium chloride concentration is 10 mM. Columns not connected by the same letter are significantly different (Tukey-Kramer HSD; α=0.05). The error bars indicate the standard error.

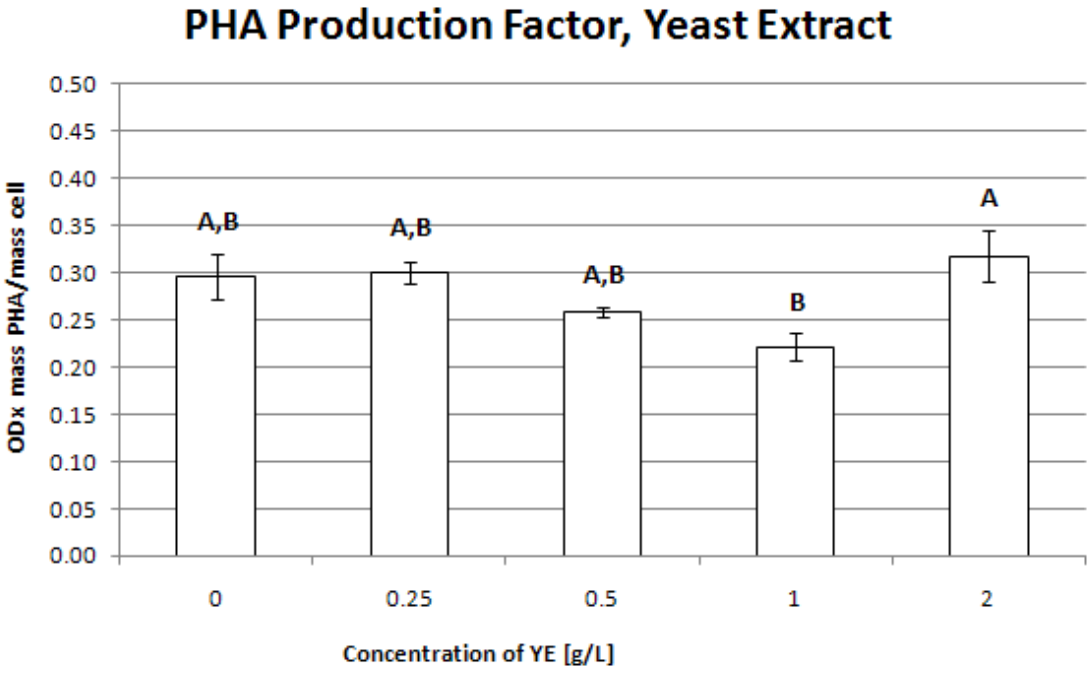

Figure 29. PHA Production Factor for various concentrations of yeast extract. The nominal RRNCO yeast extract concentration is 2 g/L. Columns not connected by the same letter are significantly different (Tukey-Kramer HSD; α=0.05). The error bars indicate the standard error.

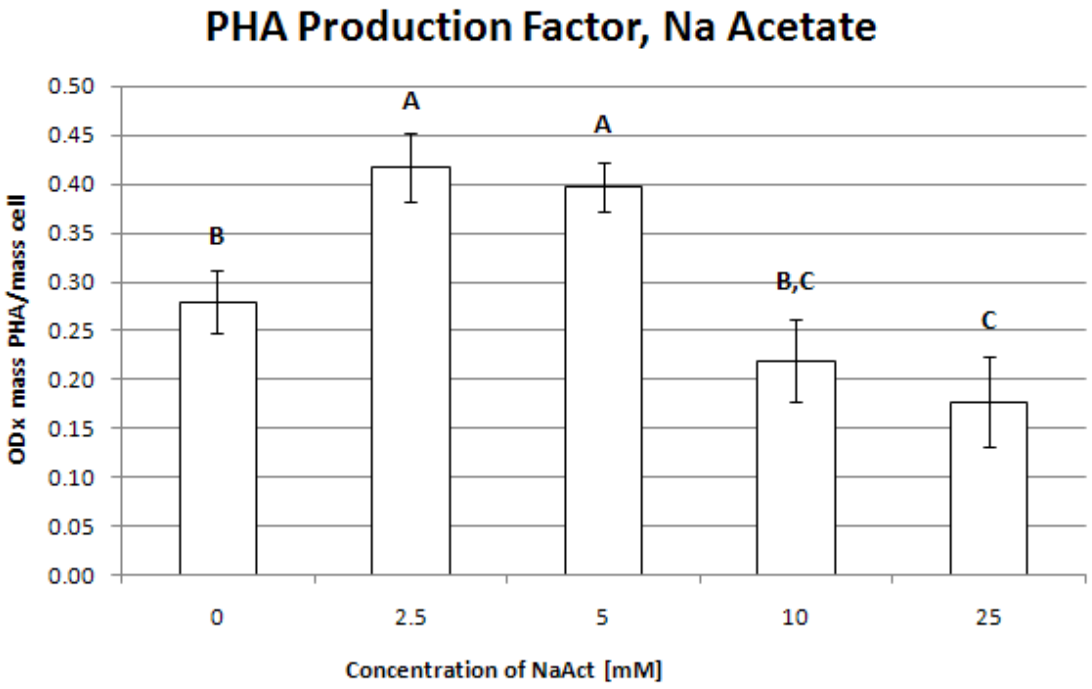

Figure 30. PHA Production Factor for various concentrations of sodium acetate. The nominal RRNCO acetate concentration is 10 mM. Columns not connected by the same letter are significantly different (Tukey-Kramer HSD; α=0.05). The error bars indicate the standard error.

5.1.2 *Discussion*

Determining how media components affect cell density was valuable since cell density is an important factor in PHA production. The maximum cell density for each of the treatments did not occur at the normal RRNCO media concentrations. For NH_4Cl and YE treatments, the maximum cell density occurred at higher respective concentrations than nominal RRNCO media.

Acetate consumption was consistent across the different levels of concentration for NH_4Cl (Figure 25). These data suggest that NH_4Cl does not control the rate of acetate consumption. When levels of NaAct were increased, consumption of acetate increased (Figure 27). This makes sense when considering most of the starting amount of acetate was consumed by the time of harvest for first three concentration levels of the NaAct treatment. Interestingly, acetate consumption decreased with increasing YE concentration (Figure 26). Since growth increased with increasing YE concentration, it seemed counter intuitive that acetate consumption would decrease. Yeast extract may have been limiting acetate consumption. Alternatively, yeast extract could contain components that could lead to acetic acid production in *R. rubrum*. Since acetate consumption is calculated by subtracting the final acetate concentration from the starting concentration, an increase in acetic acid would show up as a decrease in acetate consumption.

An optimized media was developed for scale up to the fermentation scale based on the PHA production factor results. The maximum PHA production factor from each treatment was chosen for the optimized media. The concentrations for NH_4Cl, YE, and NaAct chosen for the optimized media were 25 mM, 2 g/L, and 2.5 mM, respectively. In

cases where the optimal PHA production factor was not statistically significant from another level, mean difference, maximum optical density, and maximum PHA mass were considered when determining the optimal concentration.

The results of the hypovial experiment did not agree with literature in terms of the effect of the carbon to nitrogen balance on cellular PHA content [107, 126-128]. A high carbon to nitrogen ratio was expected, however the opposite was observed indicating an unknown presence of bio-available nitrogen. Yeast extract may contain available sources of carbon and nitrogen which would throw off the nitrogen limitation in the low NH_4Cl concentration media. Unpublished data for thermal gravimetric analysis (TGA) of three different brands of yeast extract indicated the presence of nitrogen.

5.2 MEDIA OPTIMIZATION: CENTRAL COMPOSITE DESIGN

5.2.1 *Results*

Detailed results of the central composite design experiment can be found in APPENDIX II.

5.2.1.1 *Dry Cell Mass*

The central composite design actual and predicted values for dry cell mass are presented in Table 7. The software package Design Expert 7.1.6 was used to develop the second order regression equation:

$$DCM = (2.83 \times 10^{-1}) + (5.15 \times 10^{-3})[NH_4Cl] + (2.73 \times 10^{-1})[YE] + (8.96 \times 10^{-4})[NaAct] + (-2.25 \times 10^{-3})[NH_4Cl]^2 + (-2.55 \times 10^{-4})[YE]^2 + (-5.79 \times 10^{-3})[NaAct]^2 + (-1.08 \times 10^{-4})[NH_4Cl] \cdot [YE] + (-3.47 \times 10^{-3})[NH_4Cl] \cdot [NaAct] + (1.03 \times 10^{-4})[YE] \cdot [NaAct]$$ **Equation 17**

where DCM was the dry cell mass response and [NH_4Cl], [YE], and [NaAct] were the concentrations of ammonium chloride, yeast extract, and sodium acetate respectively.

The results for the Analysis of Variance are shown in Table 8. The Model F Value of 62.34 implied that the model is significant. There was only a 0.01% chance that a Model F-Value this large could have occurred due to normal process variation. The significance of each term in the quadratic model was determined by p-values. P-values less than 0.05 indicated significant model terms. In the case of dry cell mass, all terms were significant except the quadratic terms $[YE]^2$and $[NaAct]^2$. The relative importance of each term is shown by plotting the absolute value of the t-statistic (Figure 31). The "Lack of Fit" value of 0.22 implied that the lack of fit was not significant relative to the pure error. This meant that there was a 95.2% chance that the lack of fit was due to normal process variation. The R-Squared value for the model was 0.956.

Table 7. The central composite design matrix with predicted and actual values for dry cell mass is presented.

	Factors			Response, DCM [g/L]	
Standard Order	NH4Cl [mM]	YE [g/L]	NaAct [mM]	Predicted Value	Actual Value
1	7.9	0.4	4.2	0.41	0.39
2	7.9	0.4	4.2	0.41	0.42
3	29.5	0.4	4.2	0.39	0.39
4	29.5	0.4	4.2	0.39	0.38
5	7.9	1.6	4.2	0.67	0.67
6	7.9	1.6	4.2	0.67	0.69
7	29.5	1.6	4.2	0.60	0.59
8	29.5	1.6	4.2	0.60	0.60
9	7.9	0.4	15.8	0.39	0.36
10	7.9	0.4	15.8	0.39	0.41
11	29.5	0.4	15.8	0.31	0.28
12	29.5	0.4	15.8	0.31	0.32
13	7.9	1.6	15.8	0.58	0.57
14	7.9	1.6	15.8	0.58	0.59
15	29.5	1.6	15.8	0.44	0.40
16	29.5	1.6	15.8	0.44	0.47
17	0.0	1.0	10.0	0.51	0.48
18	0.0	1.0	10.0	0.51	0.54
19	37.4	1.0	10.0	0.38	0.38
20	37.4	1.0	10.0	0.38	0.39
21	18.7	0.0	10.0	0.31	0.31
22	18.7	0.0	10.0	0.31	0.32
23	18.7	2.0	10.0	0.65	0.60
24	18.7	2.0	10.0	0.65	0.71
25	18.7	1.0	0.0	0.57	0.54
26	18.7	1.0	0.0	0.57	0.59
27	18.7	1.0	20.0	0.42	0.42
28	18.7	1.0	20.0	0.42	0.44
29	18.7	1.0	10.0	0.48	0.47
30	18.7	1.0	10.0	0.48	0.50
31	18.7	1.0	10.0	0.48	0.48
32	18.7	1.0	10.0	0.48	0.47
33	18.7	1.0	10.0	0.48	0.53
34	18.7	1.0	10.0	0.48	0.48
35	18.7	1.0	10.0	0.48	0.47
36	18.7	1.0	10.0	0.48	0.47

Table 8. The ANOVA results for the response surface quadratic model of dry cell mass are presented.

Source	Sum of Squares	*df*	Mean Square	F Value	p-value Prob > F	
Model	0.397	9	0.044	62.34	< 0.0001	Significant
A-NH4Cl	0.044	1	0.044	62.46	< 0.0001	Significant
B-YE	0.279	1	0.279	394.20	< 0.0001	Significant
C-NaAct	0.054	1	0.054	76.83	< 0.0001	Significant
AB	3.403E-03	1	3.403E-03	4.81	0.0374	Significant
AC	4.082E-03	1	4.082E-03	5.77	0.0237	Significant
BC	6.489E-03	1	6.489E-03	9.18	0.0055	Significant
A^2	4.326E-03	1	4.326E-03	6.12	0.0202	Significant
B^2	4.280E-05	1	4.280E-05	0.06	0.8076	not significant
C^2	3.319E-04	1	3.319E-04	0.47	0.4993	not significant
Residual	0.018	26	7.070E-04			
Lack of Fit	0.001	5	1.791E-04	0.22	0.9522	not significant

Figure 32 displays the 3-D surface and contour plots for dry cell mass. Each paired inset shows the surface and contour for the interactive variables of the quadratic model for dry cell mass. The variable not displayed was fixed at the nominal RRNCO concentration level while the two remaining variables were varied infinitely in the design space. The contour curves represented the dry cell mass for those infinite combinations. Dry cell mass was optimized using the Design Expert software package. For the quadratic model created, the optimal predicted dry cell mass was 0.762 g/L with optimal NH_4Cl, YE, and NaAct concentrations of 4.9 mM, 2.0 g/L, and 3.9 mM respectively.

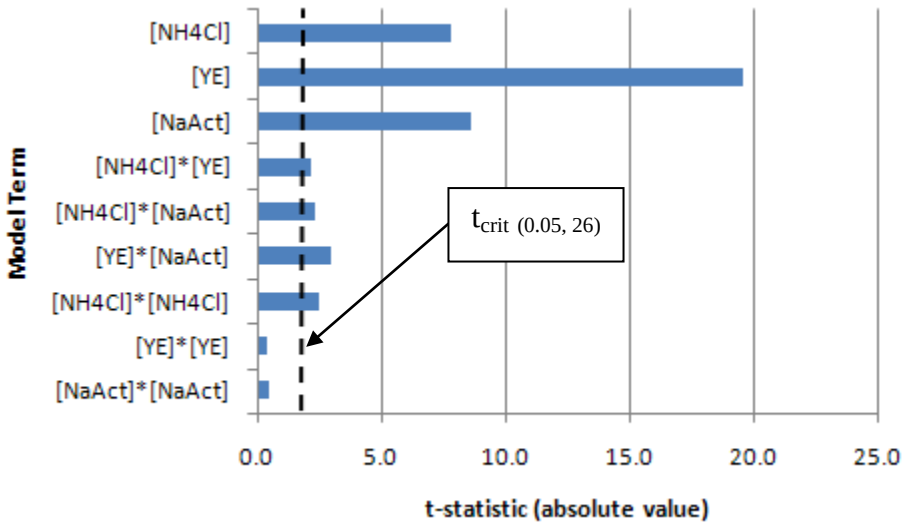

Figure 31. The absolute value of the t-statistic for each model term is shown for the dry cell mass model. The dotted line represents value of the critical t-static ($t_{crit\ (0.05,\ 26)}$ = 1.706). Values of the t-statistic greater than $t_{crit\ (0.05,\ 26)}$ correspond to significant model terms.

The model results were also examined by plotting a single factor while holding the remaining two factors constant at nominal RRNCO concentrations (Figure 33). Hypovial and CCD experimental data points were plotted along with the model for comparison. A 95% confidence interval was plotted over the range of the model design space.

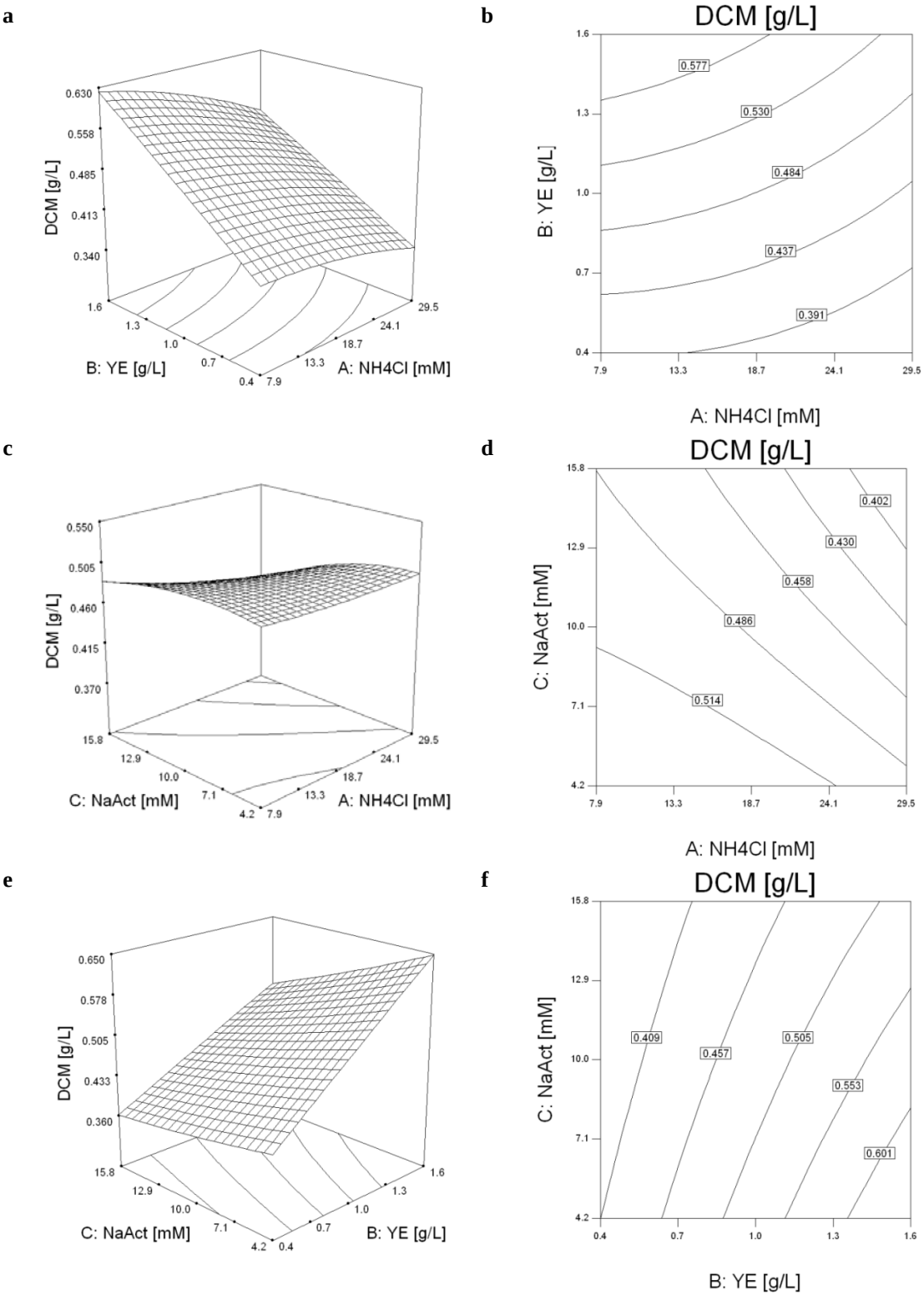

Figure 32. The interactive effects of the DCM quadratic model are plotted as 3-D response curves and contour plots. The interactive effects evaluated are NH_4Cl-YE (a & b), NH_4Cl-NaAct (c & d), and YE-NaAct (e & f).

A

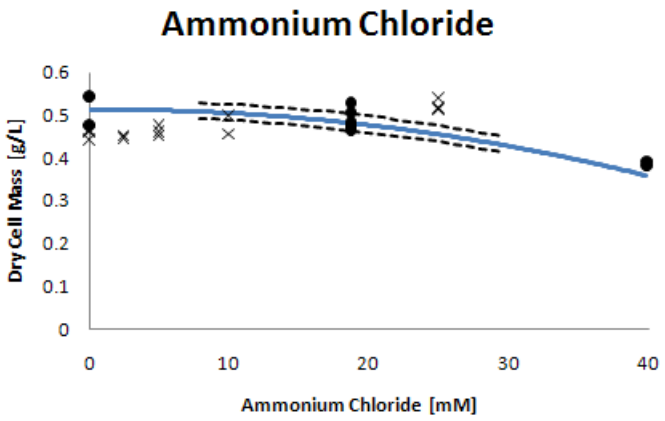

B

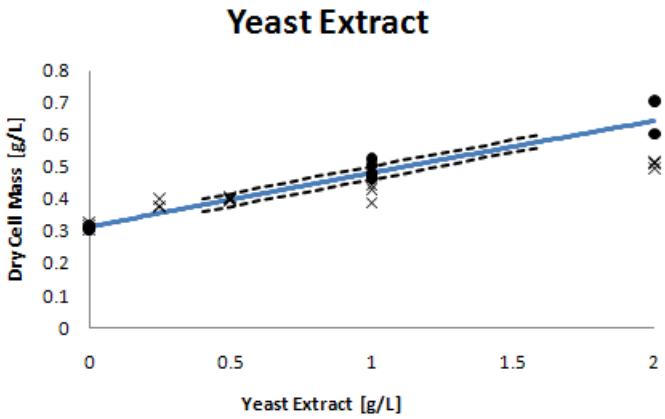

C

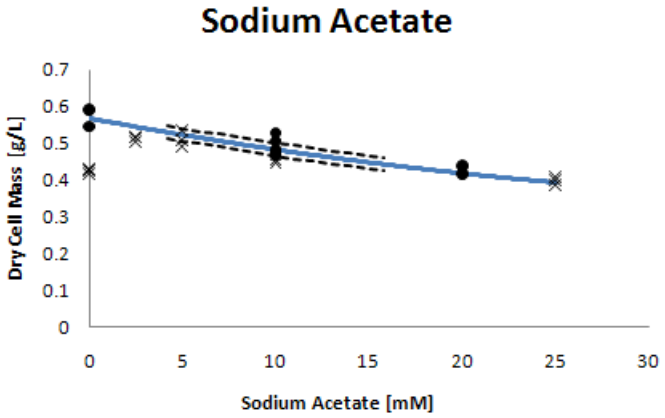

Figure 33. The dry cell mass model results are shown with two factors held constant while the third is varied. Constant factor concentrations were fixed at nominal RRNCO concentrations: A) YE – 1 g/L; NaAct – 10 mM B) NH4Cl – 18.7 mM; NaAct – 10 mM C) YE – 1 g/L; NH4Cl – 18.7 mM. The blue line represents the dry cell mass model. The dotted black line represents the 95% confidence interval for the model over the design space. Black circles represent experimental CCD data points. "X"s represent experimental hypovial data points.

5.2.1.2 *PHA Production Factor*

A second order regression equation was developed for the PHA production factor using the central composite design. The actual and predicted responses are displayed in Table 9. The PHA production factor was based on seven center points. The resulting model had the following form:

$$PHA\ production\ factor = (2.58 \times 10^{-1}) + (-1.28 \times 10^{-3})[NH_4Cl] + (-1.19 \times 10^{-1})[YE] + (-1.76 \times 10^{-2})[NaAct] + (-3.84 \times 10^{-4})[NH_4Cl]^2 + (3.78 \times 10^{-5})[YE]^2 + (3.69 \times 10^{-3})[NaAct]^2 + (1.13 \times 10^{-5})[NH_4Cl] \cdot [YE] + (5.04 \times 10^{-2})[NH_4Cl] \cdot [NaAct] + (5.06 \times 10^{-4})[YE] \cdot [NaAct] \quad \textbf{Equation 18}$$

The results for the Analysis of Variance are shown in Table 10. The Model F Value of 2.10 implied that the model was not significant. There was a 6.95% chance that a Model F-Value this large could have occurred due to normal process variation. The only significant terms in the model were [NaAct] ($p<0.05$), $[YE]^2$ ($p<0.05$), and $[NaAct]^2$ ($p<0.05$). The relative importance of each term is shown by plotting the absolute value of the t-statistic (Figure 34). The "Lack of Fit" value of 0.90 implied that the lack of fit was not significant to relative to the pure error. This meant that there was a 49.8% chance that the lack of fit was due to normal process variation. The R-Squared value for the model was 0.430. The predicted R-Squared value (-0.1527) was negative which implied that the mean was better predictor for the PHA production factor than the model.

Table 9. The central composite design matrix with the predicted and actual values for the PHA production factor is presented.

	Factors			Response, DCM [g/L]	
Standard Order	NH4Cl [mM]	YE [g/L]	NaAct [mM]	Predicted Value	Actual Value
1	7.9	0.4	4.2	0.15	0.15
2	7.9	0.4	4.2	0.09	0.15
3	29.5	0.4	4.2	0.16	0.13
4	29.5	0.4	4.2	0.10	0.13
5	7.9	1.6	4.2	0.20	0.14
6	7.9	1.6	4.2	0.09	0.14
7	29.5	1.6	4.2	0.14	0.11
8	29.5	1.6	4.2	0.10	0.11
9	7.9	0.4	15.8	0.08	0.08
10	7.9	0.4	15.8	0.07	0.08
11	29.5	0.4	15.8	0.11	0.08
12	29.5	0.4	15.8	0.03	0.08
13	7.9	1.6	15.8	0.12	0.13
14	7.9	1.6	15.8	0.13	0.13
15	29.5	1.6	15.8	0.17	0.11
16	29.5	1.6	15.8	0.10	0.11
17	0.0	1.0	10.0	0.13	0.10
18	0.0	1.0	10.0	0.11	0.10
19	37.4	1.0	10.0	0.08	0.07
20	37.4	1.0	10.0	0.04	0.07
21	18.7	0.0	10.0	0.20	0.12
22	18.7	0.0	10.0	0.10	0.12
23	18.7	2.0	10.0	0.11	0.15
24	18.7	2.0	10.0	0.15	0.15
25	18.7	1.0	0.0	0.16	0.16
26	18.7	1.0	0.0	0.19	0.16
27	18.7	1.0	20.0	0.07	0.10
28	18.7	1.0	20.0	0.12	0.10
29	18.7	1.0	10.0	0.11	0.08
30	18.7	1.0	10.0	0.02	0.08
31	18.7	1.0	10.0	0.08	0.08
32	18.7	1.0	10.0	0.09	0.08
33	18.7	1.0	10.0	0.11	0.08
34	18.7	1.0	10.0	0.04	0.08
35	18.7	1.0	10.0	0.11	0.08

Table 10. The ANOVA results for the response surface quadratic model of the PHA production factor are presented.

Source	Sum of Squares	*df*	Mean Square	F Value	p-value Prob > F	
Model	0.029	9	0.003	2.10	0.0695	not significant
A-NH4Cl	0.002	1	0.002	1.56	0.2228	not significant
B-YE	0.001	1	0.001	0.83	0.3711	not significant
C-NaAct	0.009	1	0.009	5.74	0.0244	Significant
AB	9.884E-05	1	9.884E-05	0.06	0.8026	not significant
AC	8.953E-05	1	8.953E-05	0.06	0.8119	not significant
BC	2.634E-03	1	2.634E-03	1.70	0.2041	not significant
A^2	4.490E-05	1	4.490E-05	0.03	0.8662	not significant
B^2	8.577E-03	1	8.577E-03	5.54	0.0268	Significant
C^2	7.554E-03	1	7.554E-03	4.88	0.0366	Significant
Residual	0.039	25	1.549E-03			
Lack of Fit	0.007	5	1.427E-03	0.90	0.4980	not significant

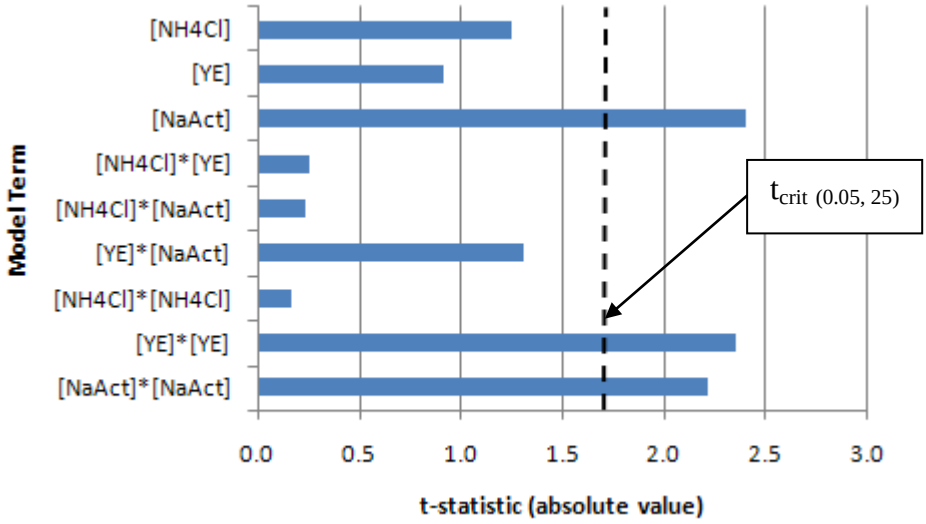

Figure 34. The absolute value of the t-statistic for each model term is shown for the dry cell mass model. The dotted line represents value of the critical t-static ($t_{crit\ (0.05,\ 25)}$ = 1.708). Values of the t-statistic greater than $t_{crit\ (0.05,\ 25)}$ correspond to significant model terms.

The PHA Production Factor model results were examined by plotting a single factor while holding the remaining two factors constant at nominal RRNCO concentrations (Figure 35). Hypovial and CCD experimental data points were plotted along with the model for comparison. A 95% confidence interval was plotted over the range of the model design space. The model was a poor fit for the experimental data in all cases which agrees with the ANOVA results.

5.2.2 *Discussion*

The PHA production factor model was not significant. According to the analysis of variance for the PHA production factor model, the mean would serve as a better predictor for the PHA production factor than the model itself. As a result, the central composite design for this data set was not a good predictor for the PHA production factor.

Although the PHA production factor was not a good predictor, the model for dry cell mass indicated that interaction effects may have been present between treatments. It also indicated the nominal RRNCO media was not optimized in terms of dry cell mass. Since dry cell mass is an integral component of PHA yield and the PHA production factor calculations, the result of the model indicated that standard RRNCO was not optimized for PHA production.

A

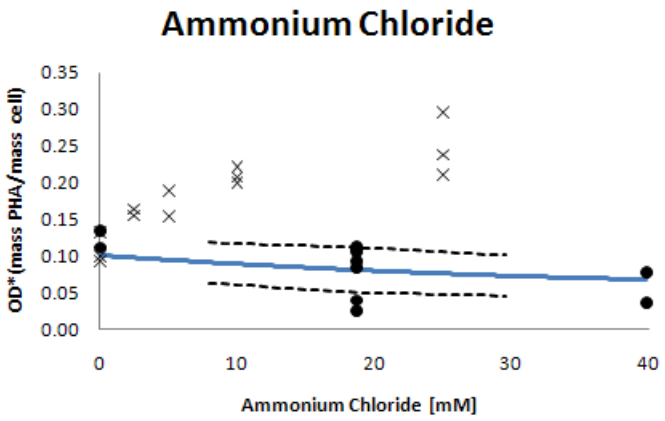

B

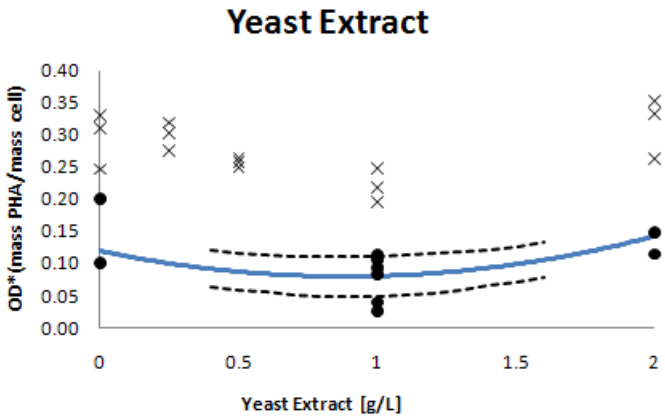

C

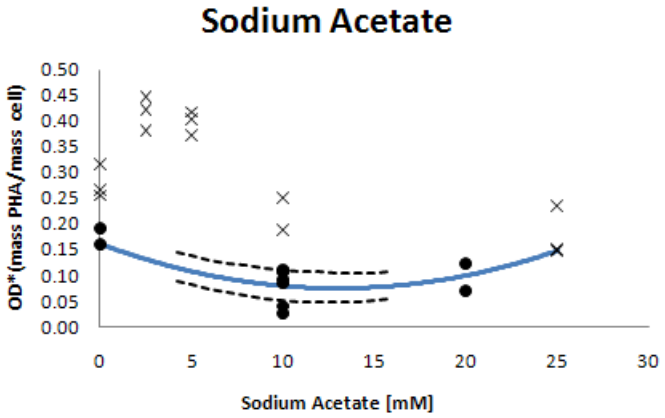

Figure 35. The PHA Production Factor model results are shown with two factors held constant while the third is varied. Constant factor concentrations were fixed at nominal RRNCO concentrations: A) YE – 1 g/L; NaAct – 10 mM B) NH_4Cl – 18.7 mM; NaAct – 10 mM C) YE – 1 g/L; NH_4Cl – 18.7 mM. The blue line represents the PHA Production Factor model. The dotted black line represents the 95% confidence interval for the model over the design space. Black circles represent experimental CCD data points. "X"s represent experimental hypovial data points.

5.3 HARVEST POINT OPTIMIZATION

5.3.1 *Results*

5.3.1.1 *Growth*

The optical density at 680 nm and dry cell mass shared very similar trends when compared on adjusted scales (Figure 36). On average, 1 absorbance unit corresponded to 0.38 g/L dry cell mass. During the linear portions of the exponential stage, the growth rate of the three replicates was calculated as 0.015 absorbance units per hour, resulting in an average doubling time of 34 hours. The average stationary phase optical density for replications A-C was 2.2, 2.8, and 2.9 absorbance units respectively. The average stationary phase dry cell mass for replications A-C was 0.8, 1.0, and 1.0 g/L dry cell mass respectively.

5.3.1.2 *PHA Yield*

The PHA yields on a dry cell mass basis followed similar trends to the growth curve during exponential growth (Figure 37). At the end of the exponential phase and early stages of stationary phase, PHA yield began to plateau and then decreased unlike optical density. For replicates A and B, the peak PHA yield occurred between 130 and 140 hours elapsed fermentation time. Replicate C PHA yields begin to level off at 130 hours, but then increase to a new peak almost 100 hours later. The mean maximum PHA yield for all replicates observed was 18.1% (dry mass basis).

A

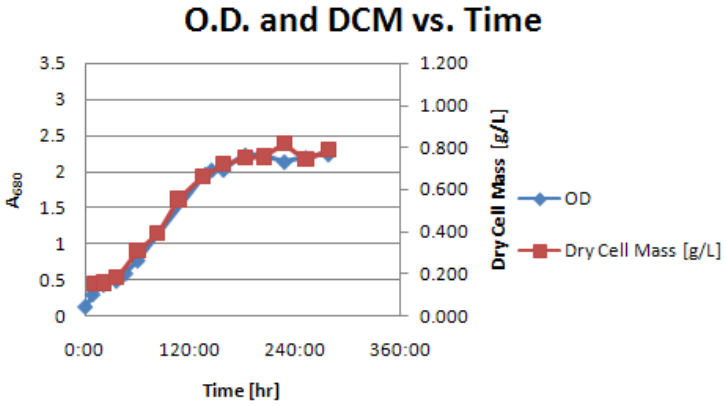

B

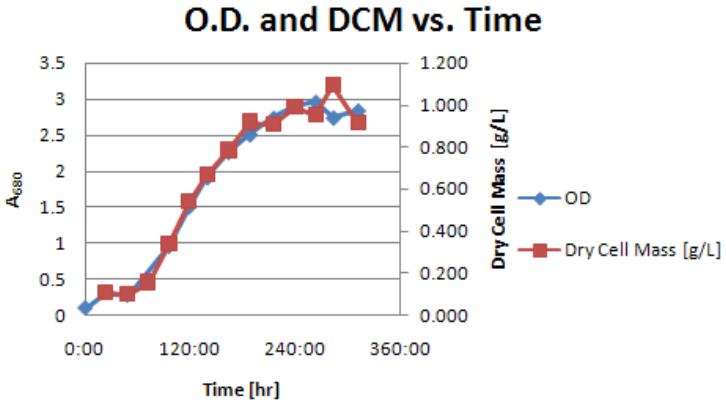

C

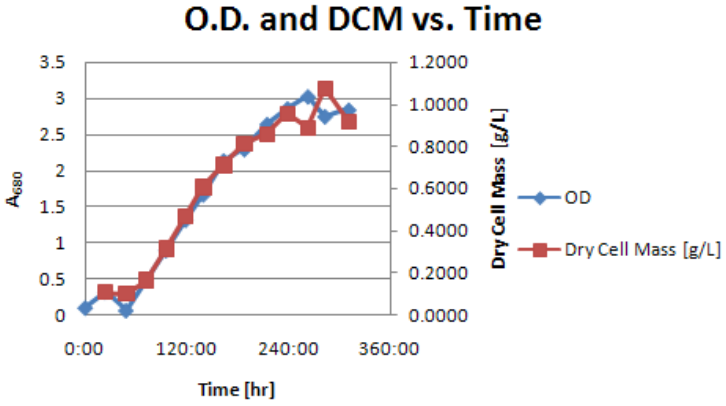

Figure 36. Optical density (absorbance 680 nm; blue diamonds) and dry cell mass (red squares) data are plotted against total elapsed fermentation time for three replicates (A, B & C). These cultures were dark grown on the fermentation scale (10 L) using modified RRNCO media (2.5 mM NH_4Cl, 2 g/L yeast extract, and 20 mM sodium acetate).

A

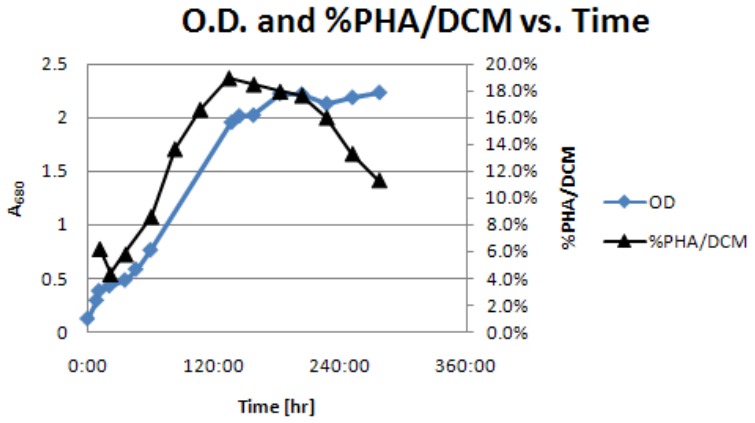

B

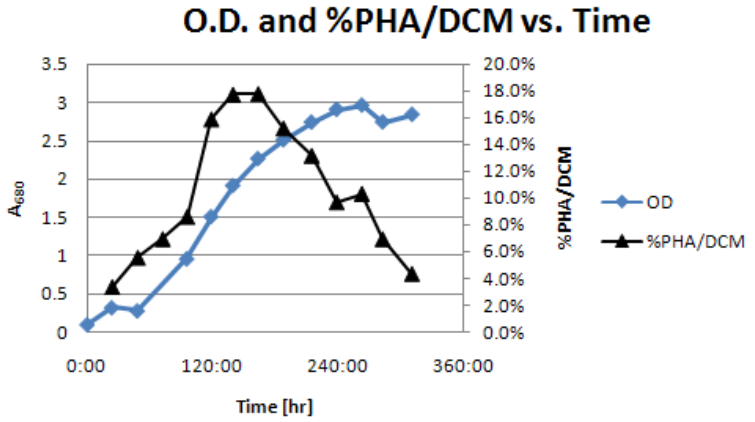

C

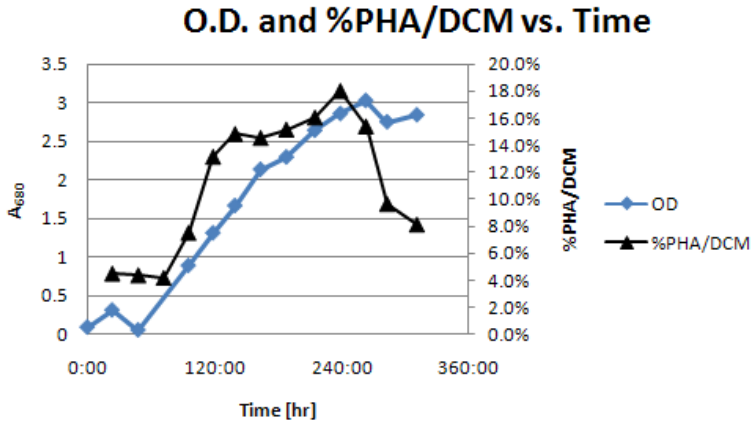

Figure 37. Optical density (absorbance 680 nm; blue diamonds) and PHA yield (black triangles) data are plotted against total elapsed fermentation time for three replicates (A, B & C). These cultures were dark grown on the fermentation scale (10 L) using modified RRNCO media (25 mM NH_4Cl, 2 g/L yeast extract, and 2.5 mM sodium acetate).

5.3.1.3 *PHA Yield and Media Acetate Concentration*

The starting acetate concentration for all replicates was 2 mM. Interestingly, media acetate concentration increased from the starting concentration, peaked, then decreased to zero (Figure 38). When comparing acetate concentration side-by-side with PHA yield, PHA yield began to decrease once the acetate concentration approached zero (Figure 38). In fact, for replicates A and B, peak PHA yield occurred at the same time the media acetate concentration reached zero.

5.3.1.4 *Exhaust Gas Composition*

During early exponential phase, exhaust CO concentration decreased with corresponding increases in H_2 and CO_2 concentration (Figure 39). The exhaust gas composition reached a new equilibrium within approximately 70 hours for all replicates. The concentration of hydrogen shifted from 28.5% to a maximum measured concentration of 32.4%, 34.1%, and 31.6% for replicates A, B, and C respectively. The level of H_2 stayed approximately the same even as PHA production increased. Carbon dioxide concentration increased from 21.5% to a maximum of 27.7% for replicate A, 28.9% for replicate B, and 28.7% for replicate C. The average equilibrium exhaust gas composition was 31.0% H_2, 40.4% CO, and 27.5% CO_2.

A

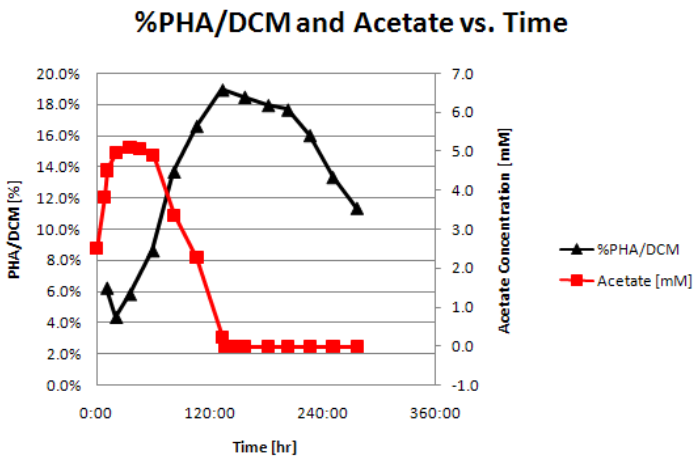

B

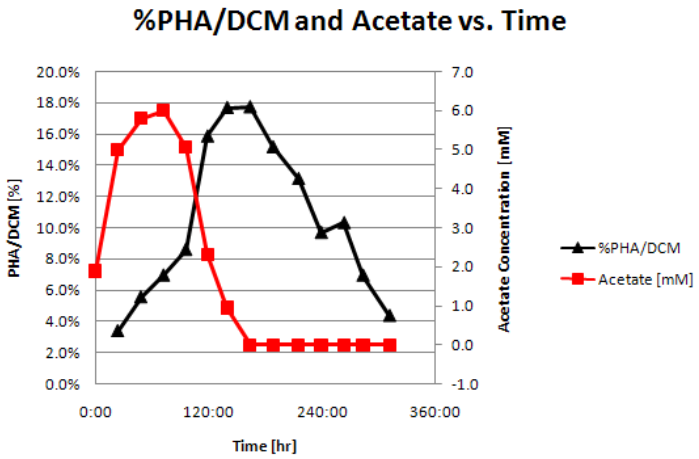

C

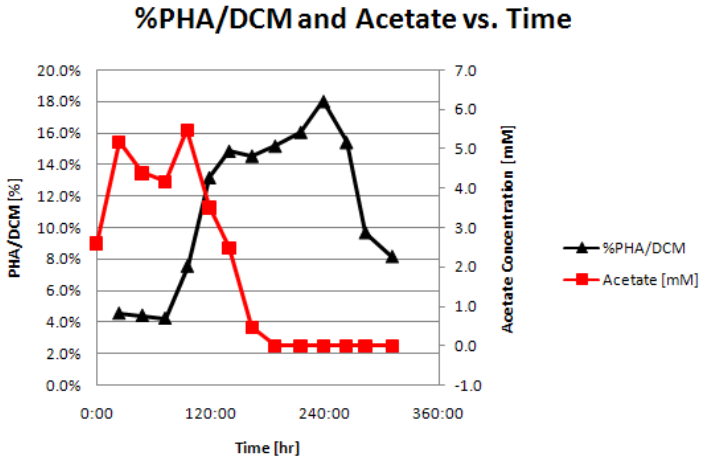

Figure 38. PHA yield (black triangles) and acetate concentration (red squares) data are plotted against total elapsed fermentation time for three replicates (A, B & C). These cultures were dark grown on the fermentation scale (10 L) using modified RRNCO media (25 mM NH_4Cl, 2 g/L yeast extract, and 2.5 mM sodium acetate).

A

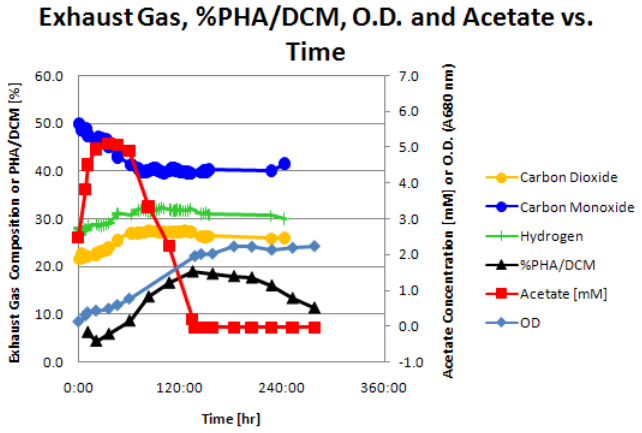

B

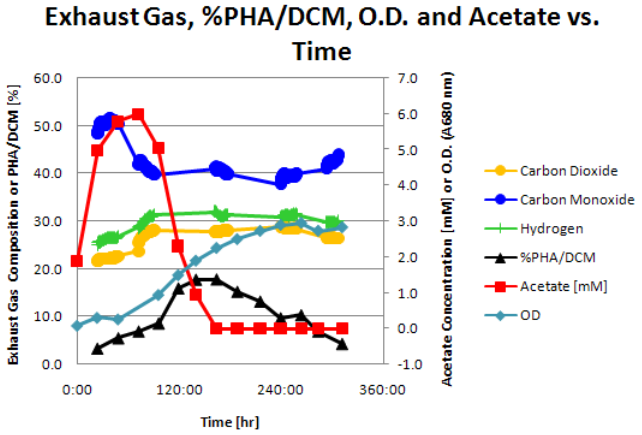

C

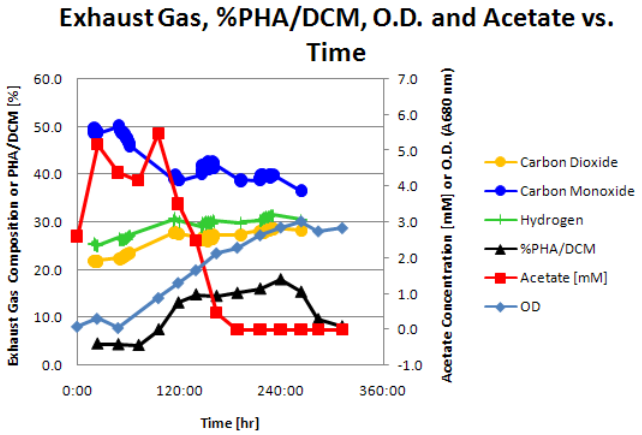

Figure 39. Exhaust gas composition (CO – blue circles, H_2 – green circles, CO_2 – yellow circles), PHA yield (black triangles), optical density (absorbance 680 nm; blue diamonds), and acetate concentration (red squares) data are plotted against total elapsed fermentation time for three replicates (A, B, &C). These cultures were dark grown on the fermentation scale (10 L) using modified RRNCO media (25 mM NH4Cl, 2 g/L yeast extract, and 2.5 mM sodium acetate).

Figure 39 shows the timing of all the events monitored during the fermentation. Acetate concentration peaked as CO concentration deceased, close to the point at which the exhaust gas reached its new equilibrium composition. Like OD, PHA yield continued to increase while CO concentration decreased. As the cells reached stationary phase, PHA yield decreased and acetate concentration reached zero.

5.3.1.5 *Transmission Electron Microscope Imaging*

TEM pictures were taken using a 200kV JEOL 2100 STEM and captured with a GATAN E1000 digital camera. Images were taken from replicate A samples collected at 21 and 134 hours elapsed fermentation time, Figure 40 and Figure 41 respectively. No staining was required for contrast because the photopigment of *R. rubrum* was electron dense. PHA inclusion bodies, which are not electron dense, could be seen as white circles inside the cells. The number of inclusion bodies per cell appeared to be similar between the two time periods, however, the size of the inclusion bodies appropriately appeared larger in the 134-hour cells.

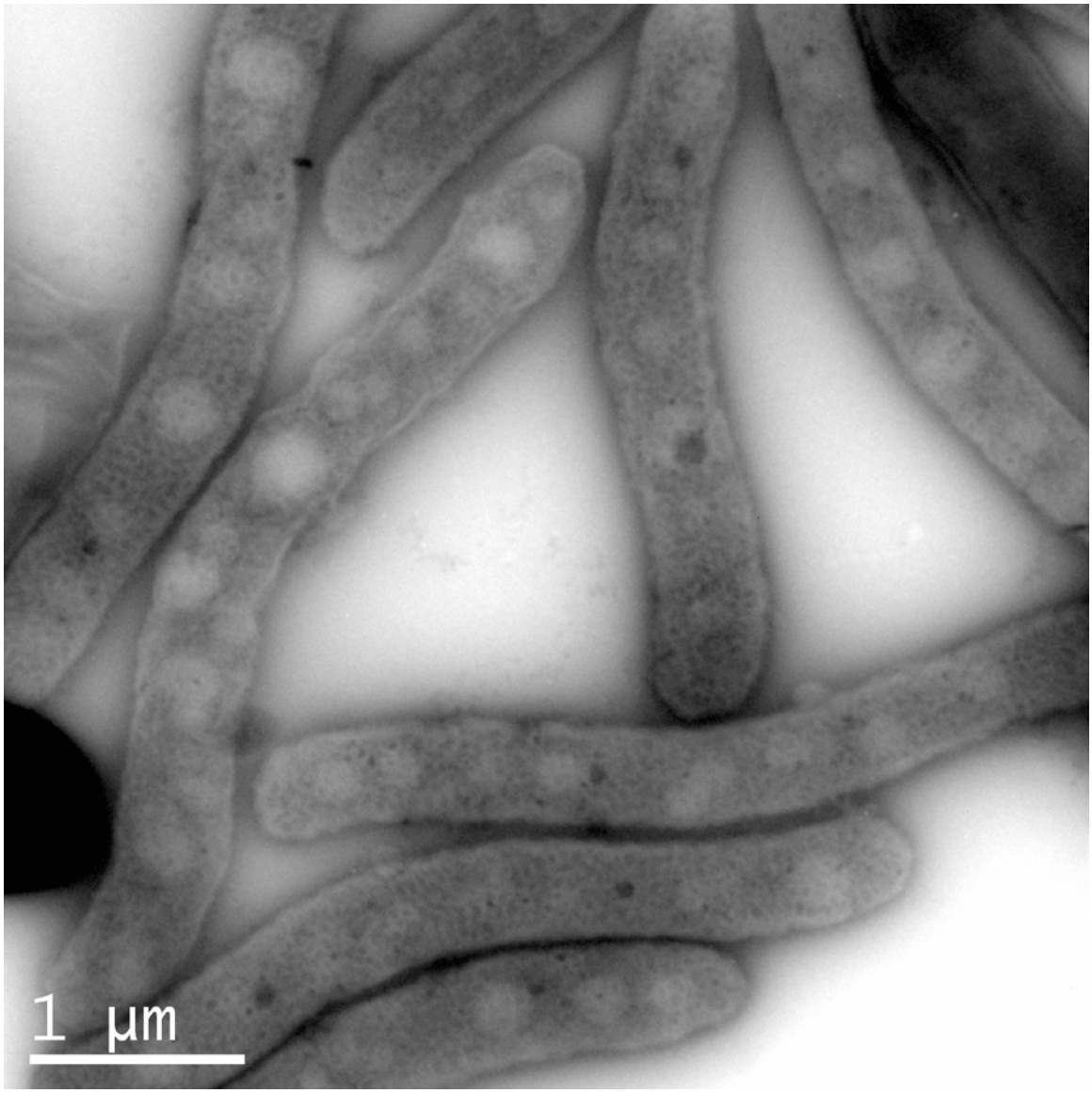

Figure 40. Transmission electron microscope picture of *R. rubrum* at 20 hours elapsed fermentation time of replicate A. PHA granules are visible as lighter colored circular inclusion bodies. The calculated PHA yield for this sampling time was 4.3% (dry cell mass basis).

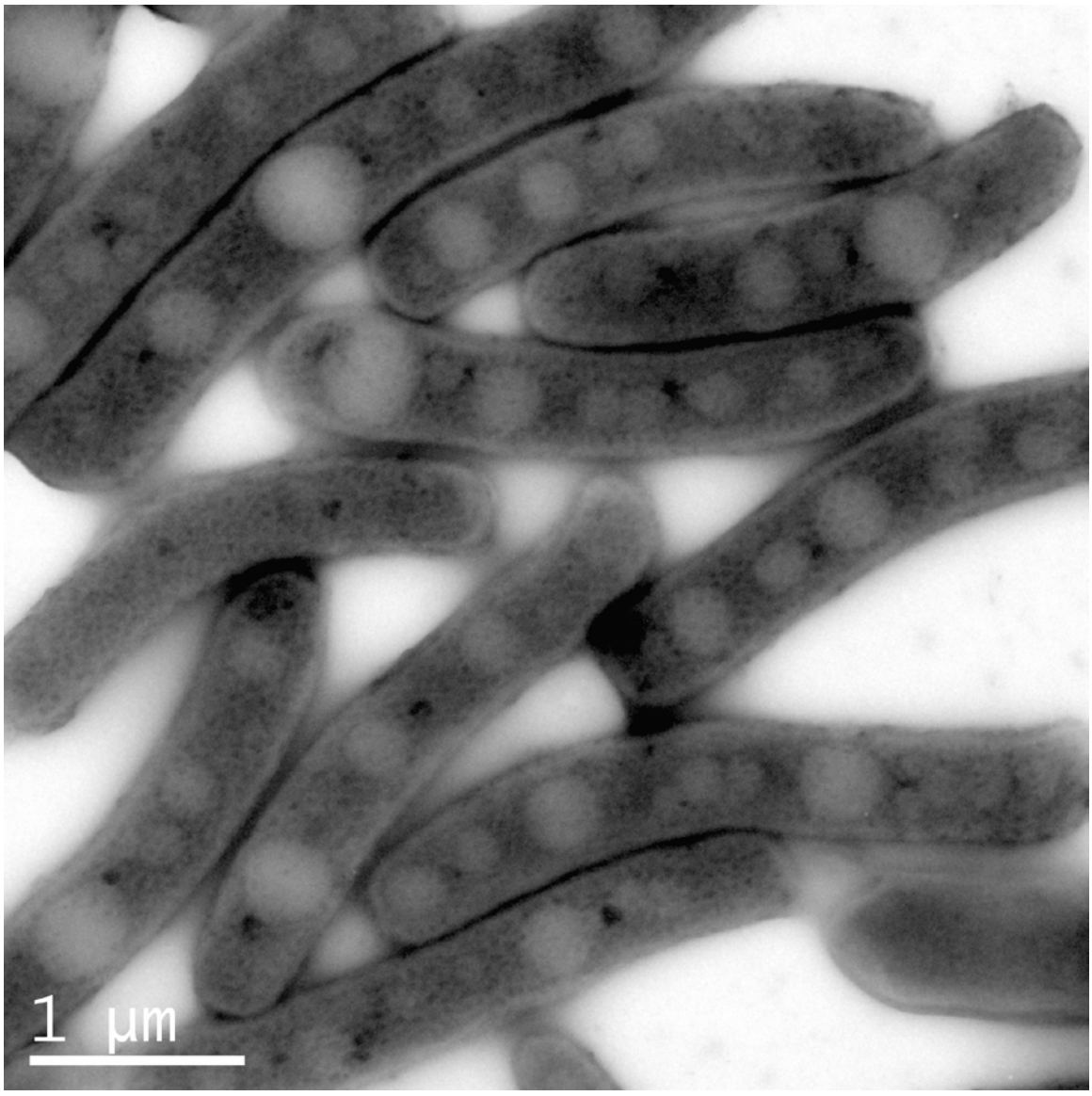

Figure 41. Transmission electron microscope picture of *R. rubrum* at 134 hours elapsed fermentation time of replicate A. PHA granules are visible as lighter colored circular inclusion bodies. The calculated PHA yield for this sampling time was 19% (dry cell mass basis).

5.3.2 *Discussion*

5.3.2.1 *Carbon Availability*

The availability of carbon is important for PHA production. PHA production increases in the presence of excess carbon [164]. In Figure 39, exhaust gas CO concentration decreased then leveled off. The observed CO uptake was likely due to mass transfer limitations. Mass transfer limits carbon uptake via CO, however acetate (and possibly even yeast extract) served as an additional source of carbon. The exhaust gas CO composition reached equilibrium while there was still cell growth (Figure 39). If CO was the only source of carbon, one would have expected the new equilibrium concentration to begin at an elapsed time similar to the start of the stationary growth phase. Instead, cell growth continued after CO concentration reached plateau. In each replicate shown in Figure 39, cell growth reached its plateau only after the CO consumption leveled off, acetate concentration decreased to zero, and PHA yield declined. PHA production likely slowed due to lack of available carbon and as a result, PHA began to be consumed or broken down as a source of carbon in these carbon limiting conditions.

5.3.2.2 *Yeast Extract*

Yeast extract may serve as a source of carbon and nitrogen and could be throwing off the C:N ratio. Kerby et al. noted that CO-dependent growth was enhanced by an undefined component in yeast extract and noticed a decrease in growth by three-fold in cultures grown in media lacking yeast extract [6]. That same

study mentions that a carbon and electron imbalance may be the result of CO dependant consumption of YE components.

CHAPTER 6. CONCLUSIONS

6.1 SYNGAS FERMENTATION FACILITY

The Syngas Fermentation Facility, comprised of five 14 L fermentors along with a custom gas mixing system, was designed and built in 1056 Black Engineering building at Iowa State University. A control program for the Syngas Fermentation System was also developed using National Instruments LabView. The program successfully integrated mass and pressure controllers with BioFlo 110 fermentor controllers for total system control and monitoring, including data logging capabilities. Remote monitoring of the control program was achieved using both remote desktop software as well as custom software for email/text message control and alerts.

6.1.1 *System Limitations*

In order to get the most out of the syngas fermentation control program, it is important to understand its limitations. In terms of hardware, the Alicat mass flow controllers have an accuracy of +/-(0.8% of Reading + 0.2% of Full Scale) [150]. The control program user must be aware of this limitation when setting low flow rates. Also, the Alicat mass flow controllers depend on gas viscosity to calculate mass flows. The complex gas compositions used in the fermentation system are unique and not available as selectable gas mixtures on the Alicat controllers. Therefore, the fermentation station mass flow controllers are set to control N_2. Wilke's viscosity equation for gas mixtures can be used to correct for this discrepancy [165]. For the fermentation hardware, the temperature can only be controlled using the fermentation program when a heating jacket

is used. The heated circulating baths currently used for temperature control are not integrated into the control system.

The fermentation control program cannot detect leaks. The ability to recognize leaks in the system is based on how the user interprets the pressure and mass flow data. Similarly, the fermentation system is not currently capable of monitoring gas cylinder levels. Empty cylinders could be detected by observing the behavior of the control program outputs. The control program can be used to isolate leaks once they are found by shutting off gas flow to the appropriate lines. Gas leaks between the cylinder gas and the gas mixing mass flow controllers can only be mitigated manually.

The remote control and monitoring system monitors all values of the control program when using the remote desktop software. Currently, only mass flow rate and pressure set points of the gas controllers are monitored and controlled via email/text message control. Remote capabilities are useful and convenient, but should not provide a false sense of security. The fermentation system should be monitored in person regularly for proper operation and safety.

In the event of a power failure to the entire system, the mass flow controllers default to an always closed state. When power is returned, the controllers will remain closed. If the control computer loses power or the control program is shut down, the mass flow controllers will hold their current set points if power is maintained to the controllers.

6.2 MEDIA OPTIMIZATION

Statistics were useful in analyzing the subtle differences in the responses of *R. rubrum* to different concentrations of media components. A high carbon to nitrogen ratio was expected for maximizing PHA production, however the opposite was observed. When compared with the literature, the results indicated an unknown presence of bio-available nitrogen [107, 126-128]. Based on preliminary TGA analysis, yeast extract appeared to be a contributor of this nitrogen. Future work could further investigate this hypothesis.

The central composite design experiment failed to produce a significant model to predict the PHA production factor; however, the model developed for predicting dry cell mass was significant. This model for dry cell mass indicated the presence of interaction effects between media components. Based on the model, nominal RRNCO media was not optimized for dry cell mass.

6.3 HARVEST POINT OPTIMIZATION

6.3.1 *Scale Up*

The scaled up fermentation experiments were less difficult to establish culture growth than the smaller scale experiments. The success rate of initial growth was almost 100%, and the stationary phase cell densities were consistently greater. The key enzyme for CO utilization, CODH, is oxygen sensitive [106]. On a smaller scale, oxygen exposure could have a more detrimental effect with less chance for recovery than on a large scale.

The fermentation scale fermentors were purged continuously with simulated syngas. This continuous gassing along with the optimized rushton impeller setup in the fermentors improved mass transfer over the hypovial scale and likely played a major role in the success experienced on the larger scale.

6.3.2 *Harvest Point Indicators*

Cell density and media acetate levels may serve as good indicators of maximum PHA production. PHA production appeared to maximize when cell growth reached late exponential phase or early stationary phase. Maximum PHA corresponded well with the point of acetate exhaustion. Both parameters are relatively inexpensive, quick, and easy to monitor. These characteristics make optical density and media acetate concentration potentially valuable tools for harvest point selection.

6.4 RECOMMENDATIONS FOR FUTURE WORK

6.4.1 *Syngas Fermentation Facility*

The following recommendations would provide enhanced capabilities to the control program depending on future usage requirements and available time and funds to work on the changes.

Currently, the system is not fully capable of monitoring gas cylinder usage. This could be accomplished by adding pressure transducers to the high pressure side of the gas cylinders. With this capability, warnings could be sent out before a cylinder is empty which would avoid gas supply interruption.

Future updates to the program could include streamlining the block diagram to reduce clutter and unnecessary redundancy in the code. Also, the list of email/test message commands could be expanded to include values for the fermentors.

6.4.2 *Yeast Extract Replacement*

Yeast extract may be acting as an additional source of available carbon and nitrogen in the growth media. PHA is also an expensive ingredient, so increasing the amount of yeast extract in the media will also increase the cost of the media. Future investigations could replace yeast extract with a vitamin mixture to better control the carbon to nitrogen ratio in the media.

6.4.3 *Novel Carbon Source Investigation*

Co-polymers of PHA can be customized by varying the carbon source fed to the bacteria [166]. *R. rubrum* grown in RRNCO media currently uses acetate as a carbon source. Acetic acid and other small carboxylic acids are found in the aqueous fraction of bio-oil derived from fast pyrolysis. The aqueous phase of liquid bio-oil may serve as an inexpensive source of carbon and could produce unique PHA co-polymers.

Another interesting idea would be to co-culture *R. rubrum* with an acetogenic syngas organism such as *Clostridium ljungdahlii*. *C. ljungdahlii* produces ethanol and acetic acid as products of syngas fermentation [167]. *R. rubrum,* which has tolerance to exogenous ethanol, could reduce acetic acid concentration in the media by incorporating it into PHA. Should the organisms not form a viable co-culture due to different pH requirements, etc., the spent media from *C. ljungdahllii* could be fed to *R. rubrum* after ethanol extraction.

6.4.4 *Examination of Other Media Components*

This thesis focused on the optimization of carbon and nitrogen sources in RRNCO media. PHA production can be initiated by limited availability of nitrogen, phosphorus, magnesium, sulfate, or oxygen (if aerobic) as well as conditions of excess carbon [107, 126-128]. Future studies could include examining other media components such as biotin, phosphate, and 3-(N-morpholino)propanesulfonic acid (MOPS).

6.4.5 *Measurement Uncertainty Improvement*

A large contributing factor to the uncertainty of the PHA measurement and derived calculations was due to the small sample volumes. Larger sample volumes and/or higher precision analytical equipment could improve the measurement uncertainty.

REFERENCES

1. Choi, D., et al., *A Techno-economic Analysis of Polyhydroxyalkanoate and Hydrogen Production from Syngas Fermentation of Gasified Biomass.* Applied Biochemistry and Biotechnology, 2009.
2. Brandl, H., et al., *Ability of the phototrophic bacterium Rhodospirillum rubrum to produce various poly ([beta]-hydroxyalkanoates): Potential sources for biodegradable polyesters.* International Journal of Biological Macromolecules, 1989. **11**(1): p. 49-55.
3. Ulmer, H.W., et al., *Bacterial production of poly(.beta.-hydroxyalkanoates) containing unsaturated repeating units by Rhodospirillum rubrum*. 1994. p. 1675-1679.
4. Maness, P.-C. and P. Weaver, *Production of poly-3-hydroxyalkanoates from CO and H2 by a novel photosynthetic bacterium.* Applied Biochemistry and Biotechnology, 1994. **45-46**(1): p. 395-406.
5. Do, Y.S., et al., *Growth of Rhodospirillum rubrum on synthesis gas: conversion of CO to H2 and poly-beta-hydroxyalkanoate.* Biotechnol Bioeng, 2007. **97**(2): p. 279-86.
6. Kerby, R.L., P.W. Ludden, and G.P. Roberts, *Carbon monoxide-dependent growth of Rhodospirillum rubrum*. 1995. p. 2241-2244.
7. Brown, R.C., *Biorenewable resources: engineering new products from agriculture*. 1st ed. 2003, Ames: Blackwell.
8. Higman, C. and M. van der Burgt, *Gasification*. 2003, Amsterdam: Elsevier.
9. Simbeck, D.R., et al., *Coal Gasification Guidebook: Status, Applications, and Technologies*. 1993, Palo Alto, CA: Electric Power Research Institute (EPRI).
10. Probstein, R.F. and R.E. Hicks, *Synthetic Fuels*. 2006, Mineola, NY: Dover Publications, Inc.
11. Lath, E. and P. Herbert, *Make CO from Coke, CO2, and O2.* Hydrocarbon Processing, 1986. **65**(8): p. 55-58.
12. McKendry, P., *Energy production from biomass (part 3): gasification technologies.* Bioresource Technology, 2002. **83**: p. 55-63.
13. Stevens, D.J., *Hot Gas Conditioning: Recent Progress with Larger-Scale Biomass Gasification Systems; Update and Summary of Recent Progress*, DOE, Editor. 2001, NREL: Gorden, CO.
14. Probstein, R.F. and R.E. Hicks, *Synthetic fuels*. 1982, New York, NY: McGraw-Hill. 302.
15. Bridgwater, A.V., *The technical and economic feasibility of biomass gasification for power generation.* Fuel and Energy Abstracts, 1995. **36**: p. 269-269.
16. Bredwell, M.D., P. Srivastava, and R.M. Worden, *Reactor Design Issues for Synthesis-Gas Fermentations.* Biotechnology Progress, 1999. **15**(5): p. 834-844.
17. Klasson, K.T., et al., *Biological production of liquid and gaseous fuels from synthesis gas.* Applied Biochemistry and Biotechnology, 1990. **24-25**: p. 857-874.

18. Datar, R.P., et al., *Fermentation of biomass-generated producer gas to ethanol.* Biotechnology and Bioengineering, 2004. **86**(5): p. 587-594.
19. Klasson, K.T., et al., *Bioconversion of synthesis gas into liquid or gaseous fuels.* Enzyme and Microbial Technology, 1992. **14**(8): p. 602-608.
20. Clausen, E.C. and J.L. Gaddy, *Biological Conversion of Synthesis Gas*, in *Topical Report: Economic Evaluations*. 1993, University of Arkansas, Fayetteville, AR for U.S. DOE: Morgantown Energy Technology Center, Morgantown, WV.
21. Balows, A., et al., eds. *The Prokaryotes. A Handbook on the Biology of Bacteria: Ecophysiology, Isolation, Identification, Applications*. 2nd ed. 1992, Springer-Verlag: New York.
22. Madigan, M.T., J.M. Martinko, and J. Parker, *Brock Biology of Microorganisms*. 9th ed. 2000, Englewood Cliffs: Prentice Hall.
23. Klasson, K., et al., *Evaluation of mass-transfer and kinetic parameters for Rhodospirillum rubrum in a continuous stirred tank reactor.* Applied Biochemistry and Biotechnology, 1993. **39-40**(1): p. 549-557.
24. Klasson, K.T., et al., *Biological conversion of synthesis gas into fuels.* International Journal of Hydrogen Energy, 1992. **17**(4): p. 281-288.
25. Younesi, H., et al., *Biohydrogen production in a continuous stirred tank bioreactor from synthesis gas by anaerobic photosynthetic bacterium: Rhodopirillum rubrum.* Bioresource Technology, 2008. **99**(7): p. 2612-2619.
26. Najafpour, G. and H. Younesi, *Bioconversion of synthesis gas to hydrogen using a light-dependent photosynthetic bacterium, Rhodospirillum rubrum* World Journal of Microbiology and Biotechnology, 2007. **Volume 23**(Number 2): p. 275-284.
27. Najafpour, G., H. Younesi, and A.R. Mohamed, *Effect of organic substrate on hydrogen production from synthesis gas using Rhodospirillum rubrum, in batch culture.* Biochemical Engineering Journal, 2004. **21**(2): p. 123-130.
28. Yagi, T., *Enzymic oxidation of carbon monoxide.* Biochim Biophys Acta, 1958. **30**(1): p. 194-195.
29. Uffen, R.L., *Metabolism of carbon monoxide.* Enzyme and Microbial Technology, 1981. **3**: p. 197-206.
30. Kim, Y.M. and G.D. Hegeman, *Oxidation of carbon monoxide by bacteria.* Int. Rev. Cytol., 1983. **81**: p. 1-32.
31. Meyer, O. and H.G. Schlegel, *Biology of Aerobic Carbon Monoxide-Oxidizing Bacteria.* Annual Review of Microbiology, 1983. **37**(1): p. 277-310.
32. Kerby, R.L., et al., *Genetic and physiological characterization of the Rhodospirillum rubrum carbon monoxide dehydrogenase system*. 1992. p. 5284-5294.
33. Brown, R.C., *Hybrid thermochemical/biological processing: Putting the cart before the horse?* Applied Biochemistry and Biotechnology, 2007. **137-140**(1): p. 947-956.
34. Henstra, A.M., et al., *Microbiology of synthesis gas fermentation for biofuel production.* Curr Opin Biotechnol, 2007. **18**(3): p. 200-6.

35. Sharak Genthner, B.R. and M.P. Bryant, *Additional characteristics of one-carbon-compound utilization by Eubacterium limosum and Acetobacterium woodii.* Applied and Environmental Microbiology, 1987. **53**(3): p. 471-476.
36. Diekert, G.B. and R.K. Thauer, *Carbon Monoxide Oxidation by Clostridium thermoaceticum and Clostridium formicoaceticum.* The Journal of Bacteriology, 1978. **136**(2): p. 597-606.
37. Genthner, B.R.S. and M.P. Bryant, *Additional characteristics of one-carbon-compound utilization by Eubacterium limosum and Acetobacterium woodii.* Applied and Environmental Microbiology, 1987. **53**(3): p. 471-476.
38. Genthner, B.R.S. and M.P. Bryant, *Growth of Eubacterium limosum with Carbon Monoxide as the Energy Source.* Applied and Environmental Microbiology, 1982. **43**(1): p. 70-74.
39. Savage, M.D., et al., *Carbon monoxide-dependent chemolithotrophic growth of Clostridium thermoautotrophicum.* Applied and Environmental Microbiology, 1987. **53**(8): p. 1902-1906.
40. Lorowitz, W.H. and M.P. Bryant, *Peptostreptococcus productus strain that grows rapidly with CO as the energy source.* Applied and Environmental Microbiology, 1984. **47**(5): p. 961-964.
41. Abrini, J., H. Naveau, and E.-J. Nyns, *Clostridium autoethanogenum, sp. nov., an anaerobic bacterium that produces ethanol from carbon monoxide.* Archives of Microbiology, 1994. **161**(4): p. 345-351.
42. Tanner, R.S., L.M. Miller, and D. Yang, *Clostridium ljungdahlii sp. nov., an Acetogenic Species in Clostridial rRNA Homology Group I.* International Journal of Systematic Bacteriology, 1993. **43**(2): p. 232-236.
43. Grethlein, A.J., et al., *Evidence for production of n-butanol from carbon monoxide by Butyribacterium methylotrophicum.* Journal of Fermentation and Bioengineering, 1991. **72**(1): p. 58-60.
44. Lynd, L., R. Kerby, and J.G. Zeikus, *Carbon monoxide metabolism of the methylotrophic acidogen Butyribacterium methylotrophicum.* The Journal of Bacteriology, 1982. **149**(1): p. 255-263.
45. Shen, G.J., et al., *Biochemical basis for carbon monoxide tolerance and butanol production by Butyribacterium methylotrophicum.* Applied Microbiology and Biotechnology, 1999. **51**(6): p. 827-832.
46. Liou, J.S.C., et al., *Clostridium carboxidivorans sp. nov., a solvent-producing clostridium isolated from an agricultural settling lagoon, and reclassification of the acetogen Clostridium scatologenes strain SL1 as Clostridium drakei sp. nov.* International Journal of Systematic and Evolutionary Microbiology, 2005. **55**(5): p. 2085-2091.
47. Krumholz, L.R. and M.P. Bryant, *Clostridium pfennigii sp. nov. Uses Methoxyl Groups of Monobenzenoids and Produces Butyrate.* International Journal of Systematic Bacteriology, 1985. **35**(4): p. 454-456.
48. Rother, M. and W.W. Metcalf, *Anaerobic growth of Methanosarcina acetivorans C2A on carbon monoxide: An unusual way of life for a methanogenic archaeon.* Proceedings of the National Academy of Sciences of the United States of America, 2004. **101**(48): p. 16929-16934.

49. Lowe, S.E., M.K. Jain, and J.G. Zeikus, *Biology, ecology, and biotechnological applications of anaerobic bacteria adapted to environmental stresses in temperature, pH, salinity, or substrates.* Microbiol Rev, 1993. **57**(2): p. 451-509.
50. Henstra, A.M., C. Dijkema, and A.J.M. Stams, *Archaeoglobus fulgidus couples CO oxidation to sulfate reduction and acetogenesis with transient formate accumulation.* Environmental Microbiology, 2007. **9**: p. 1836-1841.
51. Parshina, S.N., et al., *Carbon monoxide conversion by thermophilic sulfate-reducing bacteria in pure culture and in co-culture with Carboxydothermus hydrogenoformans.* Applied Microbiology and Biotechnology, 2005. **68**(3): p. 390-396.
52. Daumas, S., R. Cord-Ruwisch, and J.L. Garcia, *Desulfotomaculum geothermicum sp. nov., a thermophilic, fatty acid-degrading, sulfate-reducing bacterium isolated with H2 from geothermal ground water.* Antonie van Leeuwenhoek, 1988. **54**(2): p. 165-178.
53. O'Brien, J.M., et al., *Association of hydrogen metabolism with unitrophic or mixotrophic growth of Methanosarcina barkeri on carbon monoxide.* The Journal of Bacteriology, 1984. **158**(1): p. 373-375.
54. Daniels, L., et al., *Carbon Monoxide Oxidation by Methanogenic Bacteria.* The Journal of Bacteriology, 1977. **132**(1): p. 118-126.
55. Sokolova, T.G., et al., *Carboxydobrachium pacificum gen. nov., sp. nov., a new anaerobic, thermophilic, CO-utilizing marine bacterium from Okinawa Trough.* International Journal of Systematic and Evolutionary Microbiology, 2001. **51**(1): p. 141-149.
56. Slepova, T.V., et al., *Carboxydocella sporoproducens sp. nov., a novel anaerobic CO-utilizing/H2-producing thermophilic bacterium from a Kamchatka hot spring.* International Journal of Systematic and Evolutionary Microbiology, 2006. **56**(4): p. 797-800.
57. Sokolova, T.G., et al., *Carboxydocella thermautotrophica gen. nov., sp. nov., a novel anaerobic, CO-utilizing thermophile from a Kamchatkan hot spring.* International Journal of Systematic and Evolutionary Microbiology, 2002. **52**(6): p. 1961-1967.
58. Svetlitchnyi, V., et al., *Two Membrane-Associated NiFeS-Carbon Monoxide Dehydrogenases from the Anaerobic Carbon-Monoxide-Utilizing Eubacterium Carboxydothermus hydrogenoformans.* The Journal of Bacteriology, 2001. **183**(17): p. 5134-5144.
59. Jung, G.Y., et al., *A new chemoheterotrophic bacterium catalyzing water-gas shift reaction.* Biotechnology Letters, 1999. **21**(10): p. 869-873.
60. Jung, G.Y., et al., *Hydrogen production by a new chemoheterotrophic bacterium Citrobacter sp. Y19.* International Journal of Hydrogen Energy, 2002. **27**(6): p. 601-610.
61. Jung, G.Y., et al., *Isolation and characterization of Rhodopseudomonas palustris P4 which utilizes CO with the production of H2.* Biotechnology Letters, 1999. **21**(6): p. 525-529.
62. Dashekvicz, M.P. and R.L. Uffen, *NOTES: Identification of a Carbon Monoxide-Metabolizing Bacterium as a Strain of Rhodopseudomonas gelatinosa (Molisch)*

van Niel. International Journal of Systematic Bacteriology, 1979. **29**(2): p. 145-148.
63. Uffen, R.L., *Anaerobic growth of a Rhodopseudomonas species in the dark with carbon monoxide as sole carbon and energy substrate.* Proceedings of the National Academy of Sciences of the United States of America, 1976. **73**(9): p. 3298-3302.
64. Sokolova, T.G., et al., *Thermincola carboxydiphila gen. nov., sp. nov., a novel anaerobic, carboxydotrophic, hydrogenogenic bacterium from a hot spring of the Lake Baikal area.* International Journal of Systematic and Evolutionary Microbiology, 2005. **55**(5): p. 2069-2073.
65. Zavarzina, D., et al., *Thermincola ferriacetica sp. nov ., a new anaerobic, thermophilic, facultatively chemolithoautotrophic bacterium capable of dissimilatory Fe(III) reduction.* Extremophiles, 2007. **11**(1): p. 1-7.
66. Sokolova, T.G., et al., *The first evidence of anaerobic CO oxidation coupled with H 2 production by a hyperthermophilic archaeon isolated from a deep-sea hydrothermal vent.* Extremophiles, 2004. **8**(4): p. 317-323.
67. Svetlichnyi, V.A., et al., *Carboxydothermus restrictus sp. nov. - a new thermophilic anaerobic carboxydotrophic bacterium.* Mikrobiologiya, 1994. **63**: p. 523-528.
68. Sokolova, T., et al., *Novel chemolithotrophic, thermophilic, anaerobic bacteria Thermolithobacter ferrireducens gen. nov., sp. nov. and Thermolithobacter carboxydivorans sp. nov.* Extremophiles, 2007. **11**(1): p. 145-157.
69. Sokolova, T.G., et al., *Thermosinus carboxydivorans gen. nov., sp. nov., a new anaerobic, thermophilic, carbon-monoxide-oxidizing, hydrogenogenic bacterium from a hot pool of Yellowstone National Park.* International Journal of Systematic and Evolutionary Microbiology, 2004. **54**(6): p. 2353-2359.
70. Parshina, S.N., et al., *Desulfotomaculum carboxydivorans sp. nov., a novel sulfate-reducing bacterium capable of growth at 100 % CO.* International Journal of Systematic and Evolutionary Microbiology, 2005. **55**(5): p. 2159-2165.
71. Ferry, J.G., *Co Dehydrogenase.* Annual Review of Microbiology, 2003. **49**(1): p. 305-333.
72. Lindahl, P.A., *The Ni-Containing Carbon Monoxide Dehydrogenase Family: Light at the End of the Tunnel?â€* Biochemistry, 2002. **41**(7): p. 2097-2105.
73. Ragsdale, S.W., *Life with Carbon Monoxide*. 2004, Informa Healthcare. p. 165 - 195.
74. Ragsdale, S.W. and M. Kumar, *Nickel-Containing Carbon Monoxide Dehydrogenase/Acetyl-CoA Synthase*. 1996. p. 2515-2540.
75. Oelgeschläger, E. and M. Rother, *Carbon monoxide-dependent energy metabolism in anaerobic bacteria and archaea.* Archives of Microbiology, 2008. **190**(3): p. 257-269.
76. Ferry, J.G., *Co Dehydrogenase.* Annual Review of Microbiology, 1995. **49**(1): p. 305-333.
77. Meyer, O. and M. Rhode, *Enzymology and bioenergetics of carbon monoxide-oxidizing bacteria*, in *Microbial growth on C1 compounds*, R.L. Crawford and

R.S. Hanson, Editors. 1984, American Society for Microbiology: Washington, D.C. p. 26-33.
78. Bonam, D. and P.W. Ludden, *Purification and characterization of carbon monoxide dehydrogenase, a nickel, zinc, iron-sulfur protein, from Rhodospirillum rubrum*. 1987. p. 2980-2987.
79. Bonam, D., S.A. Murrell, and P.W. Ludden, *Carbon monoxide dehydrogenase from Rhodospirillum rubrum.* The Journal of Bacteriology, 1984. **159**(2): p. 693-699.
80. Ensign, S.A. and P.W. Ludden, *Characterization of the CO oxidation/H2 evolution system of Rhodospirillum rubrum. Role of a 22-kDa iron-sulfur protein in mediating electron transfer between carbon monoxide dehydrogenase and hydrogenase*. 1991. p. 18395-18403.
81. Drennan, C.L., et al., *Life on carbon monoxide: X-ray structure of Rhodospirillum rubrum Ni-Fe-S carbon monoxide dehydrogenase.* Proceedings of the National Academy of Sciences of the United States of America, 2001. **98**(21): p. 11973-11978.
82. Spangler, N.J., et al., *Spectroelectrochemical Characterization of the Metal Centers in Carbon Monoxide Dehydrogenase (CODH) and Nickel-deficient CODH from Rhodospirillum rubrum*. 1996. p. 7973-7977.
83. Feng, J. and P.A. Lindahl, *Carbon Monoxide Dehydrogenase from Rhodospirillum rubrum: Effect of Redox Potential on Catalysis&#x2020*. 2004. p. 1552-1559.
84. Drennan, C.L., T.I. Doukov, and S.W. Ragsdale, *The metalloclusters of carbon monoxide dehydrogenase/acetyl-CoA synthase: a story in pictures.* Journal of Biological Inorganic Chemistry, 2004. **9**(5): p. 511-515.
85. Hausinger, R.P., *Ni and CO: more surprises.* Nat Struct Mol Biol, 2003. **10**(4): p. 234-236.
86. Heo, J., C.M. Halbleib, and P.W. Ludden, *Redox-dependent activation of CO dehydrogenase from Rhodospirillum rubrum*. 2001. p. 7690-7693.
87. Vignais, P.M., B. Billoud, and J. Meyer, *Classification and phylogeny of hydrogenases.* FEMS Microbiology Reviews, 2001. **25**(4): p. 455-501.
88. Vignais, P., *Hydrogenases and H+-Reduction in Primary Energy Conservation*, in *Bioenergetics*. 2008. p. 223-252.
89. Muller, M., *Review Article: The hydrogenosome.* Journal of General Microbiology, 1993. **139**(12): p. 2879-2889.
90. Page-Sharp, M., C.A. Behm, and G.D. Smith, *Tritrichomonas foetus and Trichomonas vaginalis: the pattern of inactivation of hydrogenase activity by oxygen and activities of catalase and ascorbate peroxidase.* Microbiology, 1996. **142**(1): p. 207-211.
91. Appel, J. and R. Schulz, *Hydrogen metabolism in organisms with oxygenic photosynthesis: hydrogenases as important regulatory devices for a proper redox poising?* Journal of Photochemistry and Photobiology B: Biology, 1998. **47**(1): p. 1-11.

92. Thomas, H. and J.D. NABER, *Isolation, characterization and N-terminal amino acid sequence of hydrogenase from the green alga Chlamydomonas reinhardtii.* European Journal of Biochemistry, 1993. **214**(2): p. 475-481.
93. Thomas, H., M. Britta, and J.D. NABER, *Induction, localization and metal content of hydrogenase in the green alga Chlamydomonas reinhardtii.* European Journal of Biochemistry, 1994. **222**(3): p. 769-774.
94. Schnackenberg, J., R. Schulz, and H. Senger, *Characterization and purification of a hydrogenase from the eukaryotic green alga Scenedesmus obliquus.* FEBS Letters, 1993. **327**(1): p. 21-24.
95. Ueno, Y., N. Kurano, and S. Miyachi, *Purification and characterization of hydrogenase from the marine green alga, Chlorococcum littorale.* FEBS Letters, 1999. **443**(2): p. 144-148.
96. Florin, L., A. Tsokoglou, and T. Happe, *A Novel Type of Iron Hydrogenase in the Green Alga Scenedesmus obliquus Is Linked to the Photosynthetic Electron Transport Chain.* Journal of Biological Chemistry, 2001. **276**(9): p. 6125-6132.
97. Volbeda, A., et al., *Crystal structure of the nickel-iron hydrogenase from Desulfovibrio gigas.* Nature, 1995. **373**(6515): p. 580-587.
98. Higuchi, Y., T. Yagi, and N. Yasuoka, *Unusual ligand structure in Ni-Fe active center and an additional Mg site in hydrogenase revealed by high resolution X-ray structure analysis.* Structure, 1997. **5**(12): p. 1671-1680.
99. Peters, J.W., *Structure and mechanism of iron-only hydrogenases.* Current Opinion in Structural Biology, 1999. **9**(6): p. 670-676.
100. Nicolet, Y., et al., *Desulfovibrio desulfuricans iron hydrogenase: the structure shows unusual coordination to an active site Fe binuclear center.* 1999. **7**(1): p. 13-23.
101. ZIRNGIBL, C., et al., *H2-forming methylenetetrahydromethanopterin dehydrogenase, a novel type of hydrogenase without iron-sulfur clusters in methanogenic archaea.* European Journal of Biochemistry, 1992. **208**(2): p. 511-520.
102. Lyon, E.J., et al., *UV-A/blue-light inactivation of the metal-free hydrogenase (Hmd) from methanogenic archaea The enzyme contains functional iron after all.* European Journal of Biochemistry, 2004. **271**(1): p. 195-204.
103. Maness, P.C. and P. Weaver, *Evidence for three distinct hydrogenase activities in Rhodospirillum rubrum.* Applied Microbiology and Biotechnology, 2001. **57**(5): p. 751-756.
104. Fox, J.D., et al., *Characterization of the CO-induced, CO-tolerant hydrogenase from Rhodospirillum rubrum and the gene encoding the large subunit of the enzyme.* The Journal of Bacteriology, 1996. **178**(6): p. 1515-1524.
105. Fox, J.D., et al., *Characterization of the region encoding the CO-induced hydrogenase of Rhodospirillum rubrum.* The Journal of Bacteriology, 1996. **178**(21): p. 6200-6208.
106. Bonam, D., et al., *Regulation of carbon monoxide dehydrogenase and hydrogenase in Rhodospirillum rubrum: effects of CO and oxygen on synthesis and activity.* The Journal of Bacteriology, 1989. **171**(6): p. 3102-3107.

107. Dawes, E.A., P.J. Senior, and A.H.R.a.D.W. Tempest, *The Role and Regulation of Energy Reserve Polymers in Micro-organisms*, in *Advances in Microbial Physiology*. 1973, Academic Press. p. 135-266.
108. Jendrossek, D. and R. Handrick, *MICROBIAL DEGRADATION OF POLYHYDROXYALKANOATES*.* Annual Review of Microbiology, 2003. **56**(1): p. 403-432.
109. Choi, G.G., H.W. Kim, and Y.H. Rhee, *Enzymatic and non-enzymatic degradation of poly(3-hydroxybutyrate-co-3-hydroxyvalerate) copolyesters produced by Alcaligenes sp. MT-16.* Journal of Microbiology, 2004. **42**: p. 346-352.
110. Madison, L.L. and G.W. Huisman, *Metabolic Engineering of Poly(3-Hydroxyalkanoates): From DNA to Plastic.* Microbiology and Molecular Biology Reviews, 1999. **63**(1): p. 21-53.
111. Bhatt, R., et al., *PHA-rubber blends: Synthesis, characterization and biodegradation.* Bioresource Technology, 2008. **99**(11): p. 4615-4620.
112. Hazer, B. and A. Steinbüchel, *Increased diversification of polyhydroxyalkanoates by modification reactions for industrial and medical applications.* Applied Microbiology and Biotechnology, 2007. **74**(1): p. 1-12.
113. Lemoigne, M., *Produits de déshydration et de polymerisation de l'acide b-oxobutyrique.* Bull. Soc. Chem. Biol., 1926. **8**: p. 770-782.
114. Griebel, R., Z. Smith, and J.M. Merrick, *Metabolism of poly(Î²-hydroxybutyrate). I. Purification, composition, and properties of native poly(Î²-hydroxybutyrate) granules from Bacillus megaterium.* Biochemistry, 2002. **7**(10): p. 3676-3681.
115. Barnard, G.N. and J.K. Sanders, *The poly-beta-hydroxybutyrate granule in vivo. A new insight based on NMR spectroscopy of whole cells.* Journal of Biological Chemistry, 1989. **264**(6): p. 3286-3291.
116. Gross, R.A., et al., *The biosynthesis and characterization of poly(Î²-hydroxyalkanoates) produced by Pseudomonas oleovorans.* Macromolecules, 2002. **22**(3): p. 1106-1115.
117. Huisman, G.W., et al., *Metabolism of poly(3-hydroxyalkanoates) (PHAs) by Pseudomonas oleovorans. Identification and sequences of genes and function of the encoded proteins in the synthesis and degradation of PHA.* Journal of Biological Chemistry, 1991. **266**(4): p. 2191-2198.
118. Lageveen, R.G., et al., *Formation of Polyesters by Pseudomonas oleovorans: Effect of Substrates on Formation and Composition of Poly-(R)-3-Hydroxyalkanoates and Poly-(R)-3-Hydroxyalkenoates.* Applied and Environmental Microbiology, 1988. **54**(12): p. 2924-2932.
119. Lee, S.Y., *Plastic bacteria? Progress and prospects for polyhydroxyalkanoate production in bacteria.* Trends in Biotechnology, 1996. **14**(11): p. 431-438.
120. Braunegg, G., G. Lefebvre, and K.F. Genser, *Polyhydroxyalkanoates, biopolyesters from renewable resources: Physiological and engineering aspects.* Journal of Biotechnology, 1998. **65**(2-3): p. 127-161.
121. Marchessault, R.H. and G. Yu, *Crystallization and material properties of polyhydroxyalkanoates*, in *Biopolymers* A. Steinbüchel, Editor. 2004, Wiley & Sons: New York. p. 157-248.

122. Sato, H., et al., *Infrared and Raman spectroscopy and quantum chemistry calculation studies of C-H center dot center dot center dot O hydrogen bondings and thermal behavior of biodegradable polyhydroxyalkanoate.* J Mol Struct 2005. **744**: p. 35–46.
123. Tsz-Chun, M., et al., *Microbial synthesis and characterization of physiochemical properties of polyhydroxyalkanoates (PHAs) produced by bacteria isolated from activated sludge obtained from the municipal wastewater works in Hong Kong.* Applied Biochemistry and Biotechnology, 2005. **122**(1): p. 731-739.
124. Marchessault, R.H., *Tender morsels for bacteria: recent developments in microbial polyesters.* Trends Polym. Sci., 1996. **4**: p. 163-168.
125. Sudesh, K., H. Abe, and Y. Doi, *Synthesis, structure and properties of polyhydroxyalkanoates: biological polyesters.* Progress in Polymer Science, 2000. **25**(10): p. 1503-1555.
126. Repaske, R. and A.C. Repaske, *Quantitative requirements for exponential growth of Alcaligenes eutrophus.* Applied and Environmental Microbiology, 1976. **32**(4): p. 585-591.
127. Ward, A.C., B.I. Rowley, and E.A. Dawes, *Effect of Oxygen and Nitrogen Limitation on Poly-{beta}-hydroxybutyrate Biosynthesis in Ammonium-grown Azotobacter beijerinckii.* Journal of General Microbiology, 1977. **102**(1): p. 61-68.
128. Kim, Y. and R. Lenz, *Polyesters from Microorganisms*, in *Biopolyesters*. 2001. p. 51-79.
129. Steinbüchel, A. and H.E. Valentin, *Diversity of bacterial polyhydroxyalkanoic acids.* FEMS Microbiology Letters, 1995. **128**(3): p. 219-228.
130. Merrick, J.M. and M. Doudoroff, *Depolymerization of poly-{beta}-hydroxybutyrate by an intracellular enzyme system.* The Journal of Bacteriology, 1964. **88**(1): p. 60-71.
131. Griebel, R.J. and J.M. Merrick, *Metabolism of Poly-{beta}-Hydroxybutyrate: Effect of Mild Alkaline Extraction on Native Poly-{beta}-Hydroxybutyrate Granules.* The Journal of Bacteriology, 1971. **108**(2): p. 782-789.
132. Verlinden, R.A.J., et al., *Bacterial synthesis of biodegradable polyhydroxyalkanoates.* Journal of Applied Microbiology, 2007. **102**(6): p. 1437-1449.
133. Moskowitz, G.J. and J.M. Merrick, *Metabolism of poly-Beta-hydroxybutyrate. II. Enzymic synthesis of D-(-)-Beta-hydroxybutyryl coenzyme A by an enoyl hydrase from Rhodospirillum rubrum.* Biochemistry, 1969. **8**(7): p. 2748-2755.
134. Ratledge, C. and B. Kristiansen, eds. *Basic Biotechnology*. 2nd ed. 2001 Cambridge University Press: Cambridge.
135. Steinbüchel, A., et al., *Molecular basis for biosynthesis and accumulation of polyhydroxyalkanoic acids in bacteria.* FEMS Microbiology Letters, 1992. **103**(2-4): p. 217-230.
136. Rehm, B.H.A. and A. Steinbüchel, *Biochemical and genetic analysis of PHA synthases and other proteins required for PHA synthesis.* International Journal of Biological Macromolecules, 1999. **25**(1-3): p. 3-19.

137. Hu, W., et al., *Synthesis of polyhydroxyalkanoate (PHA) from excess activated sludge under various oxidation-reduction potentials (ORP) by using acetate and propionate as carbon sources.* Applied Biochemistry and Biotechnology, 2005. **121**(1): p. 289-301.
138. Slater, S., et al., *Multiple beta -Ketothiolases Mediate Poly(beta -Hydroxyalkanoate) Copolymer Synthesis in Ralstonia eutropha.* The Journal of Bacteriology, 1998. **180**(8): p. 1979-1987.
139. Asrar, J. and K.J. Gruys, *Biodegradable polyester Biopol*, in *Biopolymers. Polyesters III - Applications and Commercial Products*, Y. Doi and A. Steinbüchel, Editors. 2002, Wiley-VCH: New York.
140. *Metabolix Company History: Milestones*. 2009 [cited 2009 3 October, 2009]; Available from: http://www.metabolix.com/company/brand_popup.html.
141. Choi, J.-i. and S.Y. Lee, *Process analysis and economic evaluation for Poly(3-hydroxybutyrate) production by fermentation.* Bioprocess and Biosystems Engineering, 1997. **17**(6): p. 335-342.
142. *LabView 8.2*. 2006, National Instruments Corporation: Austin, TX. p. Visual programming software for measurement and automation systems.
143. *AlicatLabView8V01Rev5*. Device Driver 2008 [cited; Available from: http://alicatscientific.com/support.php.
144. *NBS OPC Server Wizard Version.1*. 2007, New Brunswick Scientific Co., Inc.: Edison, NJ.
145. *Modbus FAQ: About Modbus-IDA*. [Web page] 2008 [cited 2008 November 6, 2008]; Available from: http://www.modbus.org/faq.php.
146. Valentine, K., *OGIC_SMTP.vi*. 2003. p. Open source simple email client.
147. Bauer, M. *Email: Save new items immediately as files*. 2006 January 19, 2006 [cited 2006 November 1, 2008]; Available from: http://www.vboffice.net/sample.html?mnu=2&pub=37&lang=en&smp=7&cmd=showitem.
148. *RS485 Adapters, Converters, Isolators, Accessories and Technical Data* 2008 [cited 2008 13 December 2008]; Available from: http://www.bb-elec.com/RS485.asp.
149. *Multi-Drop Box Operating Bulletin*. 2007, Alicat Scientific, Inc.: Tuscon, AZ. p. 1-9.
150. *Operating Manual: 16 Series Mass and Volumetric Precision Gas Flow Controller*. 2008, Alicat Scientific, Inc.: Tuscon, AZ. p. 1-49.
151. *Operating Manual: 16 Digital Pressure and Vacuum Gauges and Controllers*. 2008, Alicat Scientific, Inc.: Tuscon, AZ. p. 1-42.
152. *Guide to Operations: BioFlo 110 Modular Benchtop Fermentor*. 2007, New Brunswick Scientific Co., Inc.: Edison, New Jersey. p. 1-180.
153. *LogMeIn Free*. 2008, LogMeIn, Inc.: Woburn, MA. p. Remote desktop software.
154. Hong, C., H. Hao, and W. Haiyun, *Process optimization for PHA production by activated sludge using response surface methodology.* Biomass and Bioenergy, 2009. **33**(4): p. 721-727.

155. Kumar, P. and T. Satyanarayana, *Optimization of culture variables for improving glucoamylase production by alginate-entrapped Thermomucor indicae-seudaticae using statistical methods.* Bioresource Technology, 2007. **98**(6): p. 1252-1259.
156. Mokhtari-Hosseini, Z.B., et al., *Statistical media optimization for growth and PHB production from methanol by a methylotrophic bacterium.* Bioresource Technology, 2009. **100**(8): p. 2436-2443.
157. Sharma, L., et al., *Process optimization for poly-[beta]-hydroxybutyrate production in a nitrogen fixing cyanobacterium, Nostoc muscorum using response surface methodology.* Bioresource Technology, 2007. **98**(5): p. 987-993.
158. Rekab, K. and M. Shaikh, *Statistical design of experiments with engineering applications*. 2005, Boca Raton: Taylor & Francis.
159. Ungerman, A.J. and T.J. Heindel, *Carbon Monoxide Mass Transfer for Syngas Fermentation in a Stirred Tank Reactor with Dual Impeller Configurations.* Biotechnology Progress, 2007. **23**(3): p. 613-620.
160. Gil, J., et al., *Biomass Gasification in Fluidized Bed at Pilot Scale with Steam and Oxygen Mixtures: Product Distribution for Very Different Operating Conditions.* Energy & Fuels, 1997. **11**(6): p. 1109-1118.
161. Gil, J., et al., *Biomass gasification in atmospheric and bubbling fluidized bed: Effect of the type of gasifying agent on the product distribution.* Biomass and Bioenergy, 1999. **17**(5): p. 389-403.
162. Wang, Y. and C.M. Kinoshita, *Experimental analysis of biomass gasification with steam and oxygen.* Solar Energy 1992. **49**(3): p. 153-158.
163. Figliola, R.S. and D.E. Beasley, *Theory and design for mechanical measurements*. 3rd ed. ed. 2000, New York: John Wiley & Sons Inc.
164. Selao, T.T., S. Nordlund, and A. NoreÌ□n, *Comparative Proteomic Studies in Rhodospirillum rubrum Grown under Different Nitrogen Conditions.* Journal of Proteome Research, 2008. **7**(8): p. 3267-3275.
165. Wilke, C.R., *A Viscosity Equation for Gas Mixtures*. 1950, AIP. p. 517-519.
166. Nikolaos V. Mantzaris, A.S.K., F. Srienc, P. Daoutidis, *Optimal carbon source switching strategy for the production of PHA copolymers*. 2001. p. 727-743.
167. Cotter, J., M. Chinn, and A. Grunden, *Ethanol and acetate production by Clostridium ljungdahlii and Clostridium autoethanogenum using resting cells.* Bioprocess and Biosystems Engineering, 2009. **32**(3): p. 369-380.

Hypovial Data: ***Ammonium Chloride Treatment*** (* = *calculation based on 2 samples*)

Mean

NH_4Cl [mM]	Final OD_{680}	(Dry cell mass)/ 1L [g/L]	(PHA mass)/ 1L [g/L]	PHA mass/ Dry cell mass [%]	Final Acetate [mM]	Acetate Used [mM]	pH	OD * (PHA mass/Dry cell mass)
0	1.251	0.457	0.039	8.6%	5.7	4.3	7.31	0.11
2.5	1.267	0.449	*0.057	*12.7%	6.0	4.0	7.36	0.16
5	1.347	0.464	*0.057	*12.3%	5.6	4.4	7.32	0.17
10	1.361	0.471	0.073	15.4%	6.2	3.8	7.31	0.21
25	1.520	0.523	0.085	16.3%	5.5	4.5	7.27	0.25

Standard Deviation

NH_4Cl [mM]	Final OD_{680}	(Dry cell mass)/ 1L [g/L]	(PHA mass)/ 1L [g/L]	PHA mass/ Dry cell mass [%]	Final Acetate [mM]	Acetate Used [mM]	pH	OD * (PHA mass/Dry cell mass)
0	0.037	0.012	0.006	1.7%	0.2	0.2	0.08	0.02
2.5	0.030	0.004	*0.001	*0.3%	0.1	0.1	0.04	0.01
5	0.097	0.012	*0.007	*1.1%	0.5	0.5	0.02	0.02
10	0.040	0.025	0.004	1.3%	0.1	0.1	0.03	0.01
25	0.013	0.015	0.013	2.8%	0.2	0.2	0.02	0.04

Standard error

NH_4Cl [mM]	Final OD_{680}	(Dry cell mass)/ 1L [g/L]	(PHA mass)/ 1L [g/L]	PHA mass/ Dry cell mass [%]	Final Acetate [mM]	Acetate Used [mM]	pH	OD * (PHA mass/Dry cell mass)
0	0.0214	0.0071	0.0037	1.0%	0.1	0.1	0.05	0.01
2.5	0.0170	0.0022	*0.0006	*0.2%	0.1	0.1	0.02	0.00
5	0.0563	0.0068	*0.0050	*0.8%	0.3	0.3	0.01	0.01
10	0.0234	0.0144	0.0021	0.7%	0.1	0.1	0.02	0.01
25	0.0077	0.0084	0.0077	1.6%	0.1	0.1	0.01	0.03

95% confidence interval (mean +/- values given below)

NH_4Cl [mM]	Final OD_{680}	(Dry cell mass)/ 1L [g/L]	(PHA mass)/ 1L [g/L]	PHA mass/ Dry cell mass [%]	Final Acetate [mM]	Acetate Used [mM]	pH	OD * (PHA mass/Dry cell mass)
0	0.0921	0.0305	0.0160	4.14%	0.5	0.5	0.20	0.05
2.5	0.0733	0.0096	*0.0071	*2.77%	0.3	0.3	0.10	0.06
5	0.2421	0.0291	*0.0635	*9.75%	1.3	1.3	0.05	0.18
10	0.1005	0.0621	0.0089	3.20%	0.2	0.2	0.08	0.03
25	0.0333	0.0361	0.0329	7.00%	0.6	0.6	0.04	0.11

Oneway Analysis of OD By NH4Cl [mM]

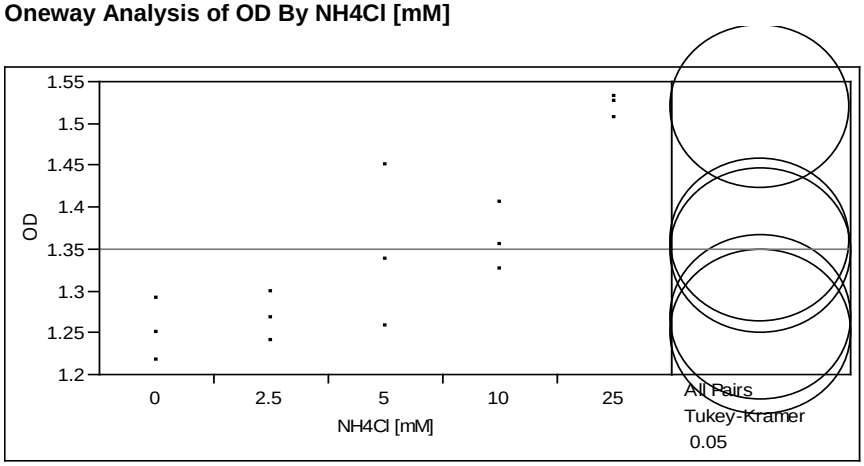

Means Comparisons

Comparisons for all pairs using Tukey-Kramer HSD

q*	Alpha
3.29108	0.05

Abs(Dif)-LSD	25	10	5	2.5	0
25	-0.13992	0.01924	0.03258	0.11241	0.12908
10	0.01924	-0.13992	-0.12659	-0.04676	-0.03009
5	0.03258	-0.12659	-0.13992	-0.06009	-0.04342
2.5	0.11241	-0.04676	-0.06009	-0.13992	-0.12326
0	0.12908	-0.03009	-0.04342	-0.12326	-0.13992

Positive values show pairs of means that are significantly different.

Level		Mean
25	A	1.5196667
10	B	1.3605000
5	B	1.3471667
2.5	B	1.2673333
0	B	1.2506667

Levels not connected by same letter are significantly different.

Level	- Level	Difference	Lower CL	Upper CL	Difference
25	0	0.2690000	0.129076	0.4089237	
25	2.5	0.2523333	0.112410	0.3922570	
25	5	0.1725000	0.032576	0.3124237	
25	10	0.1591667	0.019243	0.2990904	
10	0	0.1098333	-0.030090	0.2497570	
5	0	0.0965000	-0.043424	0.2364237	
10	2.5	0.0931667	-0.046757	0.2330904	
5	2.5	0.0798333	-0.060090	0.2197570	
2.5	0	0.0166667	-0.123257	0.1565904	
10	5	0.0133333	-0.126590	0.1532570	

Oneway Analysis of OD * (PHA mass/Dry cell mass) By NH4Cl [mM]

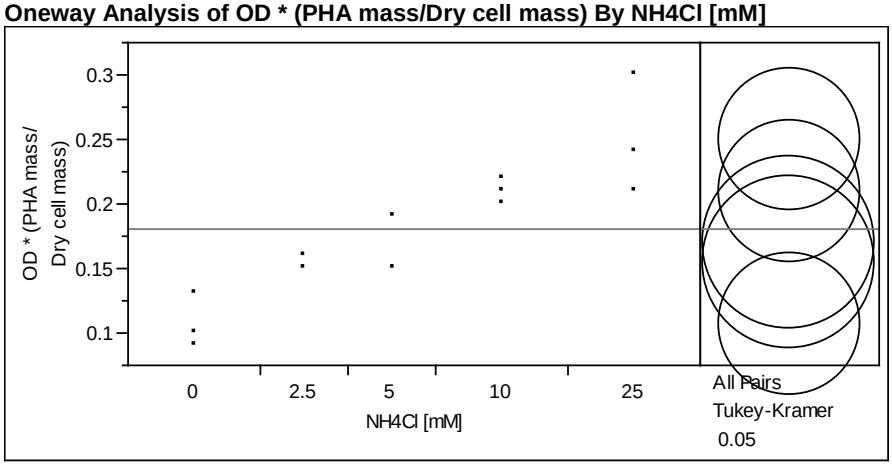

Missing Rows
2

Means Comparisons
Comparisons for all pairs using Tukey-Kramer HSD

q*	Alpha
3.45476	0.05

Abs(Dif)-LSD	25	10	5	2.5	0
25	-0.07800	-0.03800	-0.00720	0.00780	0.06534
10	-0.03800	-0.07800	-0.04720	-0.03220	0.02534
5	-0.00720	-0.04720	-0.09553	-0.08053	-0.02387
2.5	0.00780	-0.03220	-0.08053	-0.09553	-0.03887
0	0.06534	0.02534	-0.02387	-0.03887	-0.07800

Positive values show pairs of means that are significantly different.

Level				Mean
25	A			0.25000000
10	A	B		0.21000000
5	A	B	C	0.17000000
2.5		B	C	0.15500000
0			C	0.10666667

Levels not connected by same letter are significantly different.

Level	- Level	Difference	Lower CL	Upper CL	Difference
25	0	0.1433333	0.065335	0.2213316	
10	0	0.1033333	0.025335	0.1813316	
25	2.5	0.0950000	0.007795	0.1822047	
25	5	0.0800000	-0.007205	0.1672047	
5	0	0.0633333	-0.023871	0.1505380	
10	2.5	0.0550000	-0.032205	0.1422047	
2.5	0	0.0483333	-0.038871	0.1355380	
25	10	0.0400000	-0.037998	0.1179982	
10	5	0.0400000	-0.047205	0.1272047	
5	2.5	0.0150000	-0.080528	0.1105279	

Hypovial Data: *Yeast Extract Treatment*

Mean

YE [g/L]	Final OD_{680}	(Dry cell mass)/ 1L [g/L]	(PHA mass)/ 1L [g/L]	PHA mass/ Dry cell mass [%]	Final Acetate [mM]	Acetate Used [mM]	pH	OD * (PHA mass/Dry cell mass)
0	1.068	0.319	0.0885	27.7%	1.8	8.2	7.46	0.30
0.25	1.263	0.386	0.0919	23.8%	3.9	6.1	7.39	0.30
0.5	1.336	0.402	0.0778	19.3%	5.1	4.9	7.31	0.26
1	1.408	0.421	0.0663	15.7%	7.6	2.4	7.30	0.22
2	1.720	0.508	0.0937	18.4%	11.0	-1.0	7.22	0.32

Standard Deviation

YE [g/L]	Final OD_{680}	(Dry cell mass)/ 1L [g/L]	(PHA mass)/ 1L [g/L]	PHA mass/ Dry cell mass [%]	Final Acetate [mM]	Acetate Used [mM]	pH	OD * (PHA mass/Dry cell mass)
0	0.041	0.012	0.012	3.2%	1.5	1.5	0.01	0.04
2.5	0.030	0.013	0.011	2.2%	1.1	1.1	0.06	0.02
5	0.028	0.005	0.003	0.9%	1.5	1.5	0.02	0.01
10	0.041	0.028	0.009	1.4%	1.8	1.8	0.07	0.03
25	0.050	0.010	0.015	2.8%	2.8	2.8	0.02	0.05

Standard error

YE [g/L]	Final OD_{680}	(Dry cell mass)/ 1L [g/L]	(PHA mass)/ 1L [g/L]	PHA mass/ Dry cell mass [%]	Final Acetate [mM]	Acetate Used [mM]	pH	OD * (PHA mass/Dry cell mass)
0	0.0239	0.0068	0.0072	1.8%	0.8	0.8	0.01	0.02
2.5	0.0172	0.0073	0.0061	1.3%	0.6	0.6	0.04	0.01
5	0.0162	0.0029	0.0017	0.5%	0.8	0.8	0.01	0.00
10	0.0238	0.0160	0.0055	0.8%	1.0	1.0	0.04	0.01
25	0.0287	0.0059	0.0087	1.6%	1.6	1.6	0.01	0.03

95% confidence interval (mean +/- values given below)

YE [g/L]	Final OD_{680}	(Dry cell mass)/ 1L [g/L]	(PHA mass)/ 1L [g/L]	PHA mass/ Dry cell mass [%]	Final Acetate [mM]	Acetate Used [mM]	pH	OD * (PHA mass/Dry cell mass)
0	0.1027	0.0291	0.0308	7.90%	3.6	3.6	0.03	0.11
2.5	0.0739	0.0313	0.0262	5.44%	2.7	2.7	0.16	0.05
5	0.0698	0.0126	0.0073	2.23%	3.6	3.6	0.05	0.02
10	0.1023	0.0689	0.0235	3.50%	4.4	4.4	0.17	0.06
25	0.1233	0.0253	0.0373	7.00%	7.0	7.0	0.04	0.12

Oneway Analysis of OD By YE [g/L]

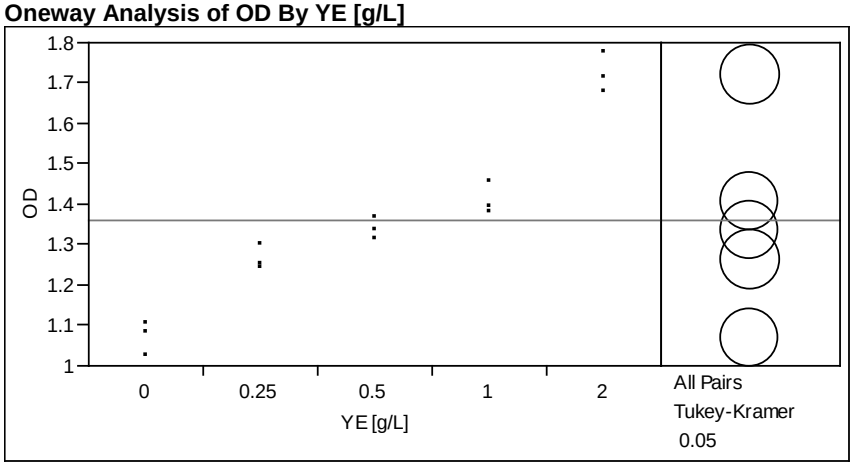

Means Comparisons
Comparisons for all pairs using Tukey-Kramer HSD

q*	Alpha
3.29108	0.05

Abs(Dif)-LSD	2	1	0.5	0.25	0
2	-0.10438	0.20762	0.27979	0.35279	0.54795
1	0.20762	-0.10438	-0.03221	0.04079	0.23595
0.5	0.27979	-0.03221	-0.10438	-0.03138	0.16379
0.25	0.35279	0.04079	-0.03138	-0.10438	0.09079
0	0.54795	0.23595	0.16379	0.09079	-0.10438

Positive values show pairs of means that are significantly different.

Level				Mean
2	A			1.7198333
1		B		1.4078333
0.5		B	C	1.3356667
0.25			C	1.2626667
0			D	1.0675000

Levels not connected by same letter are significantly different.

Level	- Level	Difference	Lower CL	Upper CL	Difference
2	0	0.6523333	0.547955	0.7567119	
2	0.25	0.4571667	0.352788	0.5615453	
2	0.5	0.3841667	0.279788	0.4885453	
1	0	0.3403333	0.235955	0.4447119	
2	1	0.3120000	0.207621	0.4163786	
0.5	0	0.2681667	0.163788	0.3725453	
0.25	0	0.1951667	0.090788	0.2995453	
1	0.25	0.1451667	0.040788	0.2495453	
0.5	0.25	0.0730000	-0.031379	0.1773786	
1	0.5	0.0721667	-0.032212	0.1765453	

Oneway Analysis of OD * (PHA mass/Dry cell mass) By YE [g/L]

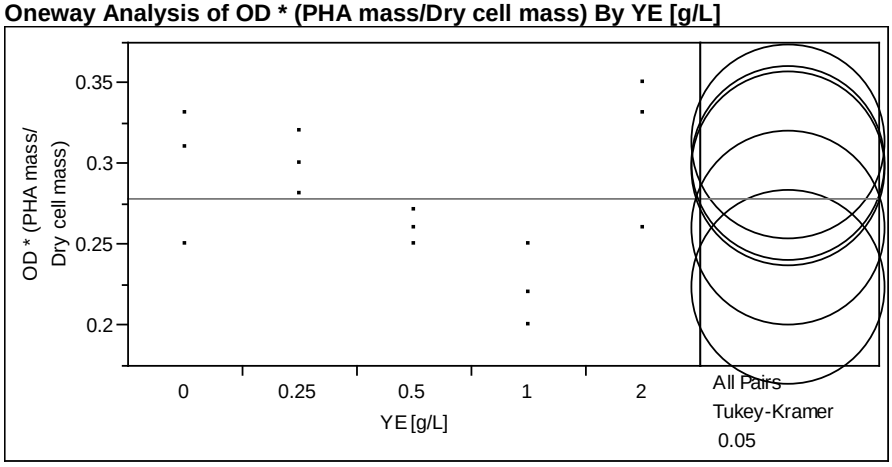

Means Comparisons
Comparisons for all pairs using Tukey-Kramer HSD

q*	Alpha
3.29108	0.05

Abs(Dif)-LSD	**2**	**0.25**	**0**	**0.5**	**1**
2	-0.08582	-0.07249	-0.06915	-0.03249	0.00418
0.25	-0.07249	-0.08582	-0.08249	-0.04582	-0.00915
0	-0.06915	-0.08249	-0.08582	-0.04915	-0.01249
0.5	-0.03249	-0.04582	-0.04915	-0.08582	-0.04915
1	0.00418	-0.00915	-0.01249	-0.04915	-0.08582

Positive values show pairs of means that are significantly different.

Level			**Mean**
2	A		0.31333333
0.25	A	B	0.30000000
0	A	B	0.29666667
0.5	A	B	0.26000000
1		B	0.22333333

Levels not connected by same letter are significantly different.

Level	**- Level**	**Difference**	**Lower CL**	**Upper CL**	**Difference**
2	1	0.0900000	0.004179	0.1758209	
0.25	1	0.0766667	-0.009154	0.1624876	
0	1	0.0733333	-0.012488	0.1591543	
2	0.5	0.0533333	-0.032488	0.1391543	
0.25	0.5	0.0400000	-0.045821	0.1258209	
0	0.5	0.0366667	-0.049154	0.1224876	
0.5	1	0.0366667	-0.049154	0.1224876	
2	0	0.0166667	-0.069154	0.1024876	
2	0.25	0.0133333	-0.072488	0.0991543	
0.25	0	0.0033333	-0.082488	0.0891543	

Hypovial Data: ***Sodium Acetate Treatment*** (* = *calculation based on 2 samples*)

Mean

NaAct [mM]	Final OD_{680}	(Dry cell mass)/ 1L [g/L]	(PHA mass)/ 1L [g/L]	PHA mass/ Dry cell mass [%]	Final Acetate [mM]	Acetate Used [mM]	pH	OD * (PHA mass/Dry cell mass)
0	1.326	0.424	0.089	21.1%	-0.1	0.1	7.31	0.28
2.5	1.660	0.511	0.129	25.1%	-0.1	2.6	7.33	0.42
5	1.689	0.510	0.120	23.5%	1.4	3.6	7.33	0.40
10	1.520	0.457	*0.066	*14.4%	6.5	3.5	7.30	0.22
25	1.366	0.399	0.052	13.0%	19.5	5.5	7.31	0.18

Standard Deviation

NaAct [mM]	Final OD_{680}	(Dry cell mass)/ 1L [g/L]	(PHA mass)/ 1L [g/L]	PHA mass/ Dry cell mass [%]	Final Acetate [mM]	Acetate Used [mM]	pH	OD * (PHA mass/Dry cell mass)
0	0.018	0.007	0.009	2.6%	0.0	0.0	0.00	0.03
2.5	0.038	0.007	0.009	1.4%	0.0	0.0	0.00	0.03
5	0.030	0.022	0.008	1.6%	0.0	0.0	0.02	0.02
10	0.009	0.010	*0.015	*2.8%	0.0	0.0	0.04	0.04
25	0.054	0.012	0.015	3.7%	0.1	0.1	0.07	0.05

Standard error

NaAct [mM]	Final OD_{680}	(Dry cell mass)/ 1L [g/L]	(PHA mass)/ 1L [g/L]	PHA mass/ Dry cell mass [%]	Final Acetate [mM]	Acetate Used [mM]	pH	OD * (PHA mass/Dry cell mass)
0	0.0105	0.0040	0.0054	1.5%	0.0	0.0	0.00	0.02
2.5	0.0221	0.0040	0.0052	0.8%	0.0	0.0	0.00	0.02
5	0.0170	0.0126	0.0045	0.9%	0.0	0.0	0.01	0.01
10	0.0050	0.0058	*0.0106	*2.0%	0.0	0.0	0.02	0.03
25	0.0314	0.0068	0.0085	2.1%	0.0	0.0	0.04	0.03

95% confidence interval (mean +/- values given below)

NaAct [mM]	Final OD_{680}	(Dry cell mass)/ 1L [g/L]	(PHA mass)/ 1L [g/L]	PHA mass/ Dry cell mass [%]	Final Acetate [mM]	Acetate Used [mM]	pH	OD * (PHA mass/Dry cell mass)
0	0.0453	0.0172	0.0231	6.35%	0.0	0.0	0.00	0.08
2.5	0.0950	0.0172	0.0223	3.54%	0.0	0.0	0.00	0.08
5	0.0733	0.0543	0.0193	4.02%	0.1	0.1	0.05	0.06
10	0.0215	0.0248	*0.1341	*25.35%	0.1	0.1	0.09	0.40
25	0.1352	0.0291	0.0368	9.19%	0.2	0.2	0.17	0.12

Oneway Analysis of OD By NaAct [mM]

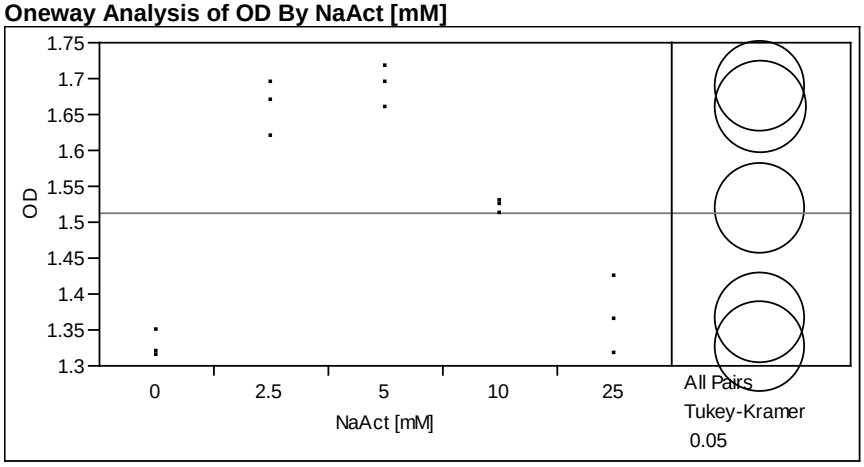

Means Comparisons
Comparisons for all pairs using Tukey-Kramer HSD

q*	Alpha
3.29108	0.05

Abs(Dif)-LSD	5	2.5	10	25	0
5	-0.09075	-0.06208	0.07825	0.23142	0.27225
2.5	-0.06208	-0.09075	0.04959	0.20275	0.24359
10	0.07825	0.04959	-0.09075	0.06242	0.10325
25	0.23142	0.20275	0.06242	-0.09075	-0.04991
0	0.27225	0.24359	0.10325	-0.04991	-0.09075

Positive values show pairs of means that are significantly different.

Level			Mean
5	A		1.6885000
2.5	A		1.6598333
10		B	1.5195000
25		C	1.3663333
0		C	1.3255000

Levels not connected by same letter are significantly different.

Level	- Level	Difference	Lower CL	Upper CL	Difference
5	0	0.3630000	0.272254	0.4537461	
2.5	0	0.3343333	0.243587	0.4250795	
5	25	0.3221667	0.231421	0.4129128	
2.5	25	0.2935000	0.202754	0.3842461	
10	0	0.1940000	0.103254	0.2847461	
5	10	0.1690000	0.078254	0.2597461	
10	25	0.1531667	0.062421	0.2439128	
2.5	10	0.1403333	0.049587	0.2310795	
25	0	0.0408333	-0.049913	0.1315795	
5	2.5	0.0286667	-0.062079	0.1194128	

Oneway Analysis of OD * (PHA mass/Dry cell mass) By NaAct [mM]

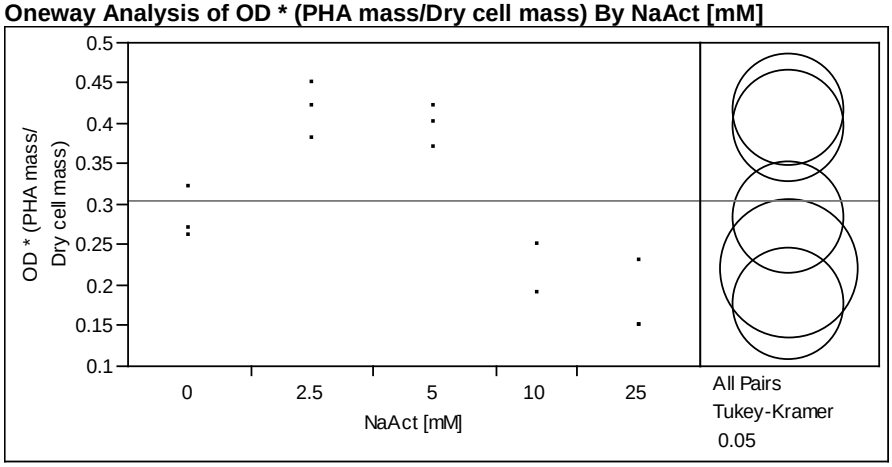

Missing Rows
1

Means Comparisons
Comparisons for all pairs using Tukey-Kramer HSD

q*	Alpha
3.36259	0.05

Abs(Dif)-LSD	2.5	5	0	10	25
2.5	-0.09969	-0.07969	0.03364	0.08520	0.14031
5	-0.07969	-0.09969	0.01364	0.06520	0.12031
0	0.03364	0.01364	-0.09969	-0.04813	0.00697
10	0.08520	0.06520	-0.04813	-0.12210	-0.06813
25	0.14031	0.12031	0.00697	-0.06813	-0.09969

Positive values show pairs of means that are significantly different.

Level				Mean
2.5	A			0.41666667
5	A			0.39666667
0		B		0.28333333
10		B	C	0.22000000
25			C	0.17666667

Levels not connected by same letter are significantly different.

Level	- Level	Difference	Lower CL	Upper CL	Difference
2.5	25	0.2400000	0.140306	0.3396944	
5	25	0.2200000	0.120306	0.3196944	
2.5	10	0.1966667	0.085205	0.3081284	
5	10	0.1766667	0.065205	0.2881284	
2.5	0	0.1333333	0.033639	0.2330278	
5	0	0.1133333	0.013639	0.2130278	
0	25	0.1066667	0.006972	0.2063611	
0	10	0.0633333	-0.048128	0.1747951	
10	25	0.0433333	-0.068128	0.1547951	
2.5	5	0.0200000	-0.079694	0.1196944	

APPENDIX II

Central Composite Design Raw Data (*nr* = not recorded)

Standard Order	NH4Cl [mM]	YE [g/L]	NaAct [mM]	O.D. Abs. 680 nm	DCM [g/L]	PHA [g/L]	PHA/DCM [%]	Final Acetate [mM]	pH	OD x PHA/DCM
1	7.9	0.4	4.2	0.9	0.393	0.063	16.10	-0.4	7.12	0.148
2	7.9	0.4	4.2	1.0	0.421	0.039	9.23	-0.4	7.13	0.089
3	29.5	0.4	4.2	0.9	0.393	0.072	18.36	-1.2	7.18	0.162
4	29.5	0.4	4.2	0.9	0.377	0.042	11.21	-1.3	7.18	0.097
5	7.9	1.6	4.2	1.6	0.673	0.084	12.54	-1.6	6.97	0.197
6	7.9	1.6	4.2	1.6	0.686	0.040	5.83	-2.0	6.98	0.093
7	29.5	1.6	4.2	1.4	0.588	0.059	10.02	-2.9	6.95	0.137
8	29.5	1.6	4.2	1.4	0.600	0.040	6.67	-3.0	6.92	0.095
9	7.9	0.4	15.8	0.8	0.363	0.034	9.48	1.2	7.19	0.077
10	7.9	0.4	15.8	0.9	0.414	0.034	8.31	1.1	7.24	0.074
11	29.5	0.4	15.8	0.7	0.278	0.045	16.08	0.0	7.29	0.106
12	29.5	0.4	15.8	0.7	0.318	0.011	3.50	0.1	7.20	0.026
13	7.9	1.6	15.8	1.4	0.566	0.050	8.84	-0.3	7.08	0.119
14	7.9	1.6	15.8	1.4	0.586	0.054	9.30	-0.1	7.08	0.128
15	29.5	1.6	15.8	1.0	0.397	0.066	16.53	-2.6	7.13	0.167
16	29.5	1.6	15.8	1.1	0.466	0.040	8.59	-1.9	7.08	0.100
17	0.0	1.0	10.0	1.1	0.477	0.057	11.89	0.2	7.13	0.133
18	0.0	1.0	10.0	1.3	0.543	0.048	8.79	0.5	7.10	0.111
19	37.4	1.0	10.0	1.0	0.382	0.030	7.85	-1.8	7.12	0.078
20	37.4	1.0	10.0	1.0	0.392	0.014	3.68	-1.6	7.11	0.036
21	18.7	0.0	10.0	0.8	0.306	0.080	26.18	1.6	7.23	0.200
22	18.7	0.0	10.0	0.8	0.316	0.041	13.03	1.7	7.20	0.099
23	18.7	2.0	10.0	1.4	0.603	0.048	7.92	-2.4	6.97	0.114
24	18.7	2.0	10.0	1.7	0.706	0.060	8.50	-1.9	6.94	0.147
25	18.7	1.0	0.0	1.3	0.544	0.066	12.04	-2.3	7.07	0.161
26	18.7	1.0	0.0	1.4	0.590	0.079	13.37	-2.0	7.08	0.193
27	18.7	1.0	20.0	1.0	0.416	0.030	7.30	-0.1	7.18	0.070
28	18.7	1.0	20.0	1.1	0.437	0.050	11.45	0.2	7.13	0.123
29	18.7	1.0	10.0	1.1	0.472	0.048	10.12	-0.5	7.10	0.108
30	18.7	1.0	10.0	1.1	0.504	0.011	2.20	-0.6	7.08	0.025
31	18.7	1.0	10.0	1.1	0.477	0.036	7.46	-0.8	7.14	0.083
32	18.7	1.0	10.0	1.0	0.467	0.041	8.81	-0.9	7.12	0.092
33	18.7	1.0	10.0	1.2	0.527	0.049	9.28	-0.5	7.04	0.112
34	18.7	1.0	10.0	1.2	0.482	0.016	3.23	-0.5	7.09	0.039
35	18.7	1.0	10.0	1.1	0.466	0.043	9.31	-0.8	7.09	0.105
36	18.7	1.0	10.0	1.2	0.468	*nr*	*nr*	-0.9	7.20	*nr*

Large Fermentor Data: *Replicate A* (*nr* = not recorded)

Elapsed time	OD	Dry Cell Mass [g/L]	*Dry Cell Mass Uncertainty [%]*	PHA [g/L]	*PHA Uncertainty [%]*	PHA/DCM [%]	*PHA/DCM Uncertainty [%]*	Acetate [mM]	pH
0:00	0.122	*nr*	*nr*	*nr*	*nr*	*nr*	*nr*	2.5	*nr*
8:29	0.294	*nr*	*nr*	*nr*	*nr*	*nr*	*nr*	3.8	*nr*
10:49	0.382	0.152	*8%*	0.009	*73%*	6.2%	*74%*	4.5	*nr*
20:42	*0.428*	0.153	*2%*	0.007	*48%*	4.3%	*48%*	5.0	*nr*
35:28	0.482	0.179	*3%*	0.010	*35%*	5.8%	*35%*	5.1	*nr*
45:45	0.584	*nr*	*nr*	*nr*	*nr*	*nr*	*nr*	5.1	*nr*
59:42	0.764	0.309	*2%*	0.027	*12%*	8.6%	*12%*	4.9	*nr*
82:11	*nr*	0.390	*3%*	0.053	*16%*	13.7%	*16%*	3.4	*nr*
106:17	*nr*	0.552	*2%*	0.092	*9%*	16.6%	*10%*	2.3	*nr*
133:46	*nr*	0.658	*2%*	0.125	*8%*	19.0%	*8%*	0.2	*nr*
136:38	1.959	*nr*	*nr*	*nr*	*nr*	*nr*	*nr*	*0.0*	*nr*
143:53	2.017	*nr*	*nr*	*nr*	*nr*	*nr*	*nr*	*0.0*	*nr*
157:18	2.025	0.719	*2%*	0.133	*5%*	18.5%	*5%*	0.0	*nr*
182:19	2.227	0.752	*2%*	0.135	*4%*	18.0%	*5%*	0.0	*nr*
203:14	2.221	0.754	*7%*	0.133	*21%*	17.7%	*22%*	0.0	*nr*
226:39	2.132	0.816	*8%*	0.131	*23%*	16.0%	*24%*	0.0	*nr*
251:05	2.191	0.743	*6%*	0.099	*24%*	13.3%	*25%*	0.0	*nr*
276:39	2.237	0.785	*7%*	0.089	*27%*	11.4%	*28%*	0.0	*nr*

Large Fermentor Data: *Replicate B* (*nr* = not recorded)

Elapsed time	OD	Dry Cell Mass [g/L]	*Dry Cell Mass Uncertainty [%]*	PHA [g/L]	*PHA Uncertainty [%]*	PHA/DCM [%]	*PHA/DCM Uncertainty [%]*	Acetate [mM]	pH
0:00	0.093	*nr*	*nr*	*nr*	*nr*	*nr*	*nr*	1.9	6.84
23:25	0.315	0.107	*5%*	0.004	*107%*	3.4%	*107%*	5.0	6.90
47:55	0.273	0.098	*7%*	0.005	*74%*	5.6%	*74%*	5.8	6.81
71:50	*nr*	0.153	*5%*	0.011	*46%*	7.0%	*46%*	6.0	6.79
95:20	0.953	0.338	*2%*	0.029	*22%*	8.6%	*22%*	5.1	6.92
118:30	1.506	0.539	*4%*	0.086	*6%*	15.9%	*7%*	2.3	6.93
139:15	1.911	0.666	*3%*	0.118	*7%*	17.7%	*7%*	0.9	6.93
163:25	2.264	0.785	*2%*	0.139	*7%*	17.8%	*7%*	0.0	7.05
187:45	2.511	0.918	*2%*	0.140	*6%*	15.2%	*6%*	0.0	7.06
214:40	2.741	0.909	*3%*	0.120	*6%*	13.2%	*7%*	0.0	7.01
238:43	2.908	0.990	*2%*	0.096	*9%*	9.7%	*9%*	0.0	6.95
262:50	2.964	0.953	*7%*	0.098	*27%*	10.3%	*28%*	0.0	7.00
282:50	2.744	1.095	*6%*	0.076	*28%*	6.9%	*28%*	0.0	6.99
310:55	2.842	0.917	*6%*	0.040	*66%*	4.4%	*67%*	0.0	7.13

Large Fermentor Data: ***Replicate C*** (*nr* = not recorded)

Elapsed time	OD	Dry Cell Mass [g/L]	*Dry Cell Mass Uncertainty [%]*	PHA [g/L]	*PHA Uncertainty [%]*	PHA/DCM [%]	*PHA/DCM Uncertainty [%]*	Acetate [mM]	pH
0:00	0.092	*nr*	*nr*	*nr*	*nr*	*nr*	*nr*	2.6	6.77
23:25	0.313	0.105	*7%*	0.005	*97%*	4.6%	*98%*	5.2	6.87
47:55	0.055	0.099	*6%*	0.004	*123%*	4.4%	*123%*	4.4	6.79
71:50	*nr*	0.161	*3%*	0.007	*67%*	4.2%	*67%*	4.2	6.77
95:20	0.889	0.312	*5%*	0.024	*42%*	7.5%	*43%*	5.5	6.97
118:30	1.312	0.467	*3%*	0.062	*13%*	13.2%	*14%*	3.5	6.94
139:15	1.665	0.605	*3%*	0.090	*10%*	14.9%	*11%*	2.5	6.92
163:25	2.135	0.711	*2%*	0.104	*7%*	14.6%	*8%*	0.5	7.03
187:45	2.294	0.812	*2%*	0.123	*6%*	15.2%	*7%*	0.0	7.03
214:40	2.639	0.857	*2%*	0.138	*5%*	16.1%	*6%*	0.0	6.98
238:44	2.857	0.955	*2%*	0.172	*5%*	18.0%	*5%*	0.0	6.98
262:47	3.025	0.886	*8%*	0.137	*20%*	15.4%	*22%*	0.0	6.99
282:50	2.749	1.074	*5%*	0.104	*19%*	9.7%	*20%*	0.0	6.98
310:55	2.840	0.915	*6%*	0.075	*23%*	8.2%	*24%*	0.0	7.10

APPENDIX IV

General Propagation of Uncertainty to a Result:

$$R' = \bar{R} \pm u_R \quad (P\%)$$

$$\bar{R} = f_1\{\bar{x}_1, \bar{x}_2, \dots, \bar{x}_L\}$$

$$u_R = f_2\{(B)_{x_1}, (B)_{x_2}, \dots, (B)_{x_L}; (P)_{x_1}, (P)_{x_2}, \dots, (P)_{x_L}\}$$

$$u_R = \sqrt{{B_R}^2 + \left(t_{v,95} P_R\right)^2}$$

Precision Index (propagation of precision through the variables):

$$P_R = \pm \sqrt{\sum_{i=1}^{L} \left[\theta_i (P)_{x_i}\right]^2}$$

Results Bias Limit (propagation of bias through the variables):

$$B_R = \pm \sqrt{\sum_{i=1}^{L} \left[\theta_i (B)_{x_i}\right]^2}$$

R= result
R'= best estimate of true value
u = uncertainty
P= precision index
B= bias limit
θ = sensitivity index
t = t-statistic

Dry Cell Mass error analysis (dcm) [g]:

dcm = dry cell mass [g]
x_1= pre mass of centrifuge tube
x_2= post mass of centrifuge tube
P_{xi} = precision error
S_{xi} = standard deviation
B_{xi} = bias error
e_1=instrument repeatability
e_2=instrument linearity

$$dcm = f(x_1, x_2) = x_2 - x_1$$

$$dcm' = \overline{dcm} \pm u_{dcm} \quad (P\%)$$

$$\overline{dcm} = f(\bar{x}_1, \bar{x}_2) = \bar{x}_2 - \bar{x}_1$$

$$\theta_{x_1} = \frac{\partial dcm}{\partial x_1}\Big|_{x=\bar{x}}$$

$$\theta_{x_2} = \frac{\partial dcm}{\partial x_2}\Big|_{x=\bar{x}}$$

$$P_{x_i} = \frac{S_{x_i}}{N^{1/2}}$$

$$B_{x_i} = \sqrt{{e_1}^2 + {e_2}^2}$$

$$P_{dcm} = \pm\sqrt{\left[\theta_{x_1}(P)_{x_1}\right]^2 + \left[\theta_{x_2}(P)_{x_2}\right]^2}$$

$$B_{dcm} = \pm\sqrt{\left[\theta_{x_1}(B)_{x_1}\right]^2 + \left[\theta_{x_2}(B)_{x_2}\right]^2}$$

$$u_{dcm} = \sqrt{{B_{dcm}}^2 + \left(t_{v,95}P_{dcm}\right)^2}$$

Dry Cell Mass error analysis (dcm_v) [g/L]:

dcm_v = volumetric dry cell mass [g/L]
V_S = sample volume [L]
res = resolution of graduated cylinder used for volume measurement

$$dcm_v = f(dcm, V_s) = \frac{dcm}{V_s} \times 1000$$

$$dcm_v{}' = \overline{dcm_v} \pm u_{dcm_v} \quad (P\%)$$

$$\overline{dcm_v} = f_1\{\overline{dcm}, V_s\} = \frac{\overline{pha}}{V_s} \times 1000$$

$$\theta_{dcm} = \frac{\partial dcm_v}{\partial dcm}\Big|_{dcm=\overline{dcm}} = \frac{1}{V_s} \times 1000$$

$$\theta_{V_s} = \frac{\partial dcm_v}{\partial V_s}\Big|_{V_s=\overline{V_s}} = \frac{-dcm}{{V_s}^2} \times 1000$$

$$u_{V_s} = B_{V_s} = \frac{1}{2} res$$

$$u_{dcm_v} = \pm\sqrt{(\theta_{dcm} \times u_{dcm}) + (\theta_{V_s} \times u_{V_s})}$$

PHA error analysis (pha) [g]:

pha = PHA mass [g]
y_1= pre mass of culture tube
y_2= post mass of culture tube
P_{xi} = precision error
S_{xi} = standard deviation
B_{xi} = bias error
e_1=instrument repeatability
e_2=instrument linearity

$$pha = f(y_1, y_2) = y_2 - y_1$$

$$pha' = \overline{pha} \pm u_{pha} \quad (P\%)$$

$$\overline{pha} = f(\bar{y}_1, \bar{y}_2) = \bar{y}_2 - \bar{y}_1$$

$$\theta_{y_1} = \frac{\partial pha}{\partial y_1}\Big|_{y=\bar{y}}$$

$$\theta_{y_2} = \frac{\partial pha}{\partial y_2}\Big|_{y=\bar{y}}$$

$$P_{y_i} = \frac{S_{y_i}}{N^{1/2}}$$

$$B_{y_i} = \sqrt{{e_1}^2 + {e_2}^2}$$

$$P_{pha} = \pm\sqrt{\left[\theta_{y_1}(P)_{y_1}\right]^2 + \left[\theta_{y_2}(P)_{y_2}\right]^2}$$

$$B_{pha} = \pm\sqrt{\left[\theta_{y_1}(B)_{y_1}\right]^2 + \left[\theta_{y_2}(B)_{y_2}\right]^2}$$

$$u_{pha} = \sqrt{{B_{pha}}^2 + \left(t_{v,95}P_{pha}\right)^2}$$

PHA error analysis (pha_v) [g/L]:

pha_v = volumetric PHA mass [g/L]
V_S = sample volume [L]
res = resolution of graduated cylinder used for volume measurement

$$pha_v = f(pha, V_s) = \frac{pha}{V_s} \times 1000$$

$$pha_v{}' = \overline{pha_v} \pm u_{pha_v} \quad (P\%)$$

$$\overline{pha_v} = f_1\{\overline{pha}, V_s\} = \frac{\overline{pha}}{V_s} \times 1000$$

$$\theta_{pha} = \frac{\partial pha_v}{\partial pha}\Big|_{pha=\overline{pha}} = \frac{1}{V_s} \times 1000$$

$$\theta_{V_s} = \frac{\partial pha_v}{\partial V_s}\Big|_{V_s=\overline{V_s}} = \frac{-pha}{{V_s}^2} \times 1000$$

$$u_{V_s} = B_{V_s} = \frac{1}{2} res$$

$$u_{pha_v} = \pm\sqrt{(\theta_{pha} \times u_{pha}) + (\theta_{V_s} \times u_{V_s})}$$

%PHA (PHA_v/DCM_v) [%]:

%PHA = PHA yield (dry cell mass basis) [%]

$$\%PHA = f(pha_v, dcm_v) = \frac{pha_v}{dcm_v} \times 100$$

$$\%PHA' = \overline{\%PHA} \pm u_{\%PHA} \quad (P\%)$$

$$\overline{\%PHA} = f_1\{\overline{pha_v}, \overline{dcm_v}\} = \frac{\overline{pha_v}}{\overline{dcm_v}} \times 100$$

$$\theta_{pha_v} = \frac{\partial \%PHA}{\partial pha_v}\Big|_{pha_v = \overline{pha_v}} = \frac{1}{\overline{dcm_v}} \times 100$$

$$\theta_{dcm_v} = \frac{\partial \%PHA}{\partial dcm_v}\Big|_{dcm_v = \overline{dcm_{v_s}}} = \frac{-\overline{pha_v}}{\overline{dcm_v}^2} \times 100$$

$$u_{\%PHA} = \pm\sqrt{\left(\theta_{pha_v} \times u_{pha_v}\right) + \left(\theta_{dcm_v} \times u_{dcm_v}\right)}$$

ACKNOWLEDGEMENTS

This work was partially supported by the Battelle Fund through the Iowa Board of Regents, USDA #683A755233, and the Iowa State University Bioeconomy Institute.

Thank you to Dr. Robert Brown for providing guidance and support as well as for the opportunity to be part of the CSET research group. Thank you to Dr. Dong Won Choi for serving as my mentor throughout this project. Thank you to Dr. Sam Jones, Patrick Johnston, Marge Rover, and the rest of the CSET staff for advice and help. I would also like to thank my fellow graduate students as well as CSET undergraduates Angelo Fruci and Amanda Machacek. Thank you to Dr. Thomas Bobik, Dr. Theodore Heindel, and Dr. Shihwu Sung for serving on my program of study committee. Dr. Bobik, Dr. Alan DiSpirito, and Dr. Heindel were gracious in letting me use equipment from their labs for my thesis research.

Most of all, I would like to thank my family and especially my wife, Kristi, for their love, support, and patience throughout this process.